

**UCSF**

**UC San Francisco Electronic Theses and Dissertations**

**Title**

Communication Between Motor Cortical Areas During Learning

**Permalink**

<https://escholarship.org/uc/item/48t860v5>

**Author**

Derosier, Katherine

**Publication Date**

2020

Peer reviewed|Thesis/dissertation

Communication Between Motor Cortical Areas During Learning

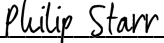
by  
Katherine Derosier

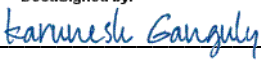
DISSERTATION  
Submitted in partial satisfaction of the requirements for degree of  
DOCTOR OF PHILOSOPHY

in  
Neuroscience


in the  
GRADUATE DIVISION  
of the  
UNIVERSITY OF CALIFORNIA, SAN FRANCISCO

Approved:

DocuSigned by:  
  
Philip Starr  
Chair

DocuSigned by:  
  
Karunesh Ganguly

DocuSigned by:  
  
Loren Frank

DocuSigned by:  
  
Mazen Kheirbek

Committee Members

Copyright 2020

by

Katherine Derosier

## **DEDICATION**

To my dog, Mera, who grudgingly allowed me to leave the house every weekday for several years to do this work.

## ACKNOWLEDGEMENTS

I have been very fortunate to have Karunesh Ganguly as my thesis advisor. One of the things I really appreciate about Karunesh is that he creates a lab environment that is supportive of a healthy work-life balance. I experienced a lot of big life events, both positive and negative, during my time at UCSF, and he was supportive every time. I also appreciate that he is proactive about scheduling meetings and always keeps an eye on the bigger picture. Regularly checking in with Karunesh and seeing how he always tried to connect my work to other projects in lab and papers he had read has probably helped me grow as a scientist more than anything else in grad school - it got me in the habit of intentionally looking at the big picture and kept me from getting caught up in details for too long.

I owe infinite thanks to Tess Veuthey, without whom none of this work would have happened. In addition to being a fantastic scientific collaborator, Tess helped me get through the toughest parts of grad school by believing in me when I didn't believe in myself. I would also like to thank Nerissa Hoglen and Daniel Silversmith for commiserating with me on bad days and being great people to bounce ideas off of. Thanks also to Preeya Khanna for suggesting a couple analyses that turned out to be very interesting, to Sravani Kondapavulur for taking time out of her other projects to help Tess and I with a key experiment, and to all of my other coworkers in the Ganguly lab for providing useful feedback at lab meetings and generally being friendly and willing to help each other out.

Thank you to my thesis committee members, Philip Starr, Loren Frank, and Mazen Kheirbek, for asking helpful questions, giving good advice, and not being too difficult to schedule things with.

Thank you to Kira Poskanzer for giving me really thoughtful life advice on multiple occasions, despite having no formal obligation to me.

Finally, I would like to thank my family. My parents have always encouraged me to do whatever I set my mind to, and taken care of me when things were hard. My sister believes in my abilities perhaps more than any other person on the planet; I hope to someday be even half as talented

as she thinks I am. My husband is always willing to brainstorm about my work, proofread my writing, or talk to me about something else when I need a distraction. I also want to thank my husband's parents for their support, especially my mother in law, who has provided us with months of free childcare. Last but not least, I would like to thank my son for giving me motivation to wrap things up.

## CONTRIBUTIONS

The **Introduction** was written by Katherine Derosier.

**Chapter 1** is reproduced in its entirety from:

Veuthey, T. L., Derosier, K., Kondapavulur, S., & Ganguly, K. (2020). Single-trial cross-area neural population dynamics during long-term skill learning. *Nature communications*, 11(1), 1-15.

T.L.V., K.D. and K.G. designed the study. T.L.V., K.D., and S.K. conducted experiments. T.L.V. and K.D. performed analyses. T.L.V., K.D., and K.G. wrote the manuscript.

**Chapter 2** was written by Katherine Derosier, Tess L. Veuthey, and Karunesh Ganguly, and represents ongoing and unpublished work. K.D., T.L.V., and K.G. designed the study. T.L.V. performed surgeries. K.D. and T.L.V. conducted experiments. K.D. performed analyses. K.D., T.L.V. and K.G. wrote the manuscript.

The **Conclusion** was written by Katherine Derosier.

# **COMMUNICATION BETWEEN MOTOR CORTICAL AREAS DURING LEARNING**

Katherine Derosier

## **ABSTRACT**

Motor cortex is known to be required for both motor learning and the execution of certain dexterous motor skills; however, much remains unknown about the communication between primary motor and premotor areas, and how it may or may not change with learning. We addressed this question by making simultaneous electrophysiological recordings of neural populations in rat primary motor (M1) and premotor (M2) cortex, first in the context of natural motor learning, and then in the context of M1 brain-computer interface (BCI) learning. In both cases, we found that activity was coordinated between the two regions. In the case of natural motor learning, we found that learning did not change the strength of M2-M1 interactions, but did increase the amount of task-related information available in the cross-area dynamics, and that these cross-area dynamics were necessary for learned behavioral improvements. In the case of BCI learning, we found that M2-M1 interactions occurred on a broader timescale than did M1-internal interactions, and that M2 population activity evolved at a slower pace. These results are consistent with a model in which M2 provides top-down contextual information to M1, which more precisely controls the output.



# TABLE OF CONTENTS

|  |    |
|--|----|
| Introduction: Why Study Motor Cortex?.....   | 1  |
| Ch. 1 Single-trial cross-area neural population dynamics during long-term skill learning ..... | 6  |
| 1.1 Abstract .....   | 6  |
| 1.2 Introduction.....  | 6  |
| 1.3 Results.....   | 8  |
| 1.3.1 Learning increases movement-modulated neurons in M1 and M2 .....                         | 8  |
| 1.3.2 Distinct cross-area dynamics versus single-unit interactions.....                        | 10 |
| 1.3.3 Correlation of cross-area activity is stable across learning.....                        | 12 |
| 1.3.4 Learning amplifies cross-area encoding of reach initiation .....                         | 12 |
| 1.3.5 Learning amplifies cross-area encoding of reach duration .....                           | 13 |
| 1.3.6 M2 local activity precedes M1 local activity .....                                       | 14 |
| 1.3.7 M2 inhibition disrupts skilled reaching.....   | 15 |
| 1.3.8 M2 inhibition preferentially disrupts M1 cross-area activity.....                        | 16 |
| 1.3.9 M2 inhibition disrupts M1 representation of movement .....                               | 17 |
| 1.4 Discussion .....   | 18 |
| 1.5 Figures.....   | 22 |
| 1.6 Methods.....   | 35 |
| 1.7 Supplementary Materials .....  | 46 |
| 1.8 References .....   | 60 |
| Ch. 2 Premotor activity during M1 brain-computer interface learning.....                       | 67 |

|       |  |    |
|-------|--|----|
| 2.1   | Abstract .....   | 67 |
| 2.2   | Introduction.....  | 67 |
| 2.3   | Results.....   | 69 |
| 2.3.1 | M2 units are modulated by a simple M1 BCI task .....                             | 69 |
| 2.3.2 | M2 population activity predicts M1 BCI-potent activity at broad timescales ..... | 70 |
| 2.3.3 | M1 direct units do not have a privileged functional relationship with M2.....    | 71 |
| 2.3.4 | M2 units are distinct from M1 indirect units .....                               | 71 |
| 2.3.5 | M2 population activity evolves at a slower pace than M1 indirect activity .....  | 72 |
| 2.4   | Discussion .....   | 72 |
| 2.4.1 | Hierarchical control of BCI performance.....                                     | 73 |
| 2.4.2 | BCIs control of static versus dynamic target states .....                        | 74 |
| 2.4.3 | Timescales of BCI learning .....   | 75 |
| 2.4.4 | Limitations and future work .....  | 75 |
| 2.5   | Figures.....   | 77 |
| 2.6   | Methods.....   | 83 |
| 2.7   | References .....   | 91 |
|       | Conclusion .....   | 95 |

## LIST OF FIGURES

|  |    |
|--|----|
| Figure 1.1 Motor skill learning is associated with increased cortical movement signals.....                    | 22 |
| Figure 1.2 Canonical Correlation Analysis identifies shared cross-area dynamics. ....                          | 24 |
| Figure 1.3 Correlation of M1-M2 cross-area activity is stable across behaviors.....                            | 26 |
| Figure 1.4 Learning increases cross-area representation of reach initiation. ....                              | 27 |
| Figure 1.5 Learning amplifies cross-area representations of reach duration.....                                | 29 |
| Figure 1.6 Local signals support a M2 to M1 hierarchy. ....  | 30 |
| Figure 1.7 M2 inhibition disrupts learned reach behavior and M1 single-unit movement modulation. ....          | 32 |
| Figure 1.8 M2 inhibition disrupts M1 cross-area movement modulation. ....                                      | 34 |
| Figure 1.9 M1 and M2 implantation coordinates.....   | 46 |
| Figure 1.10 Elaboration of reach-to-grasp learning behavior.....   | 48 |
| Figure 1.11 Fitting CCA with different bin-widths.....   | 49 |
| Figure 1.12 PCA identifies a mix of local and cross-area dynamics.....   | 51 |
| Figure 1.13 M2 saline infusions do not severely affect learned reach behavior. ....                            | 52 |
| Figure 1.14 Histological verification of M2 muscimol spread. ....  | 54 |
| Figure 2.1 Learning the BCI task.....  | 77 |
| Figure 2.2 Indirect neurons in both M2 and M1 are modulated during BCI control. ....                           | 78 |
| Figure 2.3 M2 neural activity predicts M1 BCI-potent neural activity at multiple timescales. ....              | 79 |
| Figure 2.4 Comparison of timescales of M2 and M1-indirect units' predictions of M1-direct units.....           | 80 |
| Figure 2.5 M2 population activity evolves more slowly across trials than M1 indirect population activity. .... | 82 |

## **LIST OF TABLES**

|   |    |
|---|----|
| Table 1.1 Behavior summary. ....                                      | 56 |
| Table 1.2 Implantation coordinates for all experimental animals ..... | 58 |

## **INTRODUCTION: WHY STUDY MOTOR CORTEX?**

From a certain perspective, the purpose of the brain is to produce the correct behavior at the correct time. When comparing a human to a fly, the idea of "correct" behavior is certainly more complicated, and the timescale over which the process operates may be much longer, but the principle is the same: Movement is the ultimate output of all mental processes. It is how we respond to stimuli, and how our opinions and decisions are able to influence the world. From this perspective, understanding how animals generate movements is of utmost importance to understanding the brain.

The mammalian motor system is a distributed network, involving many parts of the nervous system including cortex, striatum, thalamus, cerebellum, brain stem, and spinal cord<sup>1</sup>. Although all of these areas have movement-related activity, it has been shown that not all motor areas are strictly necessary for some motor tasks. For example, cats (and other animals) are able to perform some walking motions after a complete section of the spinal cord above the level of the limbs<sup>2</sup>, and rats that have been previously trained in a lever pressing task are still able to perform this task after a motor cortex lesion<sup>3</sup>. By combining these sorts of experiments with neural recordings from intact animals, we can generate theories about the different roles played by the parts of the motor system in different movements.

Of particular interest are intentional movements, the sort that require conscious attention, either because they are novel and unpracticed, or because they are complicated and highly dexterous. Interestingly, both the performance of dexterous motor skills and motor learning in general are thought to require motor cortex. Relatively small lesions or strokes in motor cortex can result in chronic deficits to dexterous motor skills in rodents, non-human primates, and humans<sup>4-6</sup>, and rats that had not been trained on a lever pressing task prior to a motor cortex lesion were unable to learn the task afterwards<sup>3</sup>. This indicates a special role for cortex in motor tasks that require careful online control.

In rodents, motor cortex consists of two areas: the primary motor cortex (M1), and the more rostral premotor cortex (M2; when the regions controlling the forelimbs in particular are referred to, these may be called the caudal forelimb area and the rostral forelimb area). Both areas show robust movement-related activity<sup>7</sup>, and evoke movement when electrically stimulated<sup>8-10</sup>. Anatomical studies have shown that M1 and M2 are heavily interconnected, with similar patterns of local connectivity and similar subcortical inputs and outputs<sup>11</sup>. The connections between the regions, however, suggests a hierarchical relationship, with M2 providing a strong input to M1 layer 5b, suitable for top-down control, while M1 projections to M2 appear more like feedback input<sup>12</sup>. M1 and M2 therefore likely have different roles in the learning and execution of motor skills, but these differences are only partially understood. M2 has been found to have activity related to anticipation and motor preparation<sup>13,14</sup>, and wide-field calcium imaging has found that coordinated task-related activity in M2 became earlier and more prominent with learning<sup>15</sup>. Despite this work, much is still unknown about the communication between M2 and M1, and about how input from M2 shapes M1 neural dynamics.

In Chapter 1, we investigate the role of M2-M1 communication in motor learning. By making simultaneous recordings of M2 and M1 neural populations, and using a dimensionality reduction technique that optimizes for coordinate between the regions, we are able to identify a pattern of shared cross-area population dynamics that help explain how M2 inputs shape M1 activity over the course of motor learning. We found that learning did not change the strength of M2-M1 interactions, but did increase the amount of task-related information available in the cross-area dynamics. By chemically inactivating M2 with muscimol, we show that M2 activity is necessary for execution of the reach-to-grasp task in well-trained rats. We also characterized the effect of M2 inactivation on M1 neural activity, finding that M1 neurons and population dynamics that had earlier been more strongly coordinated with M2 were more affected.

In Chapter 2, we study interactions between M2 and M1 in the context of a brain-computer interface (BCI) paradigm, where rats learn to control external cues by manipulating the firing rate

of a small set of M1 neurons. The BCI approach removes several confounds of the natural motor learning experiments. Unlike natural movement, the target neural activity pattern and the identity of the M1 neurons directly controlling the output are known and experimenter-controlled. Additionally, in natural movement, M2 and M1 have outputs to similar subcortical structures which are causally involved in movement, while in BCI, M2 can only affect the output via its input to M1. In this context, we find that M2 units are task-modulated at similar rates to M1 units that do not directly control the BCI, and that the M2 population is correlated with M1 BCI-potent activity at a broad timescale. This is in contrast to M1 indirect units, which tend to be correlated with M1 BCI-potent activity at short timescales. Furthermore, M2 single units and the M2 population as a whole are correlated with themselves over longer timescales, suggesting that M2 input to M1 is slowly-changing and modulatory.

## References

1. Purves, Dale; Augustine, George J; Fitzpatrick, David; Hall, William C; Lamantia, Anthony Samuel; Mooney, Richard D; Platt, Michael L; White, Leonard E, eds. (2018). Neuroscience (6th ed.). Sinauer Associates.
2. Rossignol, S., Chau, C., Brustein, E., Bélanger, M., Barbeau, H., & Drew, T. (1996). Locomotor capacities after complete and partial lesions of the spinal cord. *Acta neurobiologiae experimentalis*, 56, 449-464
3. Kawai, R., Markman, T., Poddar, R., Ko, R., Fantana, A. L., Dhawale, A. K., ... & Ölveczky, B. P. (2015). Motor cortex is required for learning but not for executing a motor skill. *Neuron*, 86(3), 800-812.
4. Ramanathan, D. S., Guo, L., Gulati, T., Davidson, G., Hishinuma, A. K., Won, S. J., ... & Ganguly, K. (2018). Low-frequency cortical activity is a neuromodulatory target that tracks recovery after stroke. *Nature medicine*, 24(8), 1257-1267
5. Plautz, E. J., Barbay, S., Frost, S. B., Friel, K. M., Dancause, N., Zoubina, E. V., ... & Nudo, R. J. (2003). Post-infarct cortical plasticity and behavioral recovery using concurrent cortical stimulation and rehabilitative training: a feasibility study in primates. *Neurological research*, 25(8), 801-810.
6. Dimyan, M. A., & Cohen, L. G. (2011). Neuroplasticity in the context of motor rehabilitation after stroke. *Nature Reviews Neurology*, 7(2), 76-85.
7. Hyland, B. (1998). Neural activity related to reaching and grasping in rostral and caudal regions of rat motor cortex. *Behavioural brain research*, 94(2), 255-269.
8. Neafsey, E. J., Bold, E. L., Haas, G., Hurley-Gius, K. M., Quirk, G., Sievert, C. F., & Terreberry, R. R. (1986). The organization of the rat motor cortex: a microstimulation mapping study. *Brain research reviews*, 11(1), 77-96.
9. Neafsey, E. J., & Sievert, C. (1982). A second forelimb motor area exists in rat frontal cortex. *Brain research*, 232(1), 151-156.



10. Kleim, J. A., Barbay, S., & Nudo, R. J. (1998). Functional reorganization of the rat motor cortex following motor skill learning. *Journal of neurophysiology*, *80*(6), 3321-3325.
11. Kaneko, T. (2013). Local connections of excitatory neurons in motor-associated cortical areas of the rat. *Frontiers in neural circuits*, *7*, 75.
12. Hira, R., Ohkubo, F., Tanaka, Y. R., Masamizu, Y., Augustine, G. J., Kasai, H., & Matsuzaki, M. (2013). In vivo optogenetic tracing of functional corticocortical connections between motor forelimb areas. *Frontiers in neural circuits*, *7*, 55.
13. Chen, T. W., Li, N., Daie, K., & Svoboda, K. (2017). A map of anticipatory activity in mouse motor cortex. *Neuron*, *94*(4), 866-879.
14. Murakami, M., Vicente, M. I., Costa, G. M., & Mainen, Z. F. (2014). Neural antecedents of self-initiated actions in secondary motor cortex. *Nature neuroscience*, *17*(11), 1574-1582.
15. Makino, H., Ren, C., Liu, H., Kim, A. N., Kondapaneni, N., Liu, X., ... & Komiyama, T. (2017). Transformation of cortex-wide emergent properties during motor learning. *Neuron*, *94*(4), 880-890.

# **CH. 1 SINGLE-TRIAL CROSS-AREA NEURAL POPULATION DYNAMICS DURING LONG-TERM SKILL LEARNING**

## **1.1 Abstract**

Mammalian cortex has both local and cross-area connections, suggesting vital roles for both local and cross-area neural population dynamics in cortically-dependent tasks, like movement learning. Prior studies of movement learning have focused on how single-area population dynamics change during short-term adaptation. It is unclear how cross-area dynamics contribute to movement learning, particularly long-term learning and skill acquisition. Using simultaneous recordings of rodent motor (M1) and premotor (M2) cortex and computational methods, we show how cross-area activity patterns evolve during reach-to-grasp learning in rats. The emergence of reach-related modulation in cross-area activity correlates with skill acquisition, and single-trial modulation in cross-area activity predicts reaction time and reach duration. Local M2 neural activity precedes local M1 activity, supporting top-down hierarchy between the regions. M2 inactivation preferentially affects cross-area dynamics and behavior, with minimal disruption of local M1 dynamics. Together, these results indicate that cross-area population dynamics are necessary for learned motor skills.

## **1.2 Introduction**

The connectivity pattern of mammalian cortex, characterized by both local and cross-area connections<sup>1</sup>, suggests an important role for interactions between population dynamics compartmentalized locally and those coordinated between regions. But it is unknown whether population dynamics coordinated across multiple cortical areas contribute to long-term skill learning. In the motor system, it has been shown that both premotor cortex (M2)<sup>2-6</sup> and motor

cortex (M1)<sup>7-11</sup> demonstrate changes in local population dynamics with motor learning. However, it remains unclear how cross-area dynamics between M1 and M2 are coordinated and change with long-term skill learning. Previous work on cross-area interactions during motor learning has focused on macroscopic population activity, such as local field potentials<sup>12-14</sup> and wide-field calcium signals<sup>4,15</sup>. However, such measures of aggregate activity collapse signals from a heterogeneous population of neurons into a single signal, making it difficult to resolve potentially important multiplexed signals within that population<sup>16-18</sup>. Recent work has examined cross-area dynamics during motor adaptation<sup>5</sup>, but this process is fundamentally different from new skill learning<sup>19</sup>.

How can we examine cross-area population dynamics during learning, especially when newly learned movements are still variable? To avoid the limitations of analyzing trial-averaged movement-related signals, we can instead build models by estimating prevalent population patterns from signals concatenated over time<sup>17,20,21</sup>. One common approach in well-trained animals is to use dimensionality reduction methods such as Principal Component Analysis (PCA) to capture patterns of dominant covariance within local populations<sup>5,7,11,16,22-29</sup>. Those reduced local signals can then be compared across regions<sup>5,16,30</sup>. However, since PCA finds dimensions that maximize local variance, activity patterns which do not dominate local variance are discarded. Thus, this approach may dismiss as noise neural fluctuations representing activity coordinated across areas<sup>31</sup>. Instead, cross-area activity might be identified by directly detecting covariance which is coordinated across regions<sup>5,18,32</sup>. Recent work has shown that simultaneous recordings from two visual areas can be analyzed to identify a neural shared subspace defined by the activity in each region that is maximally correlated with activity in a partner region<sup>32</sup>. Two additional studies have also identified widespread neural signals encoding facial movements<sup>18</sup> and thirst-based motivational states<sup>33</sup>. These findings suggest that signals shared across brain areas may contribute to coordinating diverse behaviors. But it remains unclear whether and how cross-area dynamics evolve during learning. Understanding these changes can help define the functional

role of cross-area activity, and provide new insight into learning mechanisms of distributed networks.

Here, we aim to assess how population dynamics shared by M2 and M1 change during motor skill learning. We hypothesize that M2-M1 shared dynamics coordinate information between the regions and contribute to learning complex behaviors. To isolate activity shared across areas, we perform simultaneous multisite recordings in M2 and M1 and use the dimensionality reduction technique Canonical Correlation Analysis (CCA) to define the axes of maximal correlation between the M2 and M1 neural populations<sup>34</sup>. By simultaneously reducing dimensionality and optimizing for M2-M1 correlation, CCA can identify cross-area signals that may be missed by methods that exclusively optimize local variance. We use the term cross-area to refer to activity in each area which is maximally correlated with activity in the partner region. We thus aim to explicitly identify cross-area dynamics during both early exploratory learning and late learned execution of a skilled movement.

In each region, we find that cross-area dynamics modulation is proportional to single-trial reaching behavior, and that modulation to reach initiation and reach duration is amplified with learning. We additionally find that local activity in M2 precedes local activity in M1, consistent with a top-down hierarchy between the signals more specific to M2 and M1. In line with this top-down functional role, M2 inhibition in well-trained animals impairs reach behavior and disrupts reach representation in M1 cross-area signals. Together, our results indicate that cross-area M2-M1 population dynamics represent a necessary component of skilled motor learning.

## **1.3 Results**

### **1.3.1 Learning increases movement-modulated neurons in M1 and M2**

We performed simultaneous recordings of population neural activity in M2 and M1 (Figure 1a, Supplementary Figure 1) in rats learning a cue-driven reach-to-grasp task, a well-established model for skill learning<sup>27,35,36</sup>. Both M2 and M1 are required for learning and execution of reach-

to-grasp movements in both rodents and primates<sup>37–39</sup>. Animals learned to successfully retrieve pellets with training (hierarchical bootstrap, 104 shuffles used here and hereafter, 27.28% ± 3.06 for Early, 57.64% ± 2.49 for Late,  $p < 0.0001$ ,  $n = 5$  rats). There were concomitant improvements in movement duration (hierarchical bootstrap, 0.30s ± 0.056 for Early, 0.20s ± 0.040 for Late,  $p = 0.0027$ ,  $n = 5$  rats) and reaction time (hierarchical bootstrap, 32.23s ± 24.58 for Early, 0.89s ± 0.18 for Late,  $p < 0.0001$ ,  $n = 5$  rats)(Figure 1b, Supplementary Figure 2, Supplementary Table 1). To examine relationships between single-neuron activity and movements, we created trial-averaged peri-event time histograms (PETHs) for both M2 and M1 in early and late learning. We used a circular shuffle test to quantify whether each neuron was significantly modulated ( $p < 0.000125$ ) (Figure 1c-d; Methods)<sup>40</sup>. Over learning, significantly more neurons in both areas were movement modulated (hierarchical bootstrap,  $n = 5$  rats; M1: 59.83% ± 8.89 for Early, 94.32% ± 4.65 for Late,  $p < 0.0001$ ; M2: 48.19% ± 13.40 for Early, 88.03% ± 5.81 for Late,  $p < 0.0001$ ), consistent with prior work arguing that learning engages and amplifies representations in both regions<sup>4,10,27,41,42</sup>. However, as PETHs represent neural activity averaged across trials, increased PETH modulation can be driven by many neural and behavioral factors. Additionally, trial-averaged activity from both early and late learning demonstrated evidence of sequential activation of neurons in a task-dependent manner<sup>10,17,21,40,43,44</sup>. While visual inspection of M1 and M2 PETHs in early and late learning suggest changes in correlated firing between areas, trial-averaged data, such as PETHs, inherently blur trial-by-trial variations in neural activity which may correspond to trial-by-trial variations in performance. Therefore, although PETHs from M1 and M2 may show temporal overlap, this does not indicate single trial correlated activity. PETHs also require time-locking to a specific aspect of movement. Thus, further analyses of single-trial data are essential for distinguishing between these confounding variables.

Without modeling single-trial activity patterns, it is unclear how movement signals in M2 and M1 correspond with single-trial performance over learning, or how task-relevant activity is coordinated between M1 and M2 on a moment-by-moment basis. Moreover, studies on population dynamics

have identified that single trial dynamics can be reliable and revealing about single-trial behavioral variation in well-trained animals<sup>18,28,45,46</sup>. However, these findings raise the fundamental questions of whether single-trial cross-area dynamics can inform our understanding of cortical communication during learning.

### 1.3.2 Distinct cross-area dynamics versus single-unit interactions

How then can we identify single trial activity patterns shared between M2 and M1? We used canonical correlation analysis (CCA), which finds linear combinations of simultaneous M2 and M1 activity that are maximally correlated with each other, to measure cross-area dynamics. The neuron weights obtained using CCA define axes in the high-dimensional M1 and M2 population spaces along which activity is most similar (see Methods). The projections of high-dimensional neural activity onto these axes provide a low-dimensional representation of shared signals (Figure 2a-b).

Our main analyses are done with CCA fit to neural data binned at 100ms, with no timelag between regions. For comparison, we also fit models to data binned at 75ms and 50ms at timelags from -500ms to +500ms. We found that for most datasets, models fit using 100ms bins with no timelag resulted in the best generalizability to held out data (see Methods and Supplementary Figure 3). Additionally, we found that neuron weights and axes generated by CCA are different from those found with PCA, which instead defines axes of maximal variance in single-area population spaces (Supplementary Figure 4). In each region, the angles between axes of maximal local covariance (using PCA) and axes of maximal cross-area correlation (using CCA) are significantly different from zero, and did not change with learning (hierarchical bootstrap,  $n=4$  rats; M2:  $59.66^\circ \pm 4.57$  for Early,  $59.34^\circ \pm 3.83$  for Late, two-sided  $p=0.92$ ; M1:  $49.84^\circ \pm 5.49$  for Early,  $59.47^\circ \pm 8.68$  for Late, two-sided  $p=0.43$ ; in all cases, all bootstrap samples were  $>30^\circ$ ,  $p<0.0001$ ).

To validate the stability of this CCA axis, we calculated 10 sets of CCA neuron weights from ten randomly selected subsets of 90% of timebins (held out data was non-overlapping). Across all

datasets, the range of weights for models using the full datasets (mean  $\pm$  std =  $0.057 \pm 0.16$  a.u.) was much larger than the variance in each neuron's weights between subsets (weight from subset – weight from full dataset, mean  $\pm$  std =  $-2.37e-05 \pm 0.02$  a. u.). That CCA weights change by a small amount when fit to different subsets of data suggests that the CCA model for M2-M1 cross-area activity is robust (Figure 2c). Further analyses were conducted without data subsampling.

To verify that the CCA-defined M2 and M1 cross-area activity models represented behaviorally significant coordinated activity, we compared the R2 between the cross-area activity to CCA models fit on trial-shuffled data. We generated a reference distribution of R2 values between the top M1 and M2 canonical variables from  $10^4$  iterations of trial-shuffled data. Canonical variables fit to the true dataset were considered significant if their R2 value exceeded the 95<sup>th</sup> percentile of the reference distribution (see Methods). Shuffling data between trials while maintaining within-trial temporal structure preserved and controlled for coarse activity fluctuations due to movement. We found that most datasets had one to three significant canonical variables (Figure 2d), confirming that CCA identified low-dimensional activity shared across M2 and M1. For one animal, the early dataset had no significant canonical variables; this animal was excluded from further analysis.

Finally, we examined whether CCA identifies cross-area relationships equivalent to those identified using a single-neuron functional connectivity measure, short-latency cross-correlations<sup>13,44,47,48</sup>. Specifically, if CCA consistently assigns high weights to M2 and M1 neurons which also have high cross-correlation values, this would indicate that CCA finds M2-M1 activity shared by individual neurons in each region. However, if the CCA weights of M2 and M1 neurons do not vary with cross-correlation values, then CCA-defined activity instead reflects distributed shared population dynamics not obvious at the single-neuron level. We found there was a weak but significant correlation between the mean CCA weights of M2-M1 neuron pairs and their short-latency normalized cross-correlation values (linear regression,  $R^2=0.0761$ ,  $p=5.98 \times 10^{-89}$ ,  $t=20.399$ ,  $n=5056$  neuron pairs from 4 rats)(Figure 2e-f). Therefore, M2 and M1 CCA neuron

weights capture aspects of short-latency correlations but can also capture additional information about cross-area dynamics (Fig 2g). This suggests that communication between cortical areas maybe be better modeled based on population-wide activity patterns rather than based on interactions between single neurons.

### 1.3.3 Correlation of cross-area activity is stable across learning

Does learning change the correlation of cross-area dynamics? If learning simply increases M1-M2 activity coordination, we would expect the correlation of M1 and M2 cross-area activity to be lower during early exploratory actions than during skilled behavior. To address this, we correlated M1 and M2 cross-area activity during three types of behavior: spontaneous behavior, exploratory reaches in early learning, and directed reaches in late learning (Figure 3a). Surprisingly, there was no difference in the mean correlation values ( $R^2$ ) of M1 versus M2 cross-area activity during the different behaviors (mixed effect model,  $0.31 \pm 0.04$  for Spontaneous,  $0.34 \pm 0.10$  for Early,  $0.30 \pm 0.08$  for Late; Spontaneous vs. Early:  $t(6)=0.46$ ,  $p=0.66$ ; Spontaneous vs. Late:  $t(6) = -0.15$ ,  $p=0.89$ ; Early vs. Late:  $t(6) = -0.74$ ,  $p=0.49$ ;  $n=4$  rats) (Figure 3b). Thus, generally increased coordination between M2 and M1 activity by itself seems unlikely to drive performance gains.

### 1.3.4 Learning amplifies cross-area encoding of reach initiation

An intriguing alternative is that learning is due to the modification of task representations within cross-area dynamics. Specifically, signals within the existing range of cross-area activity may be remapped to represent information about the task. Thus, while the overall range of M1-M2 cross-area signals may not change, high amplitude cross-area activity may now be associated with a particular behavioral state. As noted above, we observed that the door open cue was more rapidly followed by reach initiation after learning (Figure 1b), suggesting that the timing of reach initiation might be an important marker of learning. We thus explored whether M1-M2 cross-area activity could account for this change. To visualize this possibility, we plotted the M1 cross-area activity versus the M2 cross-area activity during pre-reach and at reach initiation (Figure 4a). The



histograms show the probability density functions of the respective subspace activity before and during reach initiation. Interestingly, the two behavioral states were significantly more separable after learning (mixed effect model, M2:  $0.31 \pm 0.15$  for Early,  $1.29 \pm 0.18$  for Late,  $t(6) = 5.3806$ ,  $p=0.0017$ ; M1:  $0.27 \pm 0.14$  for Early,  $1.09 \pm 0.12$  for Late,  $t(6) = 6.7227$ ,  $p=0.00053$ ;  $n=4$  rats) (Figure 4b), suggesting that high amplitude cross-area activity gained task relevance with learning.

The increased task relevance of high amplitude cross-area activity was also apparent on a single-trial basis. When viewed as single trial trajectories, peaks in cross-area activity became associated with reach initiation after learning (Figure 4c). We quantified this association across trials by building a logistic regression model to distinguish cross-area activity during two seconds before reaching versus a 400ms window at reach initiation. Strikingly, detection of reach initiation based on this cross-area activity model improved with learning (mixed effect model,  $0.66 \pm 0.03$  for Early,  $0.87 \pm 0.02$  for Late,  $t(6) = 9.77$ ,  $p=6.63 \times 10^{-5}$ ,  $n=4$  rats) (Figure 4d). Using the logistic regression model, we could then probe the time course of reach initiation prediction based on M1-M2 cross-area activity (Figure 4e). On average, while the time of reach initiation was not well predicted during early trials, it became highly predictable after learning (hierarchical bootstrap,  $0.12 \pm 0.044$  for Early,  $0.30 \pm 0.082$  for Late,  $p<0.0001$ ,  $n=4$  rats) (Figure 4f).

### 1.3.5 Learning amplifies cross-area encoding of reach duration

Does M1-M2 cross-area activity only coordinate movement initiation, or does it affect other aspects of reach performance? We examined whether single-trial M2-M1 cross-area dynamics were informative about single-trial reach duration, and whether the reach modulation of cross-area activity for movements of similar duration changed with learning. To quantify reach modulation in single-trial activity, we calculated a cross-area modulation metric (CA-modulation), which compared neural activity during reaching versus an equivalent baseline period for each trial (Figure 5a, b). This measure is equivalent to the  $d'$  (d-prime) signal sensitivity index used in signal

processing (see Methods). To directly test the relationship between behavioral performance and M1 and M2 CA-modulation, we correlated CA-modulation with reach duration on a trial-by-trial basis (Figure 5c). Interestingly, we found that CA-modulation reliably covaried with reach duration, indicating that cross-area dynamics represent information relevant to behavioral performance (mixed-effect model, M2: log slope = -0.27,  $t(1531) = -14.43$ ,  $p=2.36 \times 10^{-44}$ ; M1: log slope = -0.23,  $t(1562) = -13.88$ ,  $p=2.05 \times 10^{-41}$ ;  $n=4$  rats). Additionally, both M1 and M2 CA-modulation increased with learning (hierarchical bootstrap,  $n=4$  rats; M1:  $0.45 \pm 0.13$  for Early,  $1.97 \pm 0.44$  for Late,  $p<0.0001$ ; M2:  $0.46 \pm 0.12$  for Early,  $2.57 \pm 0.62$  for Late,  $p<0.0001$ ; Figure 5d). This modulation increase was not simply due to overall improved reach performance; instead, movements of similar duration in early and late learning were more modulated in late learning, indicating amplified representation of learned skills. Thus, the process of learning appeared to enhance reach-specific signals in cross-area population dynamics. Amplification of these task-specific signals spanning multiple brain areas may be a mechanism for coordinating network-wide activity related to salient behaviors during learning.

### 1.3.6 M2 local activity precedes M1 local activity

A prominent model of M2-M1 interactions during learning proposes a strong top-down influence from M2 to M1<sup>13,4</sup>. While cross-area activity may coordinate areas, we expected that local activity in each region might reflect a M2-to-M1 top-down relationship. For example, if M2-specific local activity temporally preceded M1-specific local activity, it would suggest that M2 is more likely to play a top-down role. To address this, we first defined local activity as the population firing not accounted for in cross-area activity. For each 100ms time bin, we projected the population firing rate vector onto the hyperplane orthogonal to the CCA subspace, and used the magnitude of this vector as our local activity value (Figure 6a). We then quantified, on a single-trial basis, the difference in median timing of M2 and M1 local activity in early and late learning (Figure 6b-c, see Methods). We found that M2 local activity consistently preceded M1 local activity in both early

and late learning (Figure 6d). These timing differences were significant when quantified via permutation testing. Specifically, we randomly assigned trial activity to either M1 or M2, computed the timing differences of the permuted data ( $10^5$  permutations), and used these differences as a reference distribution to evaluate the significance of the M2-M1 timing differences ( $p < 0.00001$ ) (Figure 6e). We used a similar approach to evaluate the change in M2-M1 temporal coupling. We thus randomly assigned M2-M1 timing differences to either early or late learning, computed the means of the permuted datasets ( $10^5$  permutations), and used the difference of those means as a reference distribution to evaluate the significance of the M2-M1 temporal coupling change with learning. M2 and M1 local activity became more tightly coupled with learning, as quantified by the significant decrease in the timing gap between their local activities with learning ( $p < 0.00001$ ) (Figure 6f). These timing results are consistent with a M2 to M1 top-down hierarchical relationship.

### 1.3.7 M2 inhibition disrupts skilled reaching

Based on our results, we expected M2 activity to be necessary for improvements in behavior with learning, as well as for amplified representations of learned movements in M1 cross-area activity. If activity shared between M2 and M1 helped to shape M1 representations, then disrupting M2-M1 cross-area activity should impact reaching behavior. To test this, we inactivated M2 in well-trained animals using the GABA agonist muscimol (Figure 7a). Unlike control saline infusions (Supplementary Figure 5), M2 inactivation caused severe performance deficits, with reaching behavior qualitatively similar to early learning (Figure 7b). M2 inactivation decreased success rate (hierarchical bootstrap,  $56.75\% \pm 5.16$  for Baseline,  $37.45\% \pm 6.88$  for Muscimol,  $p = 0.0082$ ,  $n = 6$  rats), increased reaction time (hierarchical bootstrap,  $1.26\text{s} \pm 0.28$  for Baseline,  $3.23\text{s} \pm 0.74$  for Muscimol,  $p < 0.0001$ ,  $n = 6$  rats), and increased reach duration (hierarchical bootstrap,  $0.18\text{s} \pm 0.018$  for Baseline,  $0.29\text{s} \pm 0.035$  for Muscimol,  $p < 0.0001$ ,  $n = 6$  rats). M2 saline did not decrease success rate (hierarchical bootstrap,  $54.81\% \pm 5.40$  for Baseline,  $57.84\% \pm 4.18$  for Saline,  $p = 0.7453$ ,  $n = 6$  rats), but did cause small but significant increases in reaction time (hierarchical

bootstrap,  $1.60s \pm 0.37$  for Baseline,  $2.13s \pm 0.49$  for Saline,  $p=0.0021$ ,  $n=6$  rats) and reach duration (hierarchical bootstrap,  $0.20s \pm 0.024$  for Baseline,  $0.22s \pm 0.025$  for Saline,  $p=0.0452$ ,  $n=6$  rats).

### 1.3.8 M2 inhibition preferentially disrupts M1 cross-area activity

To examine the influence of M2 inactivation on M1 neural representations, we performed simultaneous recordings in M1 and M2 during baseline performance and during M2 inactivation on the same day in well-trained animals. This approach allowed us to define the M2-M1 cross-area activity space with M2 intact, then track the effects of M2 disruption on single-unit M1 activity, M1 cross-area dynamics, and M1 local dynamics. First, we compared movement modulation of M1 single neurons during baseline reaches and M2 inactivation. Remarkably, not only did M2 inactivation disrupt M1 single-neuron movement modulation (hierarchical bootstrap,  $48.43\% \pm 16.93$  for Baseline,  $24.88\% \pm 17.01$  for M2 Muscimol,  $p=0.0137$ ,  $n=3$  rats) (Figure 7c), but the M1 neurons which contributed most to M2-M1 cross-area activity (i.e. with the highest magnitude CCA-weights) experienced greater drops in movement modulation (linear regression on  $\log(\text{CCA weight mag.})$ ,  $R^2=0.12$ ,  $t=2.81$ ,  $p=0.0067$ ,  $n=60$  neurons from 3 rats) (Figure 7e). This result is consistent with the model that M2 population activity shapes M1 population activity through M2-M1 cross-area signals.

Our data predicted that M2 inactivation might preferentially affect M1-M2 cross-area population dynamics, thereby removing top-down influence on M1, with minimal disruption of local M1 computations. Intriguingly, we found that M2 inactivation disrupted movement modulation of M2-M1 cross-area activity significantly more than the movement modulation of local M1 activity (Figure 8a). We quantified this by computing single-trial peak-to-trough values on a 1s interval centered on reach start for both cross-area and local signals. We found that across animals, both cross-area and local signals had decreased modulation with M2 inactivation, but that the decrease was significantly greater for cross-area signals (hierarchical bootstrap; M2 muscimol resulted in

a  $58.19\% \pm 8.71$  decrease in peak-to-trough amplitude for M1 cross-area signals, and a  $26.52\% \pm 7.20$  decrease for M1 local signals,  $p=0.0042$ ,  $n=3$  rats). These results indicate a degree of independence between cross-area and local dynamics. This decoupling may provide a mechanism for resilience of local dynamics, improving robustness in the event of distant network damage.

M2 inactivation resulted in a small but significant drop in firing rate across the M1 population (hierarchical bootstrap,  $24.65 \text{ Hz} \pm 2.73$  for Baseline,  $19.15 \text{ Hz} \pm 4.64$  for M2 Muscimol,  $p<0.0001$ ,  $n=3$  rats). However, histological analysis confirmed that this was not a direct effect of the muscimol itself, which did not reach M1 (Supplementary Figure 6). Instead, this effect may be due to loss of M2 inputs<sup>49</sup>. Furthermore, mean M1 local covariance did not change, indicating stability in local M1 functional connectivity (two-sided hierarchical bootstrap,  $0.24 \pm 0.063$  shared variance/total variance for Baseline;  $0.19 \pm 0.043$  shared variance/total variance for M2 Muscimol,  $p=0.28$ ,  $n=3$  rats, see Methods).

### 1.3.9 M2 inhibition disrupts M1 representation of movement

We found that M2 inactivation decreased M1 cross-area modulation during reach initiation (Figure 8b-e). We quantified this by comparing the difference in median activity along the cross-area activity axis before reach and at reach initiation (Figure 8b-d), and found that this difference was significantly smaller during M2 inhibition (mixed effect model,  $0.35 \pm 0.06$  for Baseline,  $0.03 \pm 0.09$  for M2 Muscimol,  $t(4) = -3.57$ ,  $p=0.02$ ,  $n=3$  rats). As before, we fit a logistic regression model to predict reach onset from M1 cross-area activity. We quantified the model's performance and saw that detection of reach initiation based on M1 cross-area activity decreased with M2 inhibition (mixed effect model,  $0.64 \pm 0.03$  for Baseline,  $0.52 \pm 0.04$  for M2 Muscimol,  $t(4) = -3.48$ ,  $p=0.02$ ,  $n=3$  rats) (Figure 8e), indicating that M1 cross-area dynamics were less informative about reach initiation during M2 inhibition.

In addition to disrupting reach initiation signals, we also found that M2 inhibition decreased reach modulation of M1 cross-area dynamics (hierarchical bootstrap,  $0.78 \pm 0.21$  for Baseline,  $0.27 \pm 0.050$  for M2 Musimol,  $p < 0.0001$ ,  $n = 3$  rats) (Figure 8f). This indicated that M2 input is necessary for intact M1 reach modulation and implied a M2 to M1 directionality. We additionally examined whether M2 inactivation entirely dissociated M1 cross-area modulation from behavioral performance. We found that the relationship between reach duration and M1 CA-modulation was still significant during M2 inactivation (mixed effect model, log slope =  $-0.26$ ,  $t(187) = -5.54$ ,  $p = 9.99 \times 10^{-8}$ ,  $n = 3$  rats) (Figure 8g), underscoring the fundamental relationship between M1 and behavior even during motor system disruption.

## 1.4 Discussion

This study outlines a new approach to understanding simultaneous activity shared between two cortical areas. First, we demonstrate that a computational method identifying maximally correlated activity patterns between regions can be used to isolate cross-area population dynamics. Second, we show that cross-area population dynamics become more related to both reach initiation and duration with learning. Through causal manipulations, we found that local M2 inactivation disrupted M1 cross-area dynamics as well as skilled reach execution. The M1 activity remaining in the M1-M2 cross-area dynamics axes was still predictive of single-trial behavior, indicating maintenance of meaningful movement activity in M1. However, M2 muscimol inactivation led to slower reactions to environmental cues and less efficient reaches, consistent with the hypothesis that attenuation of M2-M1 cross-area activity impairs M2 top-down guidance of behavior. These results demonstrate that M1-M2 cross-area dynamics represent and contribute to skilled execution.

There are two common approaches to understanding M2 and M1 signals during movement. First is to compare neural signals from each region in order to detect differences supporting their distinct roles. This approach has led to a model of M2 and M1 functioning within a hierarchy, with

M2 providing top-down signals to M1 related to movement planning<sup>4,5,16</sup>, timing<sup>50</sup>, and context<sup>3,50,51</sup>. In contrast, the second approach focuses on similarities between M1 and M2. Because M1 and M2 are both highly active during well-learned movements, many studies combine activity from both regions to understand cortical single-neuron and population dynamics during movement<sup>24,28,52</sup>. This allows analysis of a larger number of neurons with similar relationships to movement. These two approaches emphasizing the differences and similarities in M2 and M1 data are not mutually exclusive, but they are rarely<sup>5</sup> combined to understand how cross-area versus local signals contribute to network function.

Here we analyzed both the activity simultaneously shared across M1 and M2, and the otherwise unaccounted-for activity in each region. In any brain region, exclusively local activity is impossible to identify in-vivo, as this would require comprehensive recordings from the entire brain in order to account for activity shared with any other region. However, M1 and M2 have heavily overlapping inputs and outputs<sup>53</sup>, allowing us to consider the M1-M2 cross-area activity as encompassing most of each region's brain-wide shared activity. We found that the local dynamics in M2 and M1 had a clear temporal relationship, with M2 preceding M1, consistent with the pervasive model of top-down M2-to-M1 signals<sup>3,4</sup>. While this analysis quantified trial-by-trial timing in M2 and M1 local dynamics during early and late learning, it remains unknown whether more detailed analysis of M2 and M1 local dynamics would reveal additional trial-by-trial processes for top-down learning. However, as learning signals may initially be unpredictably related to many aspects of motor learning (timing, vigor, etc.) such work may be better accomplished in a dataset with more neurons from animals performing simpler behaviors.

Shared neural population dynamics have been identified within single brain regions<sup>7,11,28</sup>, between two hierarchical cortical regions<sup>5,16,32</sup>, and across sets of functionally diverse brain regions<sup>17,18,33</sup>. In many cases, shared dynamics are defined solely on functional relationships in neural activity, independent of behavior (but see<sup>54</sup>). This approach moves away from the view of fluctuations in neural signals as noise in a stochastic system. Instead, it frames neural activity as encompassing

a range of neural computations without apparent relation to behavior<sup>18,24,28,55</sup>. Despite this behaviorally-independent approach to understanding neural signals, one common thread in studies of cross-area activity is the dominance of movement signals within shared dynamics<sup>18,46</sup>. This privileged representation of movement emphasizes its importance as the final output of the nervous system, and suggests the possibility that movement signals have a role in shaping neural activity in a broad array of functional systems, including cognitive and motivational circuits. Here, we use learning as an intervention to change the behavioral salience of reach-to-grasp movements. In other words, we probe how learned behavioral salience of a given movement changes its representation in cross-area neural signals. We found that cross-area representations of similar movements were less modulated in early learning than late learning, consistent with a functional role for cross-area activity in amplifying neural signals for salient behaviors. This interpretation is consistent with a study of correlated variability between neurons in V4<sup>48</sup>, which found that the relationship between correlated variability and performance was the same for performance improvements driven by either attention or learning, two manipulations of behavioral salience. Thus, we posit that shared activity specifically modulates neural representations for salient behaviors.

Past work has proposed that the role of M2 is to provide top-down control and contextual information to M1<sup>4,51</sup>. Here, we provide insight into what such a signal might look like, and how it evolves with learning. In early learning, when behavior was exploratory and variable, high amplitude cross-area dynamics were less related to specific behavioral timepoints, and modulation of cross-area activity was weakly related to reaching. However, even at this early stage, reaches with more movement-modulated cross-area activity tended to have shorter durations. After learning, the relationship between cross-area activity modulation and behavior was amplified. Notably, the single-trial M1-M2 cross-area dynamics corresponding to similarly efficient, short duration reaches were not identical in early and late learning. This argues against the notion that pre-existing representations of efficient movements are selected through



learning<sup>56</sup>. Instead, our results support the idea that learning transforms and amplifies the neural signals for behaviors that are selected<sup>10</sup>. This finding also highlights the feasibility and importance of analyzing single-trials in order to understand highly variable behavioral states such as early learning.

Finally, the influence of cross-area dynamics on behavior appears to be causal, since M2 inactivation disrupted both M1 cross-area dynamics and reaching behavior, while local properties of M1 were less affected. Examining local activity during upstream inactivation provides a valuable approach to differentiating between activity dynamics generated locally and those from top-down influences. Such analyses are impossible in purely correlative studies, and, paired with same-day establishment of cross-area dynamics, demonstrate a novel approach to understanding how several patterns of covariance and information encoding overlap<sup>16,18,32,54</sup> and interact within functional neural systems<sup>5,32</sup>. Furthermore, we found that when M2 inputs are removed, M1 local shared variance does not change. This is important because there has been increasing concern that acute changes in input to an area can perturb behaviorally relevant local population relationships<sup>49,57</sup>. Importantly, rats do produce some successful reaches during both early learning and M2 inactivation, although they are less frequent and less efficient. This demonstrates that M1 can independently produce functional reach-to-grasp behavior, and suggests that top-down input from M2 is a learned signal, biasing M1 towards more effective behavior. This is concordant with long-standing models of top-down M1-M2 interactions during learning<sup>3</sup> and reinforces the view that, while M2 and M1 both represent movement, M2 is particularly important for learned, complex skills<sup>2,4,6,51,58-60</sup>.

Our results provide direct evidence that M1-M2 cross-area dynamics reflect task learning and single-trial skill performance. Knowledge of this phenomenon should help to better understand mechanisms of neural plasticity and functional properties of large-scale, hierarchical networks in the context of flexible learned behaviors.

## 1.5 Figures

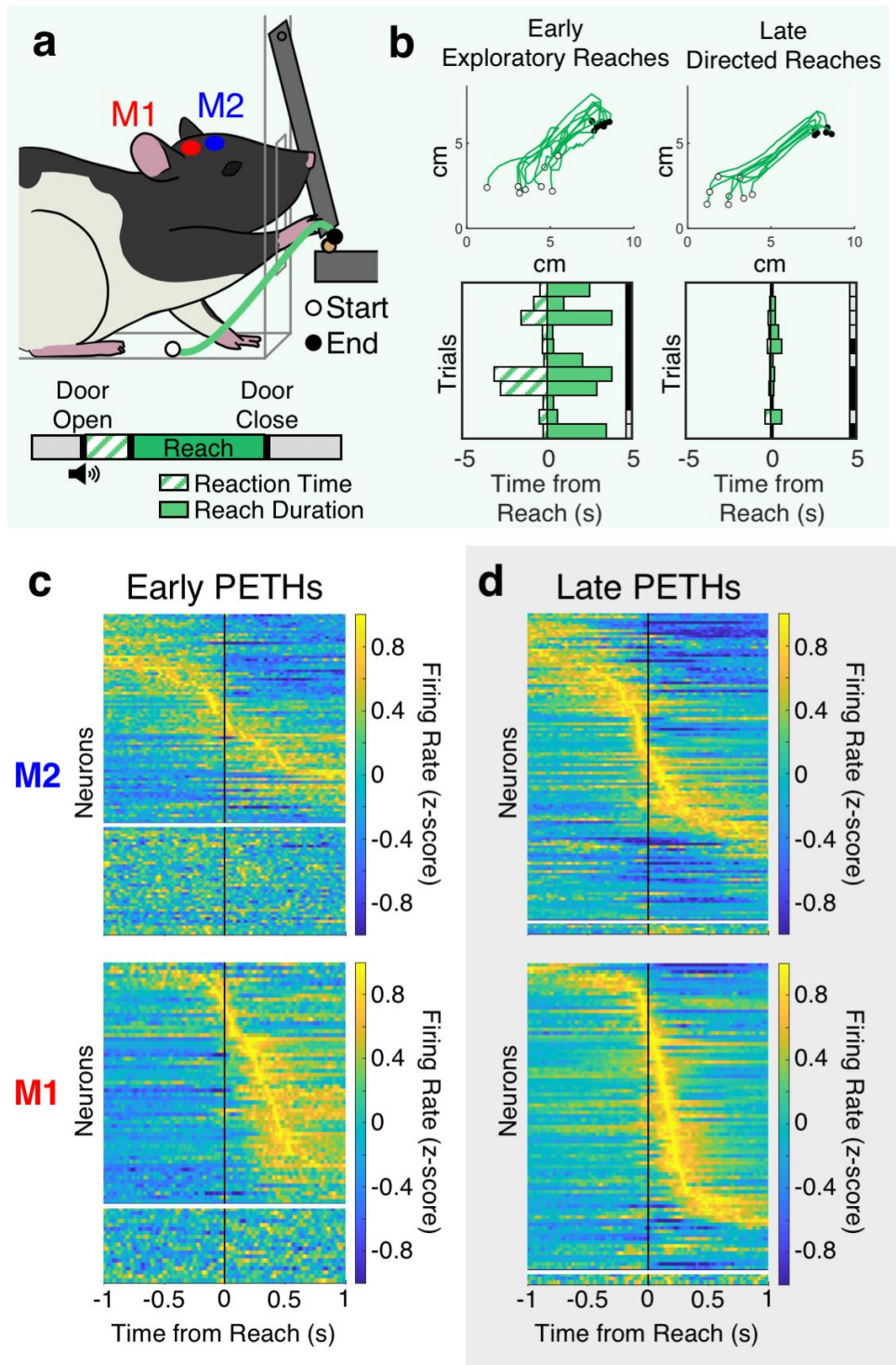
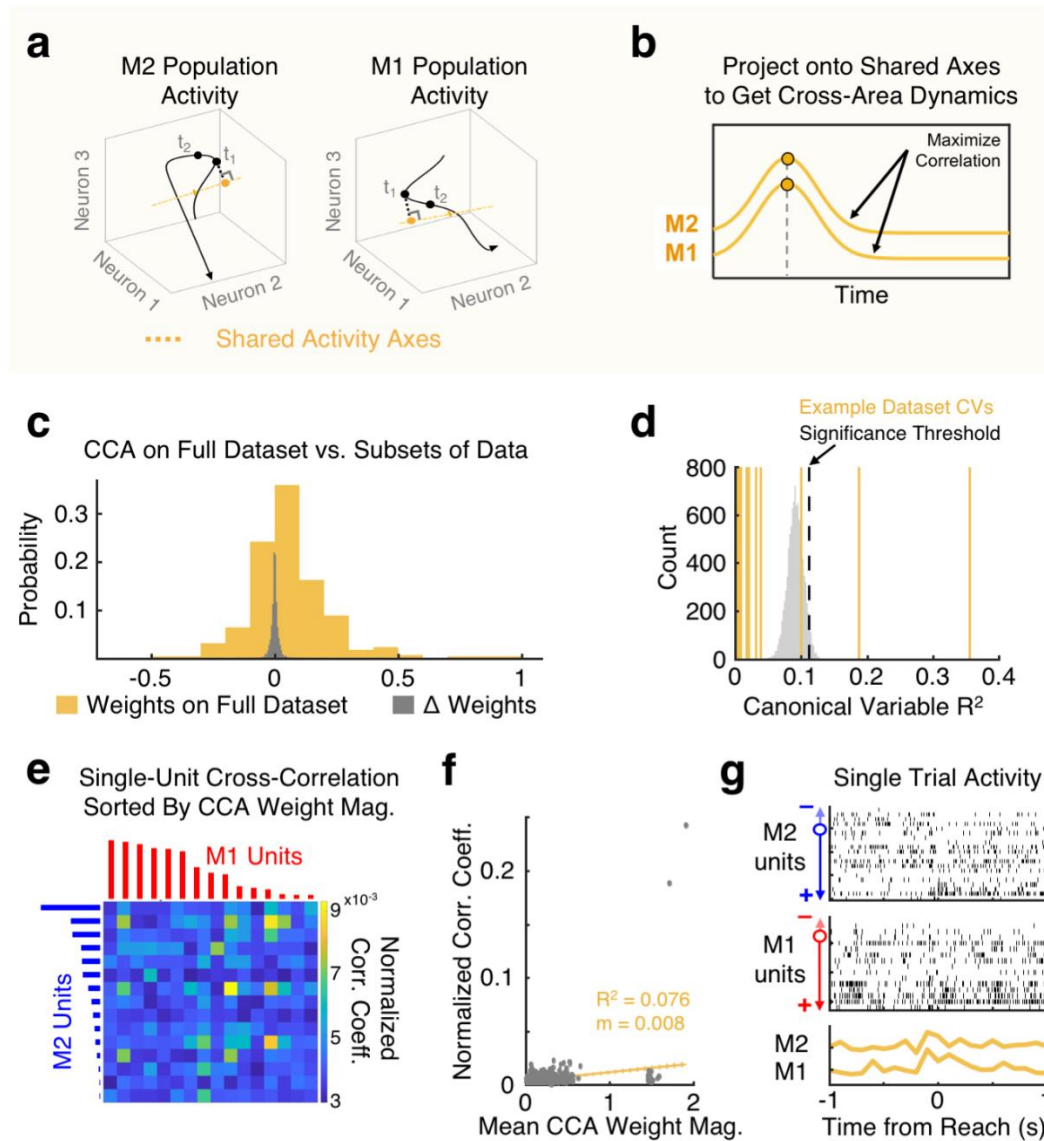


Figure 1.1 Motor skill learning is associated with increased cortical movement signals.

**(a)** (Top) Rats were trained to perform the reach-to-grasp task. (Bottom) Single-trial experimental paradigm. **(b)** Example reaches in early (left) and late (right) learning. (Top) Paw trajectories. White dot marks reach start position. Black dot marks reach end position. (Bottom) Example consecutive single-trial representations of reaction time (green striped bars) and reach duration (green bars). Right border of plot shows accuracy, with pellet retrieval success in grey and failure in black. **(c)** Population trial-averaged peri-event time histograms (PETHs) for premotor cortex (M2) (top) and primary motor cortex (M1) (bottom) units in early learning (n=5 rats). Significantly modulated neurons are shown above the white line, ordered by the time of their peak modulation. Non-significantly modulated neurons are shown below the white line, ordered by channel number. Firing rates are z-scored per-neuron for display only. **(d)** As in (c), but for late learning.



**Figure 1.2 Canonical Correlation Analysis identifies shared cross-area dynamics.**

(a) Illustration of method for identifying cross-area dynamics. A multi-dimensional neural space can be defined using the activity of each M2 (left) or M1 (right) neuron as one dimension. Neural trajectories are shown in black (artificial data). Canonical correlation analysis (CCA, yellow) is used to identify shared axes, such that when the neural trajectories are projected onto these axes, as shown in (b), the resulting trajectories, called cross-area dynamics, are maximally correlated between M2 and M1. The yellow dots for M1 and M2 illustrations are the projected values for the same timepoint in (a) and (b). (c) In yellow, distribution of CCA weights when fitting on the full datasets. In grey, distribution of weights differences from 10 subsamplings of each dataset (i.e. weight from subset – weight from full dataset). (d) Example identification of significant canonical variables (CVs, yellow lines), relative to trial-shuffled data (grey distribution,  $10^4$  shuffles). Significance threshold at 95<sup>th</sup> percentile of reference distribution. For this dataset, two CVs were significant. (e) Example comparison of CCA weight magnitude to single-neuron pairwise cross-correlations. M1 units (red) and M2 units (blue) are ordered by the absolute value of their CCA weight for the top CV. Color in the cross-correlogram indicates normalized peak correlation coefficient for

timelags between -200ms and +200ms. **(f)** Across animals, pairwise cross-correlation is correlated with mean CCA weight magnitude for that neuron pair. **(g)** CCA identifies moment-to-moment shared covariation patterns that may be hard to see by eye in single trial data. (Top) Population raster for an example trial in M2, where each row is a single neuron, sorted by CCA weight. (Middle) Population raster for the same trial in M1, sorted by CCA weight. (Bottom) The M2 and M1 cross-area dynamics for that same trial. The  $R^2$  between the M2 and M1 cross-area dynamics on this example trial is 0.3733.

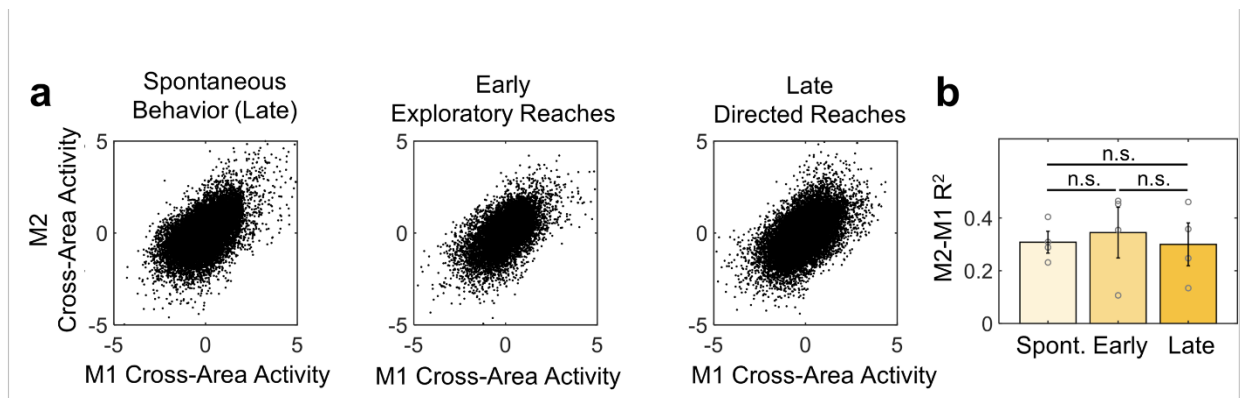


**Figure 1.3 Correlation of M1-M2 cross-area activity is stable across behaviors.**

**(a)** Correlation between M2 and M1 components of the M2-M1 cross-area population activity during (Left) spontaneous behavior, (Middle) early exploratory reaches, and (Right) late directed reaches. Spontaneous behavior was during the late learning day. Each data point is M2 and M1 data from a single 100ms bin ( $n = 4$  rats). **(b)** Quantification of (A) as crossvalidated  $R^2$  values. Bars show mean  $\pm$  SEM, open circles show data from individual animals ( $n=4$  rats). Correlation is not significantly different during spontaneous behavior, early reaches, and late reaches. Mixed-effect model, two-sided t-test, not adjusted for multiple comparisons.

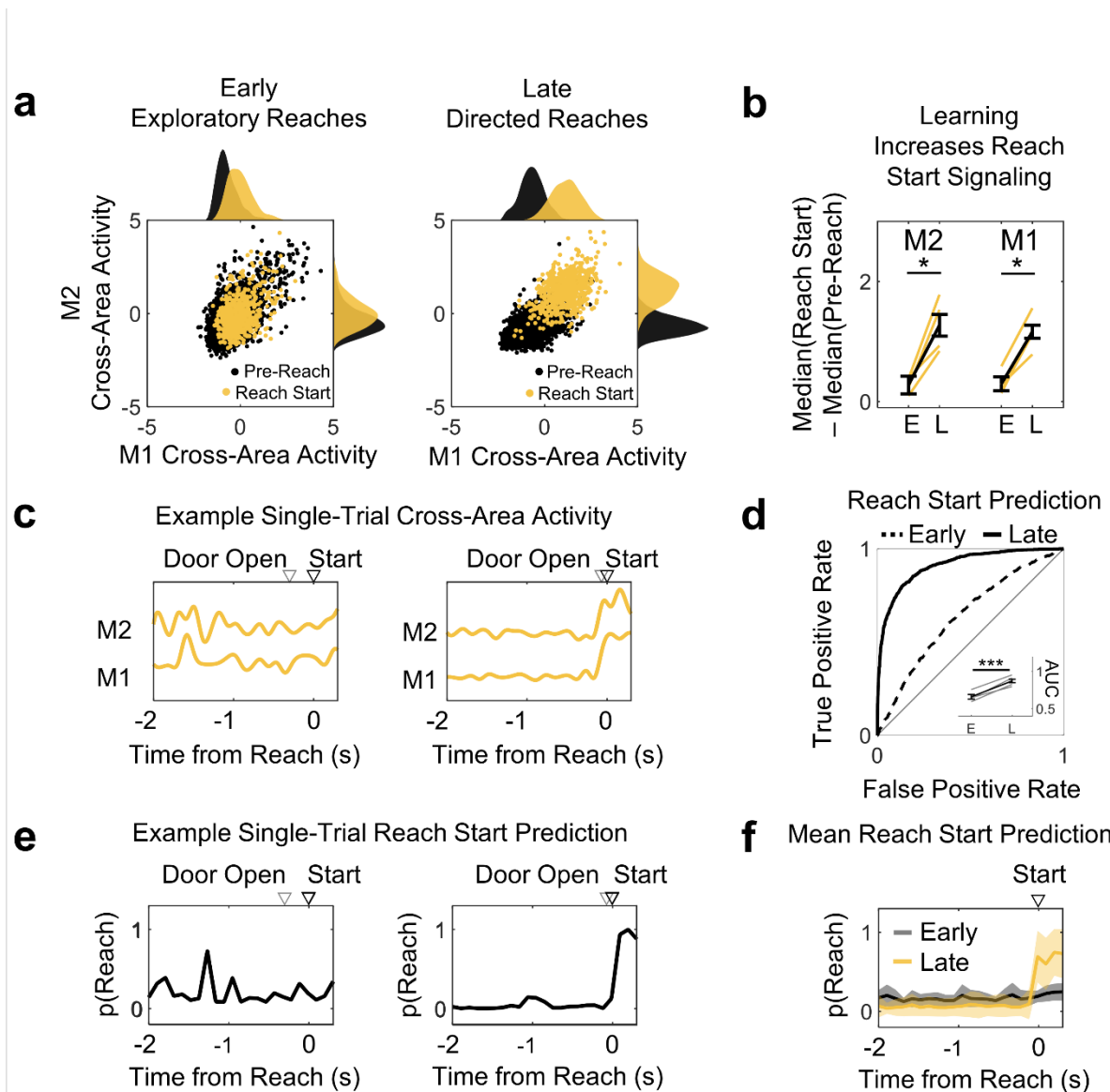


**Figure 1.4 Learning increases cross-area representation of reach initiation.**

**(a)** M2-M1 cross-area activity before reach and during reach initiation for example animal, in early (left) and late (right) learning. Probability density functions of M1 (top) and M2 (right). Pre-reach activity in black. Reach start activity in yellow. **(b)** Quantification of (a) as the difference between pre-reach and reach median activity during early and late learning for M2 ( $p=0.0017$ ) (left) and M1 ( $p=0.00053$ ) (right) cross-area activity. Yellow lines show values for individual animals, black line shows mean $\pm$ SEM,  $n=4$  rats. \*\*,  $p < 0.01$ ; \*\*\*,  $p < 0.0001$ ; two-sided t-statistics, not adjusted for multiple comparisons. **(c)** Example single-trial M2 and M1 cross-area activity before and during reach initiation. (Left) Early learning. (Right) Late learning. Time to reach initiation is indicated by triangles marking door opening (grey open triangle) and reach start (black open triangle). **(d)** ROC analysis of detection of reach initiation from M2 and M1 cross-area activity using logistic regression (example animal). (Inset) Difference in reach detection with learning quantified as the area under the curve (AUC) for all animals ( $p=6.63 \times 10^{-5}$ ). Grey lines show values for individual animals, black lines show mean $\pm$ SEM,  $n=4$  rats. \*\*\*\*,  $p < 0.0001$ . two-sided t-statistic, not adjusted for multiple comparisons. **(e)** Example single-trial prediction of reach initiation using the models

built in (d), same trials as (c). (Left) Early learning. (Right) Late learning. **(f)** Comparison of mean prediction of reach initiation during early (grey) and late (yellow) learning for example animal. Shaded region shows SEM, n=4 rats.



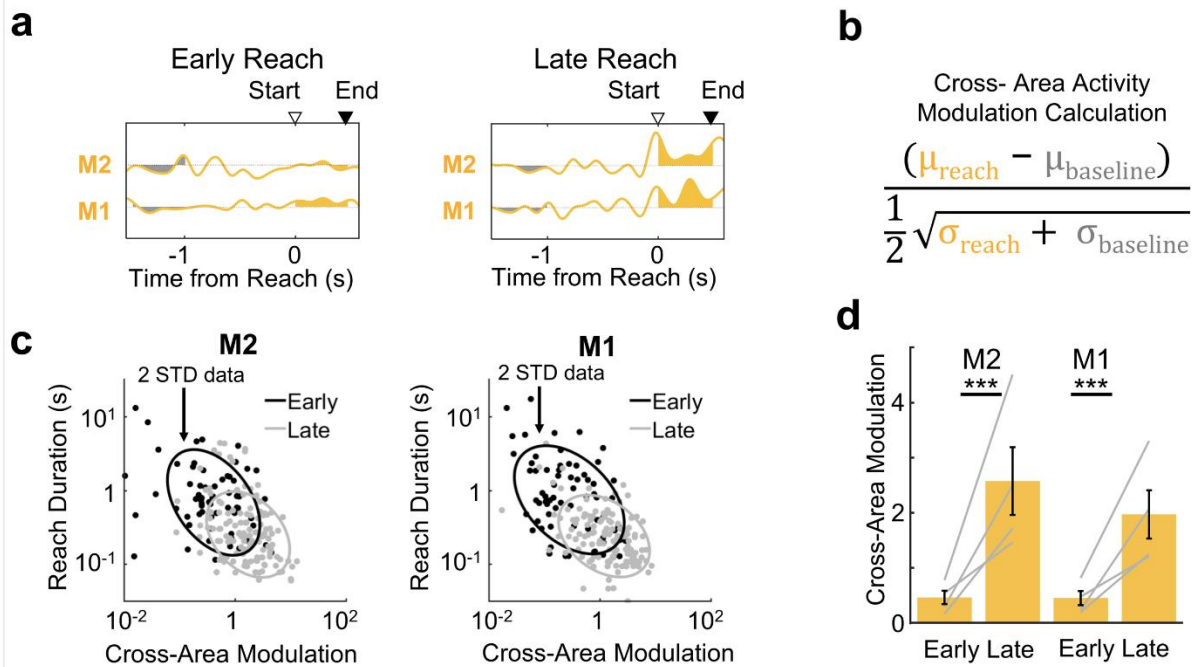


**Figure 1.5 Learning amplifies cross-area representations of reach duration.**

(a) Example single trial M2 and M1 cross-area activity in early (left) and late (right) learning. Reach duration is indicated by triangles marking reach start (open triangle) and reach end (filled triangle). Single-trial baseline modulation in grey, reach modulation in yellow. (b) Equation for calculating cross-area activity (CA) modulation (see Methods). (c) Single-trial CA-modulation predicts single-trial reach duration. Single-trial CA-modulation for M2 (left) and M1 (right) cross-area activity is plotted against single trial reach duration. Points show randomly subselected trials from early (black) and late learning (grey), with ellipses fitted to 2 standard deviations of the full datasets. All trials were used for quantification. (d) CA-modulation increases in both M1 and M2 with learning. Grey lines, also marked by black open circles, show values for individual animals, bars show mean  $\pm$  std. dev.,  $n=4$  rats. \*\*\*\*,  $p<0.0001$ . one-sided hierarchical bootstraps, not adjusted for multiple comparisons.

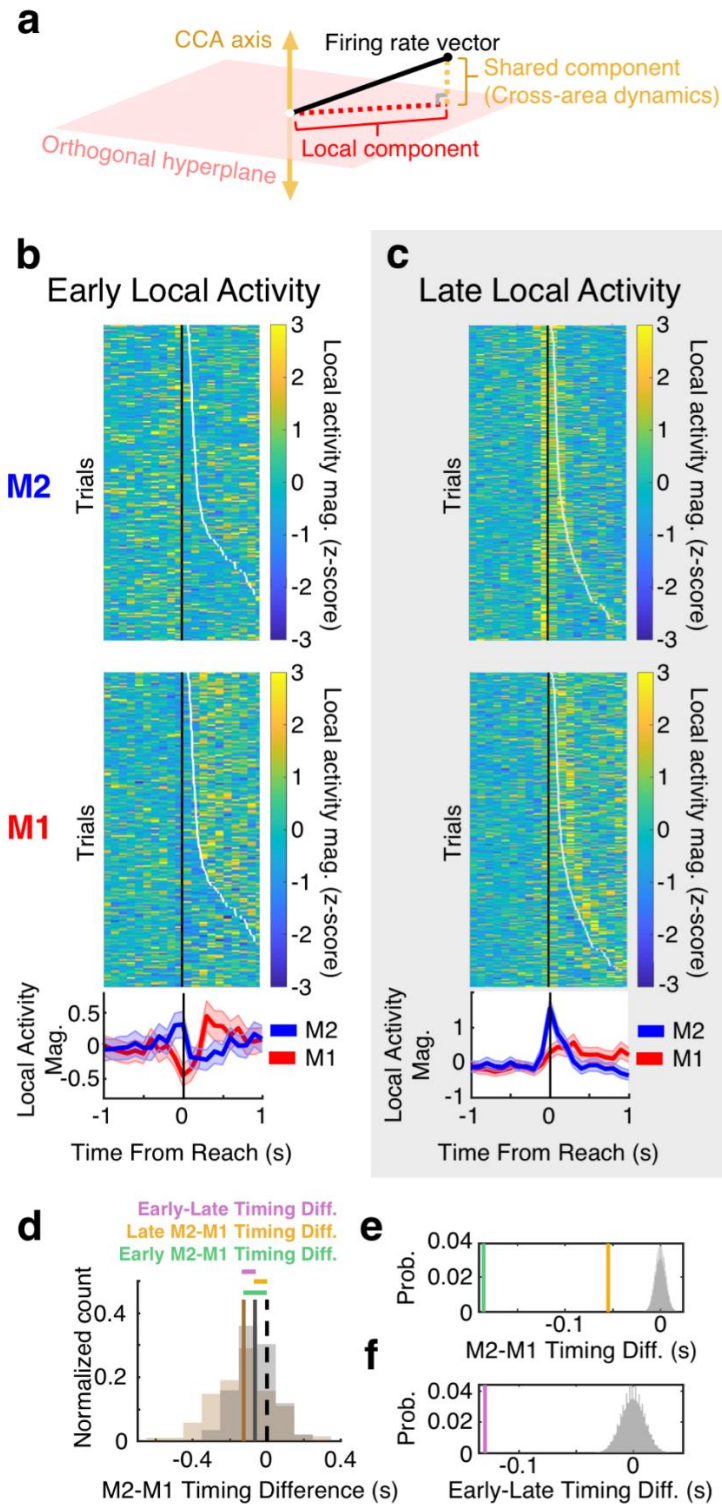


**Figure 1.6 Local signals support a M2 to M1 hierarchy.**

(a) Illustration of approach to identifying local activity using artificial data. Black line represents a population firing rate for a single time bin. Population firing was projected onto a shared axis

defined by CCA (solid yellow line) to obtain the cross-area signal (dotted yellow line), and onto the hyperplane orthogonal to the CCA subspace (light red plane), to obtain the local signal (dotted red line). **(b)** Example animal local activity in early learning (z-scored). (Top) Single trial local activity trajectories for M2. Black dots indicate reach onset and white dots indicate transition to grasp on each trial. (Middle) Single trial local activity trajectories for M1. (Bottom) Mean local activity trajectories for M2 (blue) and M1 (red). Shaded regions show SEM, n=211 trials. **(c)** As in (b), but for late learning, n=297 trials. **(d)** Distributions of timing differences between median timing of single-trial M2 and M1 local activity in early (brown) and late learning (grey) (from example animal in b, c). Black dotted line indicates zero lag in M2-M1 median timing of local activity. **(e)** Quantification of M2-M1 timing differences (n=4 rats). In grey, permutation-based reference distribution of timing differences with data randomly assigned to M1 or M2 ( $10^5$  permutations). M2 local activity significantly preceded M1 activity in early (green) and late (orange) learning. **(f)** Quantification of tighter coupling between M2 and M1 local activity from early to late learning (n=4 rats). In grey, permutation-based reference distribution of mean difference in M2-M1 timing coupling with M2-M1 timing differences randomly assigned to early or late learning ( $10^5$  permutations). The true difference in M2-M1 coupling between early and late learning (purple line) was more negative than any of the reference values, indicating that the time lag between M2 local activity and M1 local activity significantly decreased with learning.

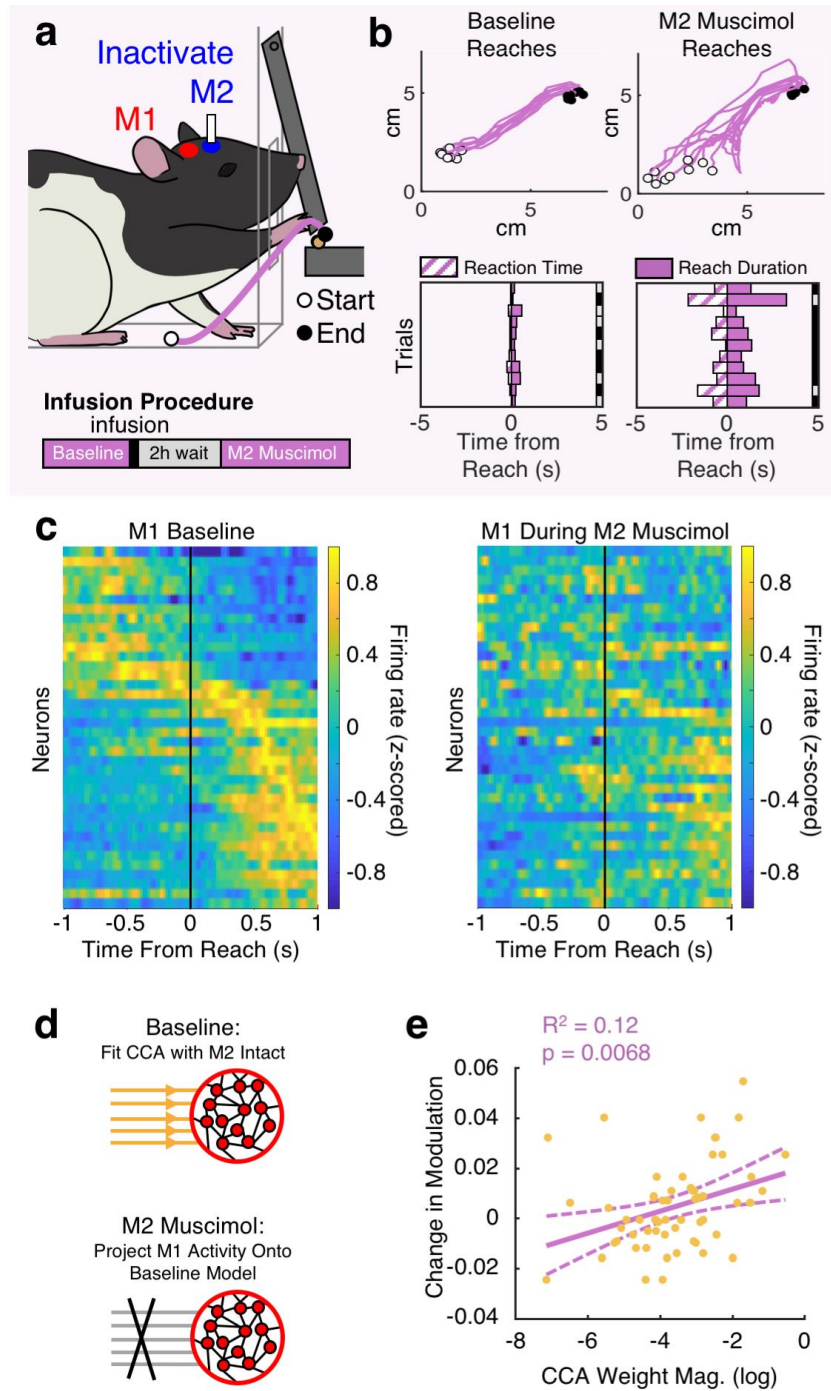


**Figure 1.7 M2 inhibition disrupts learned reach behavior and M1 single-unit movement modulation.**

(a) Rats previously trained on the reach-to-grasp task were infused with muscimol in M2. (Bottom) Experimental paradigm for evaluation of reach behavior during M2 inactivation (see Methods). (b) (Top) Example reach trajectories during baseline (left) and M2 Muscimol (right) trials. White dot marks reach start position. Black dot marks reach end position. (Bottom) Example consecutive single-trial representations of reaction time (purple striped bars) and reach duration (purple bars)

for baseline (left) and M2 muscimol inactivation (right). Right border of plot shows accuracy, with success in grey and failure in black. **(c)** Population PETH for M1 units across  $n = 3$  rats during baseline (left) and muscimol inactivation (right). Each neuron's PETH was tested for trial modulation during the baseline period using a circular shuffle test. Only neurons that were significantly modulated during the baseline period are shown, ordered by their peak time during the baseline period in both plots. Firing rates are z-scored per-neuron. **(d)** Due to the same-day inactivation paradigm, CCA weights could be computed for the baseline session, and then used with the M1 data recorded during the M2 muscimol session. **(e)** Across animals, for each neuron (yellow dot), the change in task modulation between baseline and M2 inactivation was computed (baseline – M2 muscimol), and compared to that neuron's absolute value CCA weight from the baseline period. The regression fit (purple) shows that neurons with higher magnitude CCA weights tended to have larger drops in modulation. Two-sided t-statistic, not adjusted for multiple comparisons.

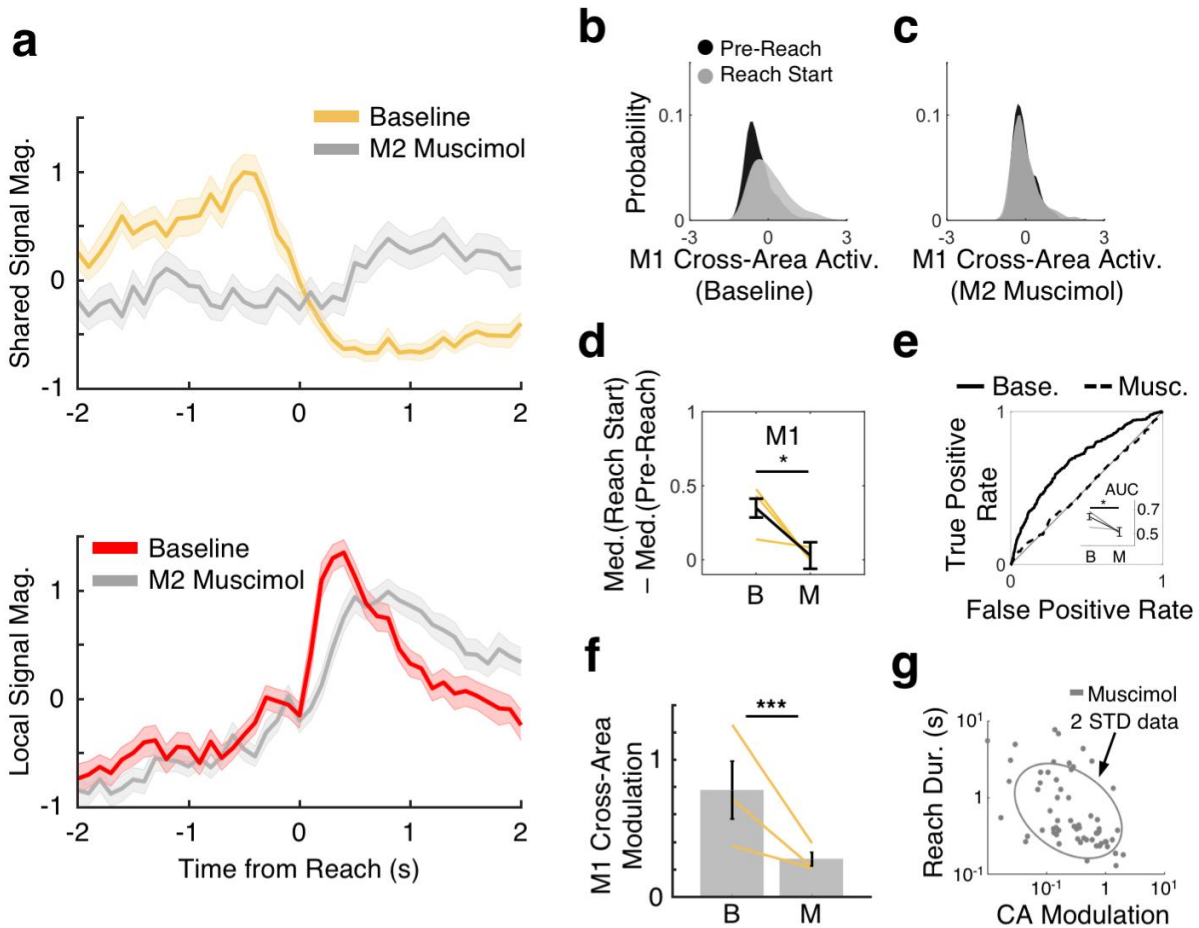


**Figure 1.8 M2 inhibition disrupts M1 cross-area movement modulation.**

**(a)** (Top) Comparison of z-scored, trial-averaged M1 cross-area activity magnitudes during baseline (yellow) and M2 inactivation (grey) for one example animal. M1 CCA weights were defined during baseline period and used to calculate cross-area activity during both baseline and M2 inactivation trials. Solid line shows mean and shaded region shows standard error of the mean. (Bottom) As above, but for M1 local signals during baseline (red) and M2 inactivation (grey), suggesting that local signals are not as impacted by M2 inactivation.  $n=91$  trials for Baseline,  $n=92$  trials for M2 Muscimol **(b)** Neural activity from M1 cross-area subspace before (black) and during (grey) reach initiation during baseline block. **(c)** As in (b), but during M2 inactivation trials. **(d)** Quantification of (b,c) as the difference between median pre-reach and reach activity during baseline and M2 inactivation trials in M1 cross-area subspace. Yellow lines show data from individual animals, black line shows mean  $\pm$  SEM,  $n=3$  rats.  $p=0.02$ . \*,  $p<0.05$ . two-sided t-statistic, not adjusted for multiple comparisons. **(e)** Detection of reach initiation from M1 cross-area subspace activity using ROC analysis on logistic regression model (example animal). (Inset) Difference in reach detection quantified as the area under the curve (AOC) for all animals. Grey lines show data from individual animals; black lines show mean  $\pm$  SEM,  $n=3$  rats.  $p=0.02$ . \*,  $p<0.05$ . two-sided t-statistic, not adjusted for multiple comparisons. **(f)** M1 cross-area activity (CA) modulation decreases significantly with M2 inactivation. Yellow lines, also marked with black open circles, show data from individual animals, bars show mean  $\pm$  std dev.,  $n=3$  rats. \*\*\*\*,  $p<0.0001$ . one-sided hierarchical bootstrap, not adjusted for multiple comparisons. **(g)** Single-trial M1 CA-modulation predicts single-trial reach duration even during M2 inactivation. Plot shows random subsampling of trials across animals, all trials were used in quantification.

## 1.6 Methods

### 1.6.1 Animal Care

All procedures were in accordance with protocols approved by the Institutional Animal Care and Use Committee at the San Francisco Veterans Affairs Medical Center. Adult male Long Evans rats (n=10, 250–400 g; Charles River Laboratories) were housed in a 12-h/12-h light–dark cycle. All experiments were done during the light cycles. Rats were housed in groups of 2 animals prior to surgery and individually after surgery.

### 1.6.2 Surgery

All surgical procedures were performed using a sterile technique under 2–4% isoflurane. Surgery involved cleaning and exposure of the skull, preparation of the skull surface (using cyanoacrylate) and then implantation of the skull screws for overall headstage stability. Reference screws were implanted posterior to lambda and ipsilateral to the neural recordings. For experiments involving physiological recordings, craniotomy and durectomy were performed, followed by implantation of the neural probes. For experiments involving only infusions, burr holes were drilled in the appropriate locations, followed by implantation of the cannulas. Postoperative recovery regimen included the administration of 0.02 mg kg<sup>-1</sup> buprenorphine for 2 days, and 0.2 mg kg<sup>-1</sup> meloxicam, 0.5 mg kg<sup>-1</sup> dexamethasone and 15 mg kg<sup>-1</sup> trimethoprim sulfadiazine for 5 days. All animals were allowed to recover for 1 week prior to further behavioral training.

### 1.6.3 Electrode array and cannula implants

Long-Evans hooded rats were implanted with two 32-channel tungsten wire probes (TDT or Innovative Neurophysiology), one each in M1 (+0.5 AP, +3.5 ML, -1.5 DV)<sup>27,38,44,61</sup> and M2 (+4.0–4.5 AP, +1.5 ML, -1.5 DV)<sup>61,62</sup>, contralateral to reaching arm (see Supplementary Table 2). Infusion cannulas were implanted in M2 (+4.0 AP, +1.5 ML, -1.5 DV) for infusion-only animals.

For rats with both M2 electrode arrays and cannulas, the cannula was attached to the lateral side of the electrode array prior to surgery.

#### 1.6.4 Functional ICMS Mapping

Two additional animals were used to confirm that forelimb movement could be evoked from both M1 and M2 (see Supplementary Figure 1). For the two mapping procedures, animals were initially anesthetized with a mixture of ketamine hydrochloride (100 mg kg<sup>-1</sup>) and xylazine (16.67 mg kg<sup>-1</sup>) delivered intraperitoneally. Supplementary 0.5-1 cc doses of the mixture were provided as needed, based on toe-pinch response. 32-channel tungsten microwire electrode arrays (Tucker Davis Technologies, ~50 k $\Omega$  input impedance at 1000 Hz) were implanted in M1 (n=1) and M2 (n=1), at a depth of 1500  $\mu$ m, targeting cortical layer V.

Consistent with prior studies<sup>63,64</sup>, we used triplet biphasic trains of 200  $\mu$ s per phase (100  $\mu$ s inter-phase interval, 333 Hz triplet) were delivered at each electrode using a constant current stimulator (IZ2, TDT) controlled by a custom Synapse program (TDT). These trains were delivered with 60-150  $\mu$ A amplitude<sup>64,65</sup>. Movements were evoked across large portions of the M1 and M2 arrays (Supplementary Figure 1). Animals were placed in a prone position such that the contralateral forelimb remained free. Stimulation was delivered at each electrode in the array with video recording at 20 frames per second. Movement, if elicited, was visible immediately after onset of stimulation, with greater amplitude of movement at higher currents and frequencies.

#### 1.6.5 Pharmacological infusions

Rats were anesthetized with 2% isoflurane before infusions. We injected 0.5 - 1  $\mu$ L (1  $\mu$ g  $\mu$ L<sup>-1</sup>)<sup>44,60</sup> of the GABA receptor agonist muscimol into contralateral M2 (infusion rate: 1nL min<sup>-1</sup>) through a chronically implanted cannula using a Hamilton infusion syringe. The infused volumes were titrated for each animal. We first started with the larger volume (1  $\mu$ L). If the animal was unable to reach within 2 hours, we downscaled to the smaller volume (0.5  $\mu$ L). The infusion syringe was left



in place for at least 5 min post-infusion. Rats were allowed to recover in their home cages for 2 hours before starting behavioral testing.

#### 1.6.6 Histology

Final placement of the electrodes was monitored online based on implantation depth and verified histologically at the end of the experiments. Rats were anesthetized with isoflurane and transcardially perfused with 0.9% sodium chloride, followed by 4% formaldehyde. The harvested brains were post-fixed for 24 h and immersed in 20% sucrose for 2 days. Coronal cryostat sections (40- $\mu$ m thickness) were mounted with permount solution (Fisher Scientific) on superfrosted coated slides (Fisher Scientific). Images of a whole section were taken by a HP scanner, and microscope images were taken by a Zeiss microscope.

#### 1.6.7 Behavioral training

We used an automated behavior paradigm to train rats to perform dexterous reach-to-grasp movements<sup>36</sup>. Rats learn to reach through a narrow slot to grasp and retrieve a 45 mg pellet from a shallow dish (i.e. pellet holder) placed ~1.5 cm outside the behavioral box<sup>35</sup>. Prior to implantation, rats were handled and habituated to the behavioral box for at least one day, then manually prompted to reach for a pellet 10-30 times to determine handedness. Handedness was determined when rats reached with the same hand for  $\geq 70\%$  of at least 10 test trials. The start of each trial was signaled with a tone and the opening of a door allowing access to the pellet. Trials ended when the door was closed, which was triggered either by the pellet being dislodged from the pellet holder, or, if this did not occur, ~15s after door opening.

#### 1.6.8 Behavioral training for learning animals

Once handedness was determined, rats were implanted with neural probes (see Surgery). For two days before behavioral training, rats were food restricted, followed by feeding animals a fixed amount during the course of training. During behavioral training, rats were placed in an automated reach box and completed 38-300 trials per day. The early learning training day was the first day

on which the rat completed at least 30 trials. The late learning training day was the second consecutive day on which the rat performed with at least 45% success rate (see Supplementary Table 1).

#### 1.6.9 Behavioral training for M2 inactivation animals

Once handedness was determined, rats were trained until their success rate reached a plateau (at least 2 consecutive days with performance above 45% and > 100 completed trials/day), after which they were implanted with infusion cannulas alone (n=3 rats), or with infusion cannulas and electrodes (n=3 rats) (see Surgery). Rats were allowed at least a week of recovery after surgery before beginning behavioral testing. Rats were re-trained until plateau performance (>2 consecutive days with performance above 40%). On M2 inactivation days, rats performed ~100 reach trials before receiving pharmacological infusions. After 2 hours of rest post-infusion, rats were re-tested for ~100 trials (see Supplementary Table 1).

#### 1.6.10 Behavioral analysis

Rat behavior was video recorded using a side view camera (30 - 100 Hz, see Supplementary Table 1) positioned outside the behavioral box, perpendicular to the main direction of movement. Each rat's reach hand was painted with an orange marker at the start of each day. Reach videos were viewed and semi-automatically scored to obtain trial success, hand position, time points for reach onset, and grasp onset. To characterize motor performance, we quantified reach duration, reaction time, maximum movement speed, and pellet retrieval success for each trial. Percent reach success is the percent of trials on which the pellet was retrieved during a single day of training, excluding trials in which the rat did not dislodge the pellet from the holder or displayed abnormal behavior (i.e. licking, reaching with the wrong hand). Reach duration for each trial was defined as the time from the start of reach to onset of grasping or when the paw first touched the pellet if no grasping occurred on that trial. Reaction time was defined as the time between the

door open cue and movement onset – note that since the rat was freely moving in the behavior box, reaction time is affected by both the rat's position and attention at the time of the cue.

#### 1.6.11 Electrophysiology data collection

We recorded extracellular neural activity using tungsten microwire electrode arrays (MEAs, n=8 rats, TDT or Innovative Neurophysiology). We recorded spike and LFP activity using a 128-channel TDT-RZ2 system (TDT). Spike data was sampled at 24,414 Hz and LFP data at 1,018 Hz. Analog headstages with a unity gain and high impedance (~1 GΩ) were used. Snippets of data that crossed a high signal-to noise threshold (4 standard deviations away from the mean) were time-stamped as events, and waveforms for each event were peak aligned. MEA recordings were sorted offline using either superparamagnetic clustering program (WaveClus66) or a density-based clustering algorithm (Mountainsort67). Clusters interpreted to be noise were discarded, but multi-units were kept for analysis. Trial-related timestamps (i.e., trial onset, trial completion, removal of pellet from pellet holder, and timing of video frames) were sent to the RZ2 analog input channel using an Arduino digital board and synchronized to neural data.

#### 1.6.12 Cross-area neural subspace and population dynamics

Shared cross-area subspaces were defined using Canonical Correlation Analysis (CCA), which identifies maximally correlated linear combinations between two groups of variables. Neural data in M2 and M1 was binned at 100ms, and data from -1s to +1s surrounding time of grasp onset was concatenated across trials and mean subtracted. CCA models were fit using the MATLAB function `canoncorr`. For analyses and figures involving times outside the -1s to +1s window around grasp, data from other time periods was projected onto these models.

CCA produces as many canonical variables (CVs) as the number of neurons in the smaller population (e.g., if there are 30 M2 neurons and 20 M1 neurons, then CCA will fit 20 CVs). The  $R^2$  values of each CV were computed using 10-fold cross-validation, and the  $R^2$  values reported in Figure 3b are for the top CV only. The cross-validation procedure used to compute the  $R^2$

values is as follows: The full dataset was randomly partitioned into 10 equal folds (ignoring trial structure, i.e. timepoints from the same trial could be assigned to different folds). Then, ten different times, one fold was assigned to be the test data and the other nine to be the training data. CCA models were fit to the training dataset. The test data was then projected onto the training model, and  $R^2$  values were computed between the M1 and M2 projections for each CV. The  $R^2$  values reported for each CV are the average across all 10 combinations of testing/training data, and are intended to measure how well the models generalize to held-out data. Other than when reporting  $R^2$  values (Figures 2d, 3b; Supplementary Figure 3a,d), or comparing weights fit on different subsets of data (Figure 2c), the CCA models used were those fit to the full datasets. To determine which CVs were significant, the  $R^2$  of each CV was compared to a bootstrap distribution made of the  $R^2$  of the top CV from CCA models fit to trial-shuffled data ( $10^4$  shuffles). Specifically, before fitting CCA, trials from M2 were concatenated in the order in which they occurred, while trials from M1 were randomly permuted prior to concatenation. This method maintains local neural patterns, as well as neural modulation which could be attributed to coarse behavioral variables that do not vary by trial, while breaking moment-by-moment relationships between the regions. Therefore, computing CCA on trial shuffled data provides a floor for the degree of correlation expected from the fact that many neurons in both regions have firing rate fluctuations around the time of grasp. A CV was considered significant if its  $R^2$  was greater than the 95<sup>th</sup> percentile of the bootstrap distribution. One animal was eliminated from further analysis because its early dataset had no significant CVs. All other datasets had 1 to 3 significant CVs. For evaluating cross-area signals (Figures 2-5, 7e, 8b-g; Supplementary Figures 3a-c, 4), only the top CV was used, as this provided a consistent dimensionality across datasets, and a signal with both magnitude and sign.

To test whether results were unique to the 100ms bin width, CCA models were also fit to data binned at 75ms and 50ms (Supplementary Figure 3). Qualitatively, CCA trajectories fit to smaller bin widths appeared noisier but had peaks at similar timepoints as the 100ms models. There was

no significant difference in  $R^2$  between the 100ms bin width and the 75ms bin width, but the 50ms bin width had a significantly smaller  $R^2$  than either the 100ms or 75ms models (two-sided hierarchical bootstrap,  $10^4$  shuffles;  $0.27 \pm 0.047$  for 100ms models,  $0.28 \pm 0.046$  for 75ms models,  $0.22 \pm 0.037$  for 50ms models;  $p=0.83$  for 100ms vs 75ms;  $p=0.016$  for 100ms vs 50ms;  $p<0.0002$  for 75ms vs 50ms;  $n=160$   $R^2$  values from 8 datasets each with 10-fold cross-validation for each condition), suggesting that larger bin sizes are needed to capture the cross-area signal. We also compared the angle between the top CV for models fit to 100ms, 75ms, and 50ms data (hierarchical bootstrap,  $10^4$  shuffles;  $13.74^\circ \pm 2.40$  for angle between 100ms model weights and 75ms model weights,  $20.04^\circ \pm 3.05$  for 100ms vs 50ms,  $18.22^\circ \pm 2.62$  for 75ms vs 50ms;  $n=8$  models per binwidth, each fit to early or late data from 4 rats). In M2, we found that the angle between the 100ms and 75ms models was significantly smaller than both the angle between the 100ms and 50ms models ( $p=0.0094$ ) and the angle between the 75ms and 50ms models ( $p=0.0041$ ). In M1, we found that the angle between the 100ms and 75ms models was significantly smaller than the angle between the 100ms and 50ms models ( $p=0.00089$ ) but not significantly smaller than the angle between the 75ms and 50ms models ( $p=0.097$ ). For all models, all bootstrap samples were less than  $45^\circ$ , suggesting that models fit to different binwidths identified similar patterns of covariation. Additionally, we fit CCA models for all three binwidths at timelags from -500ms to +500ms, and found that for 6 of 8 datasets, using 100ms bins with no lag resulted in the highest  $R^2$  values.

#### 1.6.13 Normalized cross-correlation

Normalized cross-correlations were calculated as the peak correlation coefficient for timelags between -200ms and +200ms minus the mean correlation coefficient for all timelags in that range.

#### 1.6.14 Local neural subspace and population dynamics

Local signals were computed by projection onto the hyperplane orthogonal to the cross-area subspace defined by CCA. For comparison to local signals (Figures 6, 8a), all significant CVs

were used to define the cross-area subspace, so that the local signal would be orthogonal to all significantly correlated cross-area activity. This meant that dimensionality varied across datasets, and the signals analyzed were the magnitudes of the projections onto the cross-area and local subspaces.

#### 1.6.15 Reach start decoding

To calculate the difference in cross-area subspace (CS) activity before reach initiation versus during reach initiation, we defined a pre-reach period as -2s to -0.1s before reach initiation and a reach initiation period from -0.1s to +0.3s surrounding reach initiation. CS activity from each of these periods was concatenated across trials to then calculate the median CS activity value. The difference between median CS activity during pre-reach and reach initiation was calculated for each animal.

For reach start prediction, activity from pre-reach and reach initiation was labelled as 0 or 1, respectively, which was then used as the response values to train a logistic regression model using the MATLAB function *fitglm*. The probability that CS activity values corresponded to a timepoint during reach initiation was returned as scores. We then used these scores to compute the receiver operating characteristic (ROC) curve of the classification results using the MATLAB function *perfcurve*. The area under the curve (AUC) was returned for each animal, and these values were used in mixed effect modeling to detect difference in pre-reach versus reach initiation activity during early versus late learning, and baseline versus muscimol behavior.

The logistic regression model was used to calculate the probability of reach initiation based on CS activity on single trials. We calculate the single-trial difference in the mean predicted probability of reach initiation during the pre-reach versus reach initiation periods. We compared this difference using all trials in early versus late learning, and baseline versus muscimol behavior. We plotted the median probability of reach initiation across trials aligned to reach initiation.

### 1.6.16 Neural reach modulation

Single-trial neural reach modulation of the first canonical variable from CCA was calculated using the signal processing  $d'$  (d-prime) signal sensitivity metric defined by the equation below<sup>68</sup>, where  $\mu$  indicates the mean and  $\sigma$  indicates the standard deviation of the signal. For each trial, the reach period was defined as -0.1 s before reach onset to + 0.1s after grasp onset; the baseline period was defined as a length of time equal to the reach period, ending 1s before the start of the reach period. To produce single-trial normalization, the median value from the baseline period was subtracted from both the movement signal and the baseline signal before calculating the single-trial modulation value ( $d'$ ), as below.

$$(1) \quad d' = \frac{\mu_{\text{reach}} - \mu_{\text{baseline}}}{\frac{1}{2}\sqrt{\sigma_{\text{reach}} + \sigma_{\text{baseline}}}}$$

### 1.6.17 Mean local covariance

Each neuron's shared over total variance was calculated as in Athalye et al., 2017<sup>7</sup> using code adapted from Yu et al., 2009<sup>69</sup>. Briefly, we used the factor analysis function *fastfa* to model each neuron's firing rate distribution as the sum of three elements: (1) a mean rate; (2) private variance from neuron-specific firing fluctuations not shared by the population being analyzed, and (3) shared variance driven by population signals (factors). For each neuron, shared over total variance is calculated as shared variance / (shared variance + private variance).

Using the *fastfa* function, we represent a column vector of N neurons' mean firing rates as  $\mu$  (rank N). Each neuron's private variance is an element of the diagonal matrix  $\Sigma^{\text{private}}$  (rank N x N). Each neuron's weights for creating k shared population signals are rows in the matrix U (rank N x k, where k < N). The population covariance matrix is calculated as  $\Sigma^{\text{shared}} = UUT$  (rank N x N), with the diagonal values representing the shared variance for each neuron. Therefore, the matrix of total variance for the population of neurons is represented as  $\Sigma^{\text{total}} = \Sigma^{\text{shared}} + \Sigma^{\text{private}}$ . Neuron i's

shared over total variance is  $\sum \text{shared}_{ii} / \sum \text{total}_{iii}$ . We chose to use  $k = 3$  latent shared variables using the leave-one-out strategy outlined in Yu et al., 2009<sup>69</sup>.

#### 1.6.18 Subspace alignment

The alignment between the subspaces defined by CCA and by PCA (Supplementary Figure 4) was calculated using the MATLAB function `subspace`. Weights for the top 3 PCs were included for the local subspace. Weights for only the top 1 CV were included for the shared subspace.

#### 1.6.19 Statistical analysis

Unless stated otherwise, all measurements were taken from distinct samples. We did not adjust for multiple comparisons. Normality was explicitly tested via Anderson-Darling test. For distributions that were non-normal, statistical testing was done using hierarchical bootstrap analysis, which is non-parametric<sup>70</sup> and p-values were computed as a one-sided test unless otherwise noted. For hierarchical bootstrap tests, statistics are written as mean  $\pm$  standard deviation, and data was clustered by rat identity and, where relevant, condition (early vs. late, or baseline vs. infusion). Unless otherwise noted,  $10^4$  permutations were used. For one-sided tests the lowest obtainable p-value was 0.0001, and for two-sided tests the lowest p-value obtainable was 0.0002; therefore, some p-values are reported as  $p < 0.0001$  or  $p < 0.0002$  rather than precise values. When distributions were normal, we used linear mixed effect modeling by the MATLAB function `fitlme`. For mixed effect models, statistics are written as mean  $\pm$  standard error of the mean, and rat identity was always considered a random effect. When calculating changes in neural reach modulation between early and late learning, we included reach duration as a covariate to control for changes in reach duration between early and late learning. When calculating the relationship between neural reach modulation (log) and reach duration (log), only trials with positive neural modulation were included, and we included learning stage (early vs. late) as a covariate.



**Data availability:** The data sets generated and analyzed in the current study are available from the corresponding author on reasonable request.

**Code availability:** The custom data analysis code created in MATLAB, and custom recording programs in OpenX and Synapse (TDT) are available from the corresponding author on reasonable request.

**Acknowledgments:** We thank Seok-Jon Won for assistance with perfusions and imaging. We also thank C. Campillo Rodriguez for assistance with histology; N. Hoglen, L. Tian, P. Khanna, and P. Shirvalkar for providing comments on the manuscript. **Funding:** This work was supported by fellowship awards from the National Defense Science and Engineering Graduate Fellowship (NDSEG, <https://ndseg.asee.org/>) the UCSF Discovery Fellows Program, and the Markowski-Leach Fellowship (to T.L.V.), the UCSF Medical Scientist Training Program (to T.L.V. and S.K.), the UCSF Neuroscience Graduate Program (to T.L.V. and K.D.), and the UCSF-UCB Bioengineering Graduate Program (to S.K.). Additional funds come from the Department of Veterans Affairs, Veterans Health Administration (VA Merit: 1I01RX001640 to K.G) and National Institute of Mental Health, NIH (5R01MH111871 to K.G.); and start-up funds from the UCSF Department of Neurology to K.G.. K.G. also holds a Career Award for Medical Scientists from the Burroughs Wellcome Fund (1009855) and an Independent Scientist Award (1K02NS093014) from the National Institute of Neurological Disorders and Stroke, NIH. The funders had no role in study design, data collection and analysis, decision to publish, or preparation of the manuscript.

**Author contributions:** T.L.V., K.D. and K.G. designed the study. T.L.V., K.D., and S.K. conducted experiments. T.L.V. and K.D. performed analyses. T.L.V., K.D., and K.G. wrote the manuscript.

**Competing interests:** The authors declare no competing interests.

## 1.7 Supplementary Materials

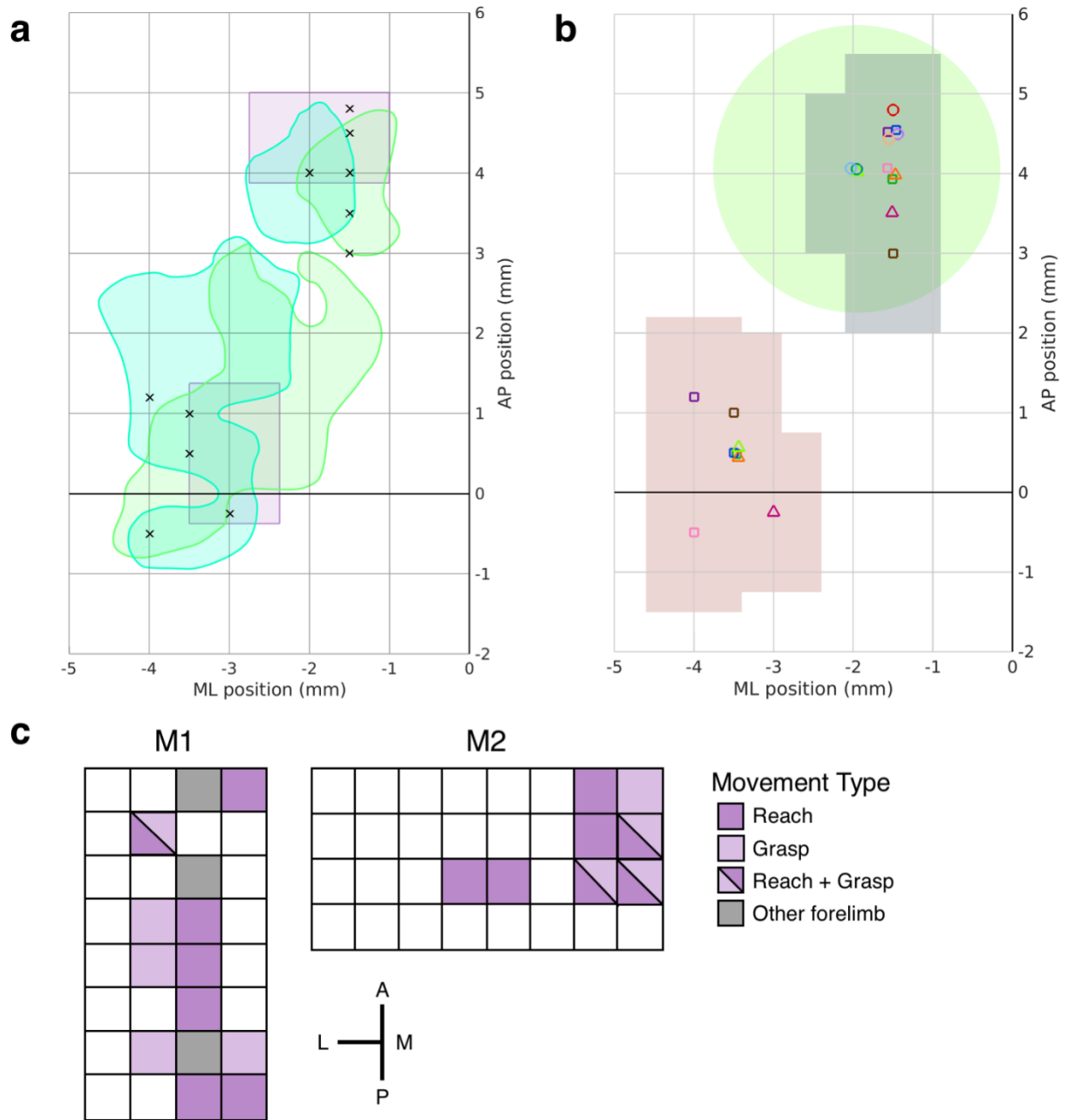


**Figure 1.9 M1 and M2 implantation coordinates.**

**(a)** Stimulation-based coordinates for M1 and M2 in Long-Evans rats. Shown in green and teal are regions where ICMS evoked forelimb movement in the two Long-Evans rats reported in Neafsey et al. 1986<sup>61</sup>; the maps were translated from diagrams of insufflated brains to flat coordinates. Shown in purple are array locations for two animals from our lab, each with a single array implanted in either M1 or M2. Electrical stimulation on these arrays evoked forelimb movements for both animals while under anesthesia. Shown as black x marks are the implantation

coordinates for animals in the present study (see Supplementary Table 2). All reaching animals were implanted contralateral to their dominant hand, but coordinates for right hemisphere implants have been transposed onto the left hemisphere. Anterior medial sites are for M2 arrays, while posterior lateral sites are for M1 arrays. We observed neural responses evoked by awake, behaving forelimb movement across both arrays in all experimental animals. **(b)** M2 muscimol spread included most M2 recording sites and excluded all M1 recording sites. Colored markers indicate center of implantation sites for experimental animals. Unlike (a), markers have been jittered at sites where multiple animals had an implant. Marker color corresponds to animal ID, and marker shape indicates animal cohort (see Supplementary Table 2 for detailed legend). Green shaded circle indicates estimated M2 muscimol spread. The center of the circle is placed at the surgical coordinates for the two animals that underwent acute injection only (see Methods), and the radius of the circle is calculated based on histology from these animals (see Supplementary Figure 6). The gray shaded region shows the combined silhouette of all M2 arrays, and the red shaded region shows the combined silhouette of all M1 arrays. As in (a), all right hemisphere implants were transposed to the left hemisphere. **(c)** Grids represent the arrays shown in purple in (a), with color indicating channels where stimulation evoked reach-like, grasp-like, or other forelimb movement. Arrays are shown in the same orientation as in (a), dimensions are not to scale.

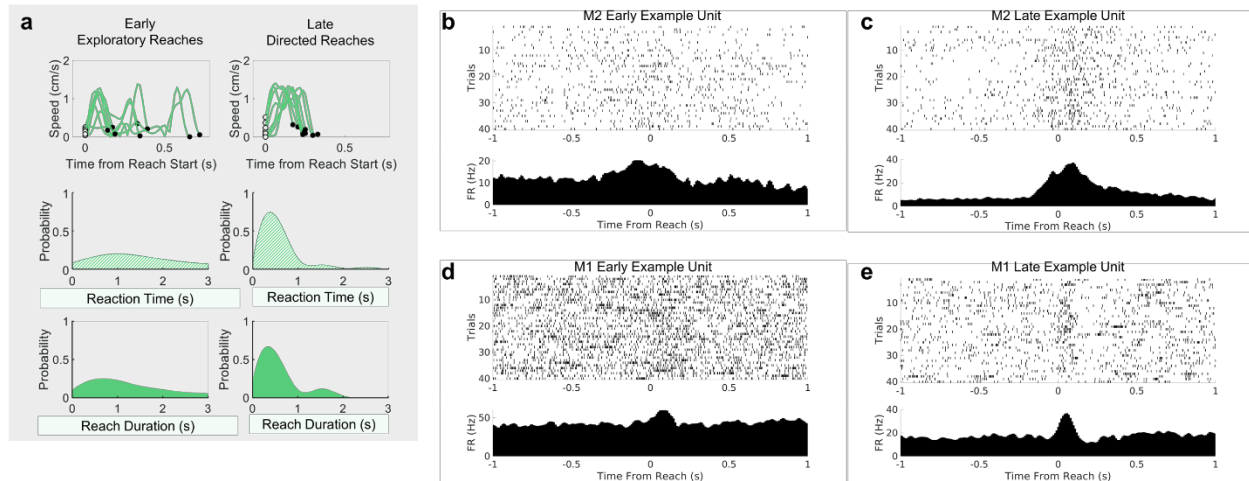


**Figure 1.10 Elaboration of reach-to-grasp learning behavior.**

(a) (Top) Speed profile for example trials in early (left) exploratory reaches and late (right) directed reaches. White dot marks reach start time. Black dot marks reach end time. Single-trial reach duration is driven by efficiency of reach targeting rather than maximal reaching speed. (Middle) Probability distribution of reaction times in early (left) exploratory reaches and late (right) directed reaches for example animal. (Bottom) Probability distribution of reach durations in early (left) exploratory reaches and late (right) directed reaches for example animal. For further details, see Supplementary Table 1. (b) Raster and PETH for example task-modulated unit from M2 in early learning. (c) Raster and PETH for example task-modulated unit from M2 in late learning. This unit was recorded on the same channel as (b). (d) Raster and PETH for example task-modulated unit from M1 in early learning, from same animal as (b,c). (e) Raster and PETH for example task-modulated unit from M1 in late learning. This unit was recorded on the same channel as (d).

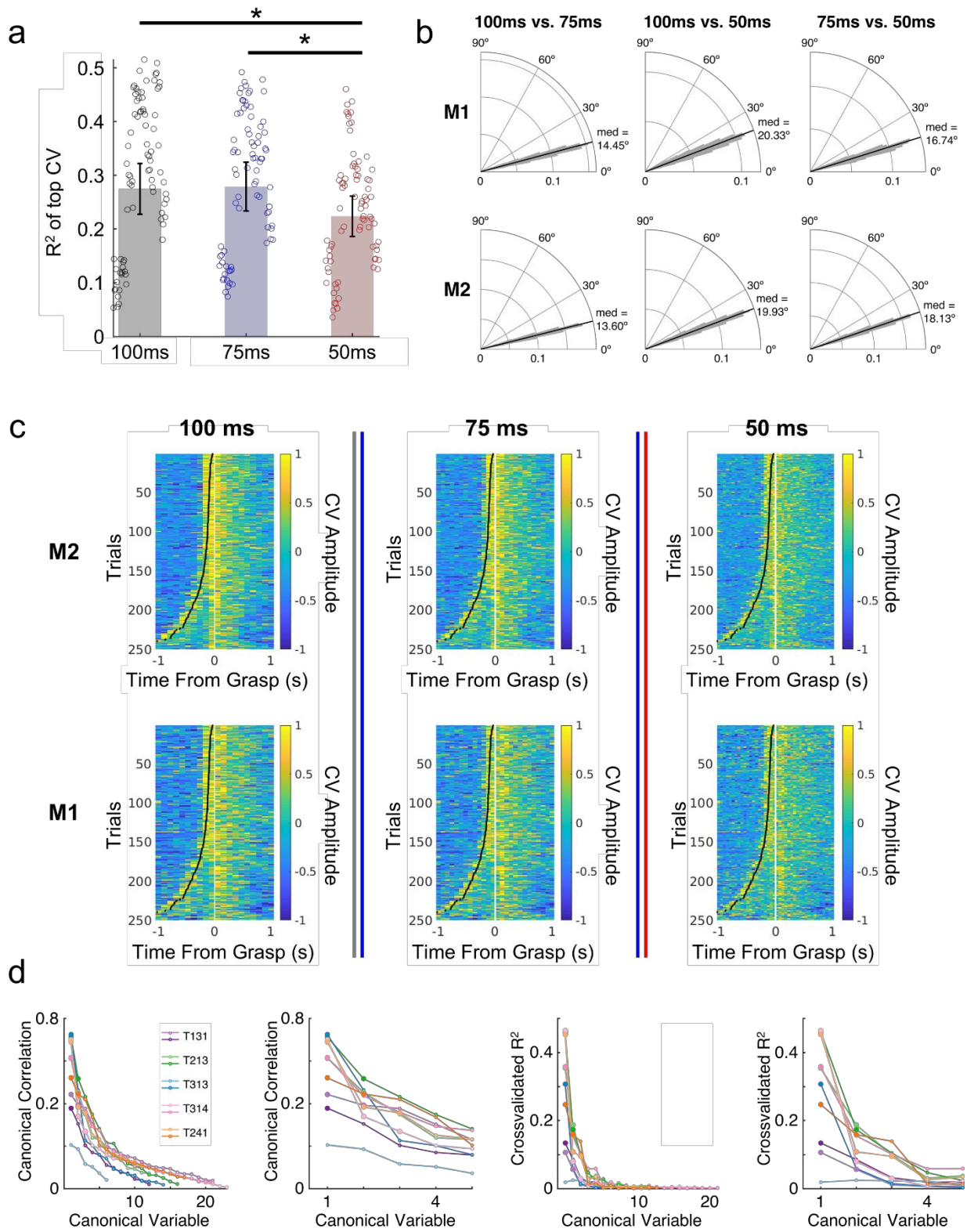
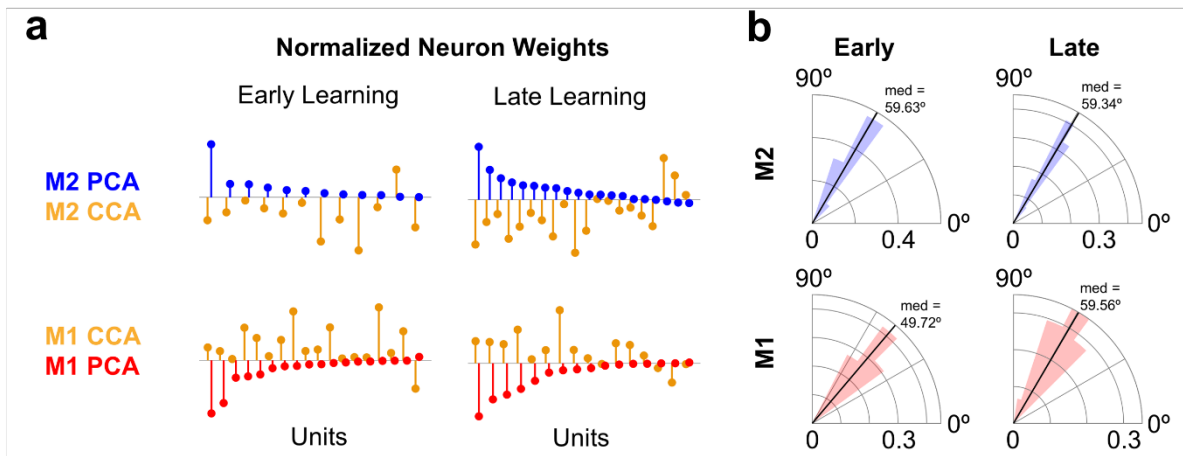


Figure 1.11 Fitting CCA with different bin-widths.

**(a)** CCA models were fit to data binned at 100, 75, and 50ms. For each dataset and model,  $R^2$  values of the top CV were computed on 10 folds of data (90% of time bins 10 ways, held out time bins were randomly chosen and non-overlapping). Bars show mean  $\pm$  std. dev.  $R^2$  values for all models fit to data at a particular binwidth, open circles show  $R^2$  values for individual models (4 animals  $\times$  2 sessions  $\times$  10 folds = 80 models per bin width).  $R^2$  values were not significantly different between the models fit on 100ms data and the models fit on 75ms data ( $p=0.83$ ), but were significantly lower for the models fit on 50ms data ( $p=0.016$  for 100ms vs 50ms;  $p<0.0002$  for 75ms vs 50ms). \*,  $p<0.05$ ; \*\*\*,  $p<0.001$ ; two-sided hierarchical bootstraps, not adjusted for multiple comparisons. **(b)** Angle between the top CVs of CCA models fit on 100ms, 75ms, or 50ms binned data. Shaded circular histogram shows bootstrap distribution of angles, black line shows median value of bootstrap distribution. Radius indicates proportion of bootstrap samples belonging to a bin. For all comparisons, the angle between models was much smaller than  $90^\circ$ , indicating that models fit on different binwidths identified similar patterns of covariation. For M2 (bottom), the angle between the 100ms and 75ms models (left) was significantly smaller than the angle between the 100ms and 50ms models (center) or between the 75ms and 50ms models (right). For M1 (top), the angle between the 100ms and 75ms models was significantly smaller than the angle between the 100ms and 50ms models, but not significantly smaller than the angle between the 75ms and 50ms models. **(c)** Single trial trajectories were qualitatively similar at different bin widths. Data shown is the same time range the models were fit on. Trials are sorted by duration and max-normalized for visualization. **(d)** Canonical correlation values (left two plots) and cross-validated  $R^2$  values (right two plots) across canonical variables. For both metrics, values drop off at a low dimensionality. Larger, filled circles indicate CVs that were statistically significant relative to models fit on trial-shuffled data (see Methods). Light colors indicate early learning datasets, dark colors indicate late learning datasets.



**Figure 1.12 PCA identifies a mix of local and cross-area dynamics.**

**(a)** Length of stems indicate weights for each neuron’s contribution to local or cross-area activity, derived using PCA and CCA respectively. Neuron weights were normalized by the maximum value for any neuron in that subspace. PCA and CCA weights are shown offset and opposing for visual clarity; for all models, more neurons had positive weights than negative. M2 and M1 subspace neuron weights in early (left) learning and late (right) learning. **(b)** Angle in multi-dimensional neural space between PCA and CCA subspaces for M2 (top) and M1 (bottom), for both early (left) and late (right) learning. Shaded histograms show bootstrap distribution of angles, solid black lines show median value of the bootstrap distribution. Radius indicates the proportion of bootstrap values in each bin.

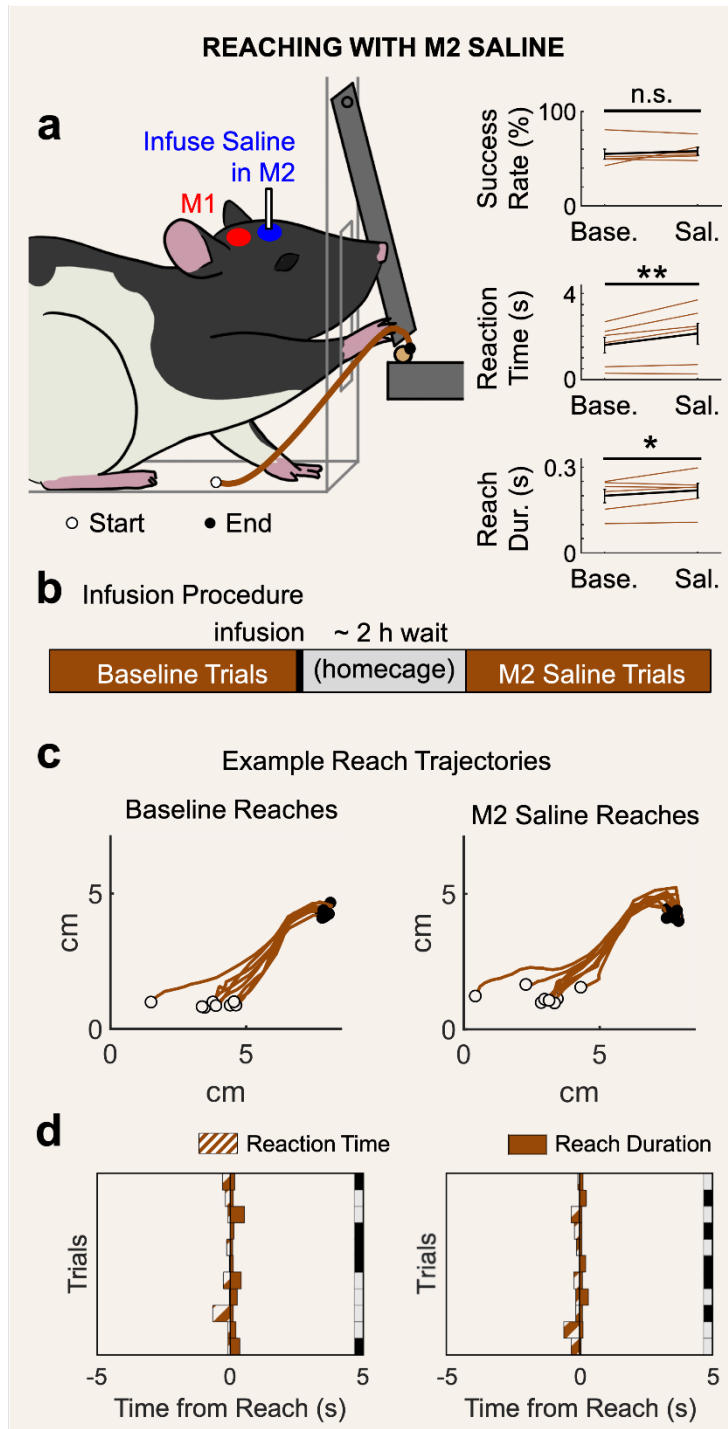


**Figure 1.13 M2 saline infusions do not severely affect learned reach behavior.**

**(a)** (Left) Rats previously trained on the reach-to-grasp task were infused with saline in M2. (Right) M2 saline increased reaction time ( $p=0.0021$ ) and reach duration ( $p=0.0452$ ), but did not decrease success rate ( $p=0.7453$ ). Brown lines show values for individual animals, black lines show mean  $\pm$  std. dev. \*,  $p<0.05$ ; \*\*,  $p<0.01$ , hierarchical bootstraps, one-sided, not adjusted for multiple-comparisons. **(b)** Experimental paradigm for evaluation of reach behavior during M2 saline infusion. **(c)** Example reach from a single animal during baseline (left) and M2 saline infusion



(right). **(d)** Example consecutive single-trial representations of reaction time and reach duration. Right border of plot shows accuracy, with success in grey and failure in black.



animals, we estimated muscimol spread to be 1.8mm from the injection site. Red arrows indicate the slices shown in (a).












**Table 1.1 Behavior summary.**



For the learning cohort, training day is measured from the first day the rat is exposed to the reaching task (excluding small number of handedness trials performed prior to implantation, see Methods). For the inactivation cohorts, animals received extensive reach training (often > 14 days) prior to their implantation and use in this study, however several of the animals also experienced extended periods of no reach training, and were therefore retrained to plateau performance prior to the muscimol and saline experiments. For these animals, training day is measured from the beginning of the most recent bout of training (same training bout for muscimol and saline experiments). For all animals, reaction time and reach duration are reported as *median (min – max)*, and measured in seconds. †Rat T313 is the animal excluded from most of the neural analyses due to having no significant CVs in the Early condition (see Methods).

| Rat ID   | Condition    | Day               | Camera Frame-rate | Trials Offered | Completed Trials | Successful Trials | Success Rate | Reaction Time          | Reach Duration       |
|--|--------------|-------------------|-------------------|----------------|------------------|-------------------|--------------|------------------------|----------------------|
| <b>Learning Cohort (Reach training + neural recordings, no inactivation)</b>               |              |                   |                   |                |                  |                   |              |                        |                      |
| T131   | Early        | Training day 1    | 30 Hz             | 313            | 183              | 43                | 23.50%       | 4.39 (0.15 - 14.73) s  | 0.23 (0.03 - 1.07) s |
|  | Late         | Training day 3    |                   | 315            | 291              | 144               | 49.49%       | 0.27 (0.15 - 11.84) s  | 0.21 (0.10 - 0.77) s |
| T213   | Early        | Training day 1    | 75 Hz             | 224            | 211              | 71                | 33.65%       | 0.34 (0.00 - 14.92) s  | 0.11 (0.00 - 0.56) s |
|  | Late         | Training day 3    |                   | 301            | 298              | 178               | 59.73%       | 0.20 (0.00 - 7.52) s   | 0.08 (0.00 - 0.32) s |
| T241   | Early        | Training day 1    | 75 Hz             | 250            | 184              | 50                | 27.17%       | 3.02 (0.32 - 24.18) s  | 0.34 (0.07 - 2.00) s |
|  | Late         | Training day 3    |                   | 300            | 273              | 162               | 59.34%       | 0.58 (0.03 - 15.76) s  | 0.32 (0.06 - 0.91) s |
| T313†  | Early        | Training day 2    | 100 Hz            | 87             | 38               | 15                | 39.47%       | 11.73 (2.51 - 29.69) s | 0.18 (0.06 - 0.66) s |
|  | Late         | Training day 15   |                   | 213            | 211              | 133               | 63.03%       | 0.33 (0.00 - 13.34) s  | 0.15 (0.05 - 0.81) s |
| T314   | Early        | Training day 1    | 100 Hz            | 299            | 142              | 28                | 19.72%       | 5.96 (0.41 - 24.39) s  | 0.38 (0.11 - 1.22) s |
|  | Late         | Training day 10   |                   | 259            | 250              | 145               | 58.00%       | 0.42 (0.00 - 12.62) s  | 0.11 (0.02 - 0.62) s |
| <b>Inactivation-Only Cohort (Reach training + infusion cannulas, no neural recordings)</b> |              |                   |                   |                |                  |                   |              |                        |                      |
| T282   | Baseline (M) | Re-training day 7 | 75 Hz             | 100            | 97               | 70                | 72.17%       | 0.37 (0.00 - 4.03) s   | 0.17 (0.01 - 0.40) s |
|  | M2 Muscimol  |                   |                   | 99             | 94               | 42                | 44.68%       | 0.59 (0.00 - 5.44) s   | 0.19 (0.01 - 0.85) s |
|  | Baseline (S) | Re-training day 7 |                   | 100            | 93               | 75                | 80.65%       | 0.04 (0.00 - 9.76) s   | 0.23 (0.01 - 0.49) s |
|  | M2 Saline    |                   |                   | 100            | 97               | 74                | 76.29%       | 0.09 (0.00 - 16.23) s  | 0.23 (0.04 - 0.80) s |
| T291   | Baseline (M) | Re-training day 8 | 100 Hz            | 106            | 105              | 45                | 42.86%       | 0.16 (0.00 - 6.48) s   | 0.11 (0.01 - 0.34) s |
|  | M2 Muscimol  |                   |                   | 105            | 90               | 31                | 34.44%       | 0.77 (0.00 - 11.15) s  | 0.16 (0.02 - 0.59) s |
|  | Baseline (S) | Re-training day 6 |                   | 100            | 100              | 50                | 50.00%       | 0.24 (0.00 - 2.31) s   | 0.10 (0.02 - 0.48) s |
|  | M2 Saline    |                   |                   | 100            | 100              | 53                | 53.00%       | 0.20 (0.00 - 6.32) s   | 0.10 (0.03 - 0.34) s |

| Rat ID  | Condition    | Day               | Camera Frame-rate | Trials Offered | Completed Trials | Successful Trials | Success Rate | Reaction Time         | Reach Duration        |
|---|--------------|-------------------|-------------------|----------------|------------------|-------------------|--------------|-----------------------|-----------------------|
| T315  | Baseline (M) | Re-training day 2 | 75 Hz             | 100            | 98               | 65                | 66.33%       | 0.94 (0.55 - 8.65) s  | 0.21 (0.03 - 0.51) s  |
|   | M2 Muscimol  |                   |                   | 100            | 82               | 34                | 41.46%       | 2.35 (0.89 - 17.05) s | 0.37 (0.03 - 0.91) s  |
|   | Baseline (S) | Re-training day 2 |                   | 111            | 101              | 50                | 49.51%       | 1.79 (0.88 - 13.81) s | 0.25 (0.04 - 0.72) s  |
|   | M2 Saline    |                   |                   | 139            | 125              | 60                | 48.00%       | 2.13 (0.84 - 16.47) s | 0.29 (0.03 - 0.87) s  |
| <b>Inactivation + Recording Cohort (Reach training + infusion cannulas + neural recordings)</b> |              |                   |                   |                |                  |                   |              |                       |                       |
| T336  | Baseline (M) | Re-training day 2 | 63.58 Hz          | 99             | 91               | 38                | 41.76%       | 1.47 (0.63 - 11.76) s | 0.22 (0.06 - 0.51) s  |
|   | M2 Muscimol  |                   |                   | 100            | 93               | 20                | 21.51%       | 4.82 (0.94 - 13.40) s | 0.30 (0.09 - 1.00) s  |
|   | Baseline (S) | Re-training day 2 |                   | 106            | 79               | 44                | 55.70%       | 1.36 (0.66 - 6.94) s  | 0.23 (0.03 - 0.39) s  |
|   | M2 Saline    |                   |                   | 149            | 118              | 66                | 55.93%       | 1.93 (0.83 - 12.52) s | 0.22 (0.05 - 0.44) s  |
| T349  | Baseline (M) | Re-training day 3 | 63.58 Hz          | 97             | 97               | 61                | 62.89%       | 1.07 (0.55 - 7.05) s  | 0.19 (0.06 - 0.58) s  |
|   | M2 Muscimol  |                   |                   | 199            | 81               | 13                | 16.05%       | 5.00 (0.31 - 13.89) s | 0.36 (0.15 - 0.72) s  |
|   | Baseline (S) | Re-training day 3 |                   | 109            | 103              | 44                | 42.72%       | 1.44 (0.00 - 13.86) s | 0.23 (0.06 - 0.52) s  |
|   | M2 Saline    |                   |                   | 99             | 96               | 60                | 62.50%       | 1.61 (0.64 - 12.79) s | 0.23 (0.06 - 0.42) s  |
| T391  | Baseline (M) | Re-training day 3 | 100 Hz            | 113            | 89               | 48                | 53.93%       | 0.91 (0.00 - 7.56) s  | 0.15 (0.028 - 0.55) s |
|   | M2 Muscimol  |                   |                   | 136            | 85               | 56                | 65.88%       | 1.57 (0.00 - 15.27) s | 0.17 (0.04 - 2.74) s  |
|   | Baseline (S) | Re-training day 3 |                   | 112            | 92               | 48                | 52.17%       | 1.91 (0.00 - 12.33) s | 0.13 (0.05 - 0.66) s  |
|   | M2 Saline    |                   |                   | 122            | 94               | 51                | 54.26%       | 2.50 (0.04 - 16.99) s | 0.13 (0.05 - 1.66) s  |

**Table 1.2 Implantation coordinates for all experimental animals**

| Rat ID   | Handedness | Implant      | Stereotaxic coordinates (mm) | Marker in Supp. Fig. 1b   |
|--|------------|--------------|------------------------------|---|
| <b>Learning Cohort</b> ( <i>Reach training + neural recordings, no inactivation</i> )                    |            |              |                              |   |
| T131   | Left       | M2 array     | ML: 1.5; AP: +4.5; DV: -1.8  |    |
|  |            | M1 array     | ML: 4.0; AP: +1.2; DV: -1.7  |   |
| T213   | Left       | M2 array     | ML: 1.5; AP: +4.0; DV: -1.5  |    |
|  |            | M1 array     | ML: 3.5; AP: +0.5; DV: -1.5  |   |
| T241   | Right      | M2 array     | ML: 1.5; AP: +4.5; DV: -1.5  |    |
|  |            | M1 array     | ML: 3.5; AP: +0.5; DV: -1.5  |   |
| T313†  | Right      | M2 array     | ML: 1.5; AP: +4.0; DV: -1.5  |    |
|  |            | M1 array     | ML: 4.0; AP: -0.5; DV: -1.5  |   |
| T314   | Right      | M2 array     | ML: 1.5; AP: +3.0; DV: -1.5  |    |
|  |            | M1 array     | ML: 3.5; AP: +1.0; DV: -1.4  |   |
| <b>Inactivation-Only Cohort</b> ( <i>Reach training + infusion cannulas, no neural recordings</i> )      |            |              |                              |   |
| T282   | Right      | M2 cannula L | ML: 1.5; AP: +4.8; DV: -1.7  |   |
|  |            | M2 cannula R | ML: 1.5; AP: +4.5; DV: -1.5  |   |
| T291   | Right      | M2 cannula L | ML: 1.5; AP: +4.5; DV: -1.7  |  |
|  |            | M2 cannula R | ML: 1.5; AP: +4.5; DV: -1.5  |   |
| T315   | Right      | M2 cannula L | ML: 1.5; AP: +4.5; DV: -1.7  |  |
|  |            | M2 cannula R | ML: 1.5; AP: +4.5; DV: -1.5  |   |
| <b>Inactivation + Recording Cohort</b> ( <i>Reach training + infusion cannulas + neural recordings</i> ) |            |              |                              |   |
| T336   | Right      | M2 array     | ML: 1.5; AP: +4.0; DV: -1.6  |  |
|  |            | M2 cannula   | ML: 2.5; AP: +4.0; DV: -1.6  |   |
|  |            | M1 array     | ML: 3.5; AP: +0.5; DV: -1.6  |   |
| T349   | Right      | M2 array     | ML: 1.5; AP: +3.5; DV: -1.6  |  |
|  |            | M2 cannula   | ML: 2.0; AP: +3.5; DV: -1.6  |   |
|  |            | M1 array     | ML: 3.0; AP: -0.25; DV: -1.6 |   |
| T391   | Right      | M2 array     | ML: 2.0; AP: +4.0; DV: -1.6  |  |
|  |            | M2 cannula   | ML: 2.5; AP: +4.0; DV: -1.6  |   |
|  |            | M1 array     | ML: 3.5; AP: +0.5; DV: -1.6  |   |

| Rat ID   | Handedness | Implant        | Stereotaxic coordinates (mm) | Marker in Supp. Fig. 1b   |
|--|------------|----------------|------------------------------|---|
| <b>Acute Fluorescent Muscimol Injection Cohort</b> |            |                |                              |   |
| T409   | N/A        | M2 injection L | ML: 2.0; AP: +4.0; DV: -1.5  |  |
|  |            | M2 injection R | ML: 2.0; AP: +4.0; DV: -1.5  |   |
| T410   | N/A        | M2 injection L | ML: 2.0; AP: +4.0; DV: -1.5  |  |
|  |            | M2 injection R | ML: 2.0; AP: +4.0; DV: -1.5  |   |

## 1.8 References

1. Sporns, O., Chialvo, D., Kaiser, M. & Hilgetag, C. Organization, development and function of complex brain networks. *Trends in Cognitive Sciences* **8**, 418–425 (2004).
2. Cao, V. Y. *et al.* Motor Learning Consolidates Arc-Expressing Neuronal Ensembles in Secondary Motor Cortex. *Neuron* (2015).
3. Hikosaka, O., Nakamura, K., Sakai, K. & Nakahara, H. Central mechanisms of motor skill learning. *Current Opinion in Neurobiology* **12**, 217–222 (2002).
4. Makino, H. *et al.* Transformation of Cortex-wide Emergent Properties during Motor Learning. *Neuron* **94**, 880-890.e8 (2017).
5. Perich, M. G., Gallego, J. A. & Miller, L. E. A Neural Population Mechanism for Rapid Learning. *Neuron* **100**, 964-976.e7 (2018).
6. Tanji, J. Sequential Organization of Multiple Movements: Involvement of Cortical Motor Areas. *Annual Review of Neuroscience* **24**, 631–651 (2001).
7. Athalye, V. R., Ganguly, K., Costa, R. M. & Carmena, J. M. Emergence of Coordinated Neural Dynamics Underlies Neuroprosthetic Learning and Skillful Control. *Neuron* **93**, 955-970.e5 (2017).
8. Ganguly, K., Dimitrov, D. F., Wallis, J. D. & Carmena, J. M. Reversible large-scale modification of cortical networks during neuroprosthetic control. *Nature Neuroscience* **14**, 662–667 (2011).
9. Kawai, R. *et al.* Motor Cortex Is Required for Learning but Not for Executing a Motor Skill. *Neuron* **86**, 800–812 (2015).
10. Peters, A. J., Chen, S. X. & Komiyama, T. Emergence of reproducible spatiotemporal activity during motor learning. *Nature* **510**, 263–267 (2014).
11. Sadtler, P. T. *et al.* Neural constraints on learning. *Nature* **512**, 423–426 (2014).



12. Arce-McShane, F. I., Ross, C. F., Takahashi, K., Sessle, B. J. & Hatsopoulos, N. G. Primary motor and sensory cortical areas communicate via spatiotemporally coordinated networks at multiple frequencies. *Proceedings of the National Academy of Sciences* **113**, 5083–5088 (2016).
13. Koralek, A. C., Jin, X., Long li, J. D., Costa, R. M. & Carmena, J. M. Corticostriatal plasticity is necessary for learning intentional neuroprosthetic skills. *Nature* **483**, 331–335 (2012).
14. Loonis, R. F., Brincat, S. L., Antzoulatos, E. G. & Miller, E. K. A Meta-Analysis Suggests Different Neural Correlates for Implicit and Explicit Learning. *Neuron* **96**, 521-534.e7 (2017).
15. Chen, T.-W., Li, N., Daie, K. & Svoboda, K. A Map of Anticipatory Activity in Mouse Motor Cortex. *Neuron* **94**, 866-879.e4 (2017).
16. Kaufman, M. T., Churchland, M. M., Ryu, S. I. & Shenoy, K. V. Cortical activity in the null space: permitting preparation without movement. *Nature Neuroscience* **17**, 440 (2014).
17. Runyan, C. A., Piasini, E., Panzeri, S. & Harvey, C. D. Distinct timescales of population coding across cortex. *Nature* **548**, 92–96 (2017).
18. Stringer, C. *et al.* Spontaneous behaviors drive multidimensional, brainwide activity. *Science* **364**, eaav7893 (2019).
19. Doyon, J. & Benali, H. Reorganization and plasticity in the adult brain during learning of motor skills. *Current Opinion in Neurobiology* **15**, 161–167 (2005).
20. Cunningham, J. P. & Yu, B. M. Dimensionality reduction for large-scale neural recordings. *Nat Neurosci* **17**, 1500–1509 (2014).
21. Mackevicius, E. L. *et al.* Unsupervised discovery of temporal sequences in high-dimensional datasets, with applications to neuroscience. *eLife* **8**, e38471 (2019).
22. Gulati, T., Ramanathan, D. S., Wong, C. C. & Ganguly, K. Reactivation of emergent task-related ensembles during slow-wave sleep after neuroprosthetic learning. *Nat Neurosci* **17**, 1107–1113 (2014).

23. Lara, A. H., Cunningham, J. P. & Churchland, M. M. Different population dynamics in the supplementary motor area and motor cortex during reaching. *Nature Communications* **9**, 2754 (2018).
24. Laubach, M., Wessberg, J. & Nicolelis, M. A. L. Cortical ensemble activity increasingly predicts behaviour outcomes during learning of a motor task. *Nature* **405**, 567–571 (2000).
25. Laurent, G. Olfactory network dynamics and the coding of multidimensional signals. *Nature Reviews Neuroscience* **3**, 884–895 (2002).
26. Lin, I.-C., Okun, M., Carandini, M. & Harris, K. D. The Nature of Shared Cortical Variability. *Neuron* **87**, 644–656 (2015).
27. Ramanathan, D. S., Gulati, T. & Ganguly, K. Sleep-Dependent Reactivation of Ensembles in Motor Cortex Promotes Skill Consolidation. *PLoS Biol* **13**, e1002263 (2015).
28. Shenoy, K. V., Sahani, M. & Churchland, M. M. Cortical Control of Arm Movements: A Dynamical Systems Perspective. *Annual Review of Neuroscience* **36**, 337–359 (2013).
29. Yttri, E. A. & Dudman, J. T. Opponent and bidirectional control of movement velocity in the basal ganglia. *Nature* **533**, 402–406 (2016).
30. Wagner, M. J. *et al.* Shared Cortex-Cerebellum Dynamics in the Execution and Learning of a Motor Task. *Cell* **177**, 669-682.e24 (2019).
31. Huk, A. C. & Hart, E. Parsing signal and noise in the brain. *Science* **364**, 236–237 (2019).
32. Semedo, J. D., Zandvakili, A., Machens, C. K., Yu, B. M. & Kohn, A. Cortical Areas Interact through a Communication Subspace. *Neuron* (2019).
33. Allen, W. E. *et al.* Thirst regulates motivated behavior through modulation of brainwide neural population dynamics. *Science* **364**, eaav3932 (2019).
34. Hotelling, H. Relations Between Two Sets of Variates. *Biometrika* **28**, 321–377 (1936).
35. Whishaw, I. Q. & Pellis, S. M. The structure of skilled forelimb reaching in the rat: A proximally driven movement with a single distal rotatory component. *Behavioural Brain Research* **41**, 49–59 (1990).

36. Wong, C. C., Ramanathan, D. S., Gulati, T., Won, S. J. & Ganguly, K. An automated behavioral box to assess forelimb function in rats. *Journal of Neuroscience Methods* **246**, 30–37 (2015).
37. Darling, W. G., Pizzimenti, M. A. & Morecraft, R. J. Functional Recovery Following Motor Cortex Lesions in Non-Human Primates: Experimental Implications for Human Stroke Patients. *J Integr Neurosci* **10**, 353–384 (2011).
38. Ramanathan, D. S. *et al.* Low-frequency cortical activity is a neuromodulatory target that tracks recovery after stroke. *Nature Medicine* **24**, 1257–1267 (2018).
39. Whishaw, I. Q., Pellis, S. M., Gorny, B. P. & Pellis, V. C. The impairments in reaching and the movements of compensation in rats with motor cortex lesions: an endpoint, videorecording, and movement notation analysis. *Behavioural Brain Research* **42**, 77–91 (1991).
40. Rothschild, G., Eban, E. & Frank, L. M. A cortical–hippocampal–cortical loop of information processing during memory consolidation. *Nat Neurosci* **20**, 251–259 (2017).
41. Kargo, W. J. Improvements in the Signal-to-Noise Ratio of Motor Cortex Cells Distinguish Early versus Late Phases of Motor Skill Learning. *Journal of Neuroscience* **24**, 5560–5569 (2004).
42. Kargo, W. J. & Nitz, D. A. Early skill learning is expressed through selection and tuning of cortically represented muscle synergies. *The Journal of neuroscience* **23**, 11255–11269 (2003).
43. Buzsáki, G. Neural Syntax: Cell Assemblies, Synapsembles, and Readers. *Neuron* **68**, 362–385 (2010).
44. Lemke, S. M., Ramanathan, D. S., Guo, L., Won, S. J. & Ganguly, K. Emergent modular neural control drives coordinated motor actions. *Nature Neuroscience* **1** (2019).

45. Kiani, R., Cueva, C. J., Reppas, J. B. & Newsome, W. T. Dynamics of Neural Population Responses in Prefrontal Cortex Indicate Changes of Mind on Single Trials. *Current Biology* **24**, 1542–1547 (2014).
46. Musall, S., Kaufman, M. T., Juavinett, A. L., Gluf, S. & Churchland, A. K. Single-trial neural dynamics are dominated by richly varied movements. *Nat Neurosci* **22**, 1677–1686 (2019).
47. Narayanan, N. S. & Laubach, M. Methods for Studying Functional Interactions Among Neural Populations. *Methods Mol Biol* **489**, (2009).
48. Ni, A. M., Ruff, D. A., Alberts, J. J., Symmonds, J. & Cohen, M. R. Learning and attention reveal a general relationship between population activity and behavior. *Science* **359**, 463–465 (2018).
49. Otchy, T. M. *et al.* Acute off-target effects of neural circuit manipulations. *Nature* **528**, 358–363 (2015).
50. Mushiake, H., Inase, M. & Tanji, J. Neuronal activity in the primate premotor, supplementary, and precentral motor cortex during visually guided and internally determined sequential movements. *Journal of Neurophysiology* **66**, 705–718 (1991).
51. Saiki, A. *et al.* Different Modulation of Common Motor Information in Rat Primary and Secondary Motor Cortices. *PLoS ONE* **9**, e98662 (2014).
52. Hyland, B. Neural activity related to reaching and grasping in rostral and caudal regions of rat motor cortex. *Behavioural Brain Research* **94**, 255–269 (1998).
53. Rouiller, E. M., Moret, V. & Liang, F. Comparison of the Connectional Properties of the Two Forelimb Areas of the Rat Sensorimotor Cortex: Support for the Presence of a Premotor or Supplementary Motor Cortical Area. *Somatosensory & Motor Research* **10**, 269–289 (1993).
54. Kobak, D. *et al.* Demixed principal component analysis of neural population data. *eLife* <https://elifesciences.org/articles/10989> (2016) doi:10.7554/eLife.10989.

55. Russo, A. A. *et al.* Motor Cortex Embeds Muscle-like Commands in an Untangled Population Response. *Neuron* **97**, 953-966.e8 (2018).
56. Costa, R. M. A selectionist account of de novo action learning. *Current Opinion in Neurobiology* **21**, 579–586 (2011).
57. Jazayeri, M. & Afraz, A. Navigating the Neural Space in Search of the Neural Code. *Neuron* **93**, 1003–1014 (2017).
58. Shima, K. & Tanji, J. Neuronal Activity in the Supplementary and Presupplementary Motor Areas for Temporal Organization of Multiple Movements. *Journal of Neurophysiology* **84**, 2148–2160 (2000).
59. Svoboda, K. & Li, N. Neural mechanisms of movement planning: motor cortex and beyond. *Current Opinion in Neurobiology* **49**, 33–41 (2018).
60. Smith, N. J., Horst, N. K., Liu, B., Caetano, M. S. & Laubach, M. Reversible inactivation of rat premotor cortex impairs temporal preparation, but not inhibitory control, during simple reaction-time performance. *Front. Integr. Neurosci.* **4**, 124 (2010).
61. Neafsey, E. J. *et al.* The organization of the rat motor cortex: A microstimulation mapping study. *Brain Research Reviews* **11**, 77–96 (1986).
62. Murakami, M., Vicente, M. I., Costa, G. M. & Mainen, Z. F. Neural antecedents of self-initiated actions in secondary motor cortex. *Nat Neurosci* **17**, 1574–1582 (2014).
63. Takemi, M. *et al.* Rapid Identification of Cortical Motor Areas in Rodents by High-Frequency Automatic Cortical Stimulation and Novel Motor Threshold Algorithm. *Front. Neurosci.* **11**, (2017).
64. Ramanathan, D., Conner, J. M. & H. Tuszynski, M. A form of motor cortical plasticity that correlates with recovery of function after brain injury. *Proc Natl Acad Sci U S A* **103**, 11370–11375 (2006).

65. Conner, J. M., Culberson, A., Packowski, C., Chiba, A. A. & Tuszynski, M. H. Lesions of the Basal Forebrain Cholinergic System Impair Task Acquisition and Abolish Cortical Plasticity Associated with Motor Skill Learning. *Neuron* **38**, 819–829 (2003).
66. Quiroga, R. Q., Nadasdy, Z. & Ben-Shaul, Y. Unsupervised spike detection and sorting with wavelets and superparamagnetic clustering. *Neural Comput* **16**, 1661–1687 (2004).
67. Chung, J. E. *et al.* A Fully Automated Approach to Spike Sorting. *Neuron* **95**, 1381-1394.e6 (2017).
68. Macmillan, N. A. & Creelman, C. D. *Detection theory: a user's guide*. (Lawrence Erlbaum Associates, 2005).
69. Yu, B. M. *et al.* Gaussian-Process Factor Analysis for Low-Dimensional Single-Trial Analysis of Neural Population Activity. *Journal of Neurophysiology* **102**, 614–635 (2009).
70. Saravanan, V., Berman, G. J. & Sober, S. J. Application of the hierarchical bootstrap to multi-level data in neuroscience. Preprint at <https://www.biorxiv.org/content/10.1101/819334v1> (2019).
71. Paxinos, G., & Watson, C. (1986). *The rat brain in stereotaxic coordinates*, 2nd edR Academic Press. New York.

## **CH. 2      PREMOTOR ACTIVITY DURING M1 BRAIN-COMPUTER INTERFACE LEARNING**

### **2.1 Abstract**

In brain-computer interface (BCI) experiments, neural activity is used to drive the movement of external devices or stimuli. With practice, subjects learn to produce experimenter-defined target neural states to achieve reward. As with natural motor learning, BCI learning depends on other brain areas, but little is known about the role of other cortical areas not used as input to the BCI. Here, we trained rats to perform an M1 BCI task, and analyzed the activity patterns of M2 neurons and M1 indirect neurons, i.e. those that were not used as input to the BCI. We found that there were task-modulated neurons in both populations, and that both populations could be used to predict M1 BCI-potent activity. Compared to M1 indirect units, M2 units were correlated with BCI-potent activity at a broader range of timescales, and their activity evolved at a slower timescale as well. We also found that M2 units predicted the activity of M1 indirect units as well as BCI-potent activity. We suggest that M2 population dynamics provide a continuous modulatory influence on M1 population activity.

### **2.2 Introduction**

Brain-computer interfaces (BCI) provide an important opportunity to study and understand neural activity. In BCI experiments, specific neural activity patterns are selected as target goals. The neurons necessary for this neural activity are exclusively and directly responsible for task accomplishment. Most studies focus on BCI performance and the activity of direct neurons that drive the decoder. However, due to the heavily interconnected nature of neural networks, other neurons in the functional network are likely to be necessary for and affected by BCI learning.

A particularly interesting question is the relative contributions of neurons embedded in the BCI control circuit as compared to neurons in other areas that project to the BCI control circuit. There

is a growing body of work that indicates that local neurons that are not part of the BCI decoder (“indirect local neurons”) are modulated in a manner that is analogous to (“direct neurons”) during the process of learning<sup>1-5</sup>. Interestingly, a recent study of BCI control in the non-human primate M1 found that neurons in other motor cortical regions (“cross-area indirect neurons”) were modulated during BCI learning<sup>6</sup>. These studies suggest that, although only a subset of neurons is required to accomplish BCI tasks, local and cross-area indirect neurons are implicated in BCI control. Consistent with this, Korelek et al., (2012)<sup>2</sup> showed that M1 BCI learning depends on striatal plasticity. An open question is how local and cross-area indirect neurons differentially contribute to BCI control. This question is essential to understanding how complex, modular neural networks function when trained to perform specific neural patterns.

Here, we focus specifically on the role of premotor cortex (M2) during the performance of a simple M1 BCI task. M2 is one of the dominant inputs to M1<sup>7-10</sup>, and M2 activity is necessary for learning and control of natural motor tasks<sup>11-15</sup>. Also, while M2 and M1 have similar representations of movement<sup>16</sup>, M2 may represent more information about task context than M1<sup>17-20</sup>. Consequently, M2 is likely crucial for guiding context-sensitive neural activity, such as BCI performance. In our experiments, we allowed BCI control using a small subset of M1 neurons; we also monitored M2 neurons and indirect local M1 neurons as the animal learnt BCI control. We confirm that indeed M2 neurons were modulated during the BCI learning using only a subset of M1 neurons. However, we found evidence for different mean timescales M2 neural activity modulation than for M1-indirect neurons. Intriguingly, M2’s long temporal task modulation is correlated with M1-direct neural activity at many timescales and time lags, suggesting continuous rather than intermittent influence on M1 activity. Also, as M2 neural activity is equally predictive of M1 direct and indirect neural activity, we suggest that M2 interacts with M1 as a whole for BCI tasks, rather than specifically modulating direct neurons as a task-relevant functional group. Together, our results suggest that, in BCI task performance, M2 population dynamics provide continuous influence on M1 population activity, rather than intermittent pulses.



## 2.3 Results

### 2.3.1 M2 units are modulated by a simple M1 BCI task

We recorded simultaneously from both M1 and M2 in rats learning a simple linear BCI task<sup>1-5</sup>. In each recording session, a subset of M1 neurons were chosen to drive the decoder (M1 direct, or M1d, units). M1 neurons that were excluded from the decoder were considered indirect (M1i) units. The M1 direct units were split into two groups: the positive pool (M1d<sup>+</sup>) and the negative pool (M1d<sup>-</sup>), each consisting of 1 to 4 arbitrarily selected units (Figure 1c). At each timestep during the experiments, online firing rates were computed for all of the M1 direct units. Firing rates were summed within the two pools, and then the summed negative pool firing rate was subtracted from the positive pool to obtain the “neural state” used to drive the BCI. Neural state values were compared to a baseline distribution, and a trial was successful when the neural state exceeded a target threshold (see Methods). Therefore, rats were rewarded when they increase the difference in firing rate between the positive and negative pools. Feedback was given via the movement of a water spout (all n=4 rats) and by a visual cue placed outside the behavior box (n=3 rats)(Figure 1b). Water reward was delivered upon successful task completion; trials that were not completed within 15 (n=1 rat) or 10 (n=3 rats) seconds were considered failures and were punished with a time out. Rats were generally able to learn the task over the course of 100 to 200 trials, as indicated by increased success rate (Figure 1d).

First, we asked whether M2 units and M1 indirect units were task modulated. Although these neurons do not directly drive the BCI decoder (Figure 2a), it is possible that they directly affect the M1 direct units. We computed peri-event time histograms (PETHs) for all offline-sorted units relative to the end of successful trials, and used a circular shuffle modulation test to determine which units were significantly modulated. We found that 31.68% of M2 units and 36.02% of M1 indirect units were significantly modulated, compared to 70.83% of offline-sorted units from channels that had contained an online-sorted direct unit (Figure 2b,c). This indicates that during

this relatively early stage of BCI training, a large portion of recorded M1 and M2 neurons are involved in rats' attempts to perform the BCI task, even though only a few neurons were directly causal to the BCI.

### 2.3.2 M2 population activity predicts M1 BCI-potent activity at broad timescales

Although we found that many M2 neurons were significantly task-modulated, it is not necessarily the case that their activity pattern is related to BCI control: an M2 neuron could have a stereotyped activity pattern without being correlated with moment-by-moment BCI activity. To address this question, we used generalized linear models (GLMs) to perform regression predicting M1 BCI-potent activity from M2 population activity ("GLM-2D models", Figure 3a). First, M1 BCI-potent activity was reconstructed, re-binned at different binwidths, used as the response variable in the GLMs. The predictors were binned M2 firing rates, where each neuron appeared more than once with variable time lags ranging from -0.2s to +0.2s relative to the M1 BCI-potent activity. Models were fit for data binned at 15, 25, 35, 50, and 100ms. Crossvalidated  $R^2$  values were computed for all binwidth models (Figure 3b), and weight structures were qualitatively similar across binwidths. Further analysis was performed with 25ms binwidth models. Model significance was computed for 25ms models by comparison to a reference distribution of models fit to trial-shuffled data. By this metric, M2 population activity had significant predictive power for moment-by-moment M1 BCI-potent activity in all datasets (see Methods).

Next, we examined the temporal structure of the regression weights. Looking at single units, we observed that many M2 units had large regression weights at multiple time lags, often including both positive and negative weights (Figure 3d). Across the population, different M2 units had their largest magnitude weight at a wide range of time lags (Figure 3c). Across all datasets, the distribution of time lags at which any neuron had its largest magnitude regression weight was not significantly different from a uniform distribution (Figure 3e; Bootstrap,  $p=0.2435$ , see Methods for

details). We hypothesized that this broad timescale of correlation reflects the complex and often polysynaptic connectivity between M2 and M1.

### 2.3.3 M1 direct units do not have a privileged functional relationship with M2

Next, we wondered whether M2 activity was particularly predictive of M1 direct unit activity, or whether it had similar predictive power for any arbitrarily chosen subset of M1 units. To address this, we randomly chose M1 indirect units to use as “surrogate direct” units, matched in number to the M1 direct units from each dataset, and built GLMs to predict their activity as before (“GLM-2I models”). For each dataset, we repeated this process with 50 different sets of M1 indirect units. As with the GLM-2D models, we found that many M2 units had large regression weights at multiple time lags, with both positive and negative weights (Figure 4c). The distribution of time lags for maximally predictive weights was also consistent with a uniform distribution (Figure 4d,e; Bootstrap,  $p=0.491$ ). For the 25ms models, we also compared crossvalidated  $R^2$  values, and found that the  $R^2$  values for the GLM-2D models were within the range of  $R^2$  values for the GLM-2I models (Figure 4b), and were not significantly different from the mean GLM-2I  $R^2$  models for 6 of 7 datasets (permutation tests,  $p = 0.1164, 0.1568, 0.8609, 0.9609, 0.3701, 0.6454$ ), but was significantly greater than the mean for the remaining dataset (permutation test,  $p=0.0192$ ). This suggests that, at least at this early stage of learning, the complex causal relationships between M2 and M1 have not been reshaped by the BCI task, and, if M2 activity is causally involved in task performance, its influence on M1 does not seem to be specific to direct units.

### 2.3.4 M2 units are distinct from M1 indirect units

Do M2 and M1 indirect units have similar roles? M2 and M1 are heavily interconnected, include task-modulated indirect units, and are jointly involved in natural motor tasks. To test this idea, we built GLMs to predict M1 BCI-potent activity from M1 indirect population activity (“GLM-ID models”). Unlike the GLM-2D and GLM-2I models, predictor units in GLM-ID models tended to have large weights for small time lags (Figure 4f), and simultaneous data ( $\tau=0$ ) was most

commonly given the largest magnitude weight (Figure 4g,h). In contrast to the GLM-2D and GLM-2I models, the distribution of time lags with the largest magnitude weights was significantly non-uniform (Bootstrap,  $p < 0.00001$ ). Additionally, the GLM-ID models had higher crossvalidated  $R^2$  values than the GLM-2D models (Figure 4b; Permutation test,  $p = 0.0079$ ). Together, this shows that there is a meaningful difference between M2 and M1 indirect units' functional relationship with M1 direct units. Specifically, M1 indirect units tend to be more correlated with M1 BCI-potent activity than M2 units, and at shorter time lags; perhaps reflecting their belonging to the same local population.

### 2.3.5 M2 population activity evolves at a slower pace than M1 indirect activity

Finally, we examined M2 and M1 indirect populations activity immediately before successful trial completion, and how this activity relates to trial outcome. We observed that M2 population activity included broad modulation near the end of successful trials (Figure 2b), and hypothesized that M2 population activity was changing at a slower timescale than M1 indirect population activity. We tested this hypothesis in two ways. First, we computed single unit autocorrelation functions, and found that the average width-at-half-max was significantly wider for M2 units than for M1 indirect units (Permutation test,  $p < 0.00001$ ). Second, we binned neural data at 50ms and correlated M2 or M1i population vectors with their respective population vectors during the final 2s of correct trials; we found that the mean correlation coefficient was significantly higher for M2 than M1i (Figure 5; Permutation test,  $p < 0.00001$ ).

## 2.4 Discussion

In this study, we demonstrate differential roles for M2 and M1 during brain-computer interface task performance. Specifically, we trained rats to perform a M1 BCI task and compared characteristics of M2 population activity with the activity of M1 indirect neurons excluded from the BCI decoder. We found that many M2 and M1 indirect neurons were task modulated, and that M2 population activity is correlated with moment-to-moment BCI performance at a broad range of

time lags. We also found that M2-based models predicting either M1 direct or M1 indirect activity had similar  $R^2$  values, and their regression weights were similarly distributed across time lags, suggesting that M1 direct units do not have a privileged relationship with M2. In contrast, models predicting M1 direct unit activity from M1 indirect unit activity had higher  $R^2$  values, and most predictive power was found at small time lags. Furthermore, M2 population activity patterns changed more slowly than M1 indirect population activity. Together, this supports a model of M1-M2 communication in which M2 provides a consistent pattern of input to M1, on a slower timescale than communication within M1. Within this framework, moment-to-moment control of the BCI is largely internal to M1, and perhaps contextual or other top-down input is provided by M2. Understanding of these differential roles can provide insight into natural movement control and can be harnessed to improve design of multi-area BCIs.

#### 2.4.1 Hierarchical control of BCI performance

BCI experiments provide an opportunity to select target neural patterns in a region of interest, and to analyze neural correlates of task performance in other brain regions. The creation of an arbitrary neural pattern eliminates many of the confounds associated with natural movements, including multi-area control of natural movements, and baseline correlations in population activity across brain regions<sup>11,21,22</sup>. In BCIs, the target neural pattern is unlikely to be correlated with unrelated processes in other brain regions. Therefore, correlations between BCI direct neuron output and other neural populations' activity allow us to make hypotheses about which regions are involved in BCI performance without having to disrupt the circuit through artificial regional inactivations. For example, here, the correlation between M2 and M1 direct neurons is weaker and at longer timescales than the correlation between M1 indirect and direct neurons. This suggests that M2 provides inputs to M1 that are task-specific, but temporally imprecise; in contrast, internal M1 population dynamics are more robust but are temporally limited. One interpretation is that M1 indirect units are better positioned to steer M1 direct units to the target

state, while M2 units appear more likely to provide a modulatory input. This is analogous to the finding in sensory systems that task information in higher level regions is present at greater latencies and maintained for longer durations<sup>23</sup>.

#### 2.4.2 BCIs control of static versus dynamic target states

BCIs are often framed as a substitute for natural movement, but there are important differences between BCI and natural movement tasks. For one, while natural movements involve body parts which must move continuously through space, BCIs need not have this restriction. Studies also suggest that, within motor cortex, neural activity during natural movement progresses through continuous states<sup>24</sup>. However, high-dimensional neural activity is not inherently constrained by continuous paths through activity space. Instead, neural activity can jump between states. This has been exploited in NHP and human experiments in which participants use a BCI to type on a digital keyboard<sup>25</sup> rather than trace paths through virtual space, as is more common with artificial limb research. In the simple BCI used in our experiments, BCI control occurred over discrete time bins and output was only smoothed over short timescales. Neural activity was therefore less constrained to be continuous than for BCIs mimicking dynamic movements<sup>6</sup>. Furthermore, the target neural activity pattern was a single static state, and the approach to it was unconstrained within the BCI-potent space. Because of this, it may be appropriate to compare the BCI task to reaction time and waiting time tasks, rather than natural movement. In waiting time tasks, animals must hold a position until an arbitrary internal threshold is reached, similar to common simple BCI paradigms in which the target neural activity must be maintained for a set period of time for trial success. Waiting experiments have demonstrated encoding of hold time within mPFC<sup>26</sup> and M2<sup>19</sup> single neurons, with single neurons displaying a variety of activity patterns, including a slow ramp to threshold. This may be similar to the slow evolution of M2 activity seen here.

In contrast to the static neural activity targeted in simple BCI tasks, natural movements are thought to require execution of dynamic paths in high-dimensional neural space<sup>27</sup>. There is also evidence

that natural movements are initiated more quickly if they are preceded by preparatory activity in the same high-dimensional direction as the neural activity required for the movement<sup>24</sup>. Therefore, to better understand natural movement dynamics, experimenters may want to use BCIs with dynamic rather than static neural activity targets<sup>28,29</sup>.

### 2.4.3 Timescales of BCI learning

Natural motor learning is widely considered to occur in several phases, from early exploration to a well-consolidated over-trained state<sup>30-33</sup>. There is evidence that cortical regions are necessary for early learning, while sub-cortical regions are necessary for well-learned performance<sup>15</sup>. It is likely that a similar process underlies BCI learning. Here, we focus on an early, still largely exploratory, stage of BCI learning by using a single-session training paradigm. BCI studies which included a sleep consolidation period<sup>3,5,34</sup> or which used multi-day learning paradigms<sup>1,35</sup> have found that M1 indirect units become less modulated with learning. It is possible that at later stages of learning, M2 task-modulation is similarly decreased; however, it is also possible that consolidation has a different effect on local and cross-area indirect neurons. To our knowledge, only one other study has analyzed the activity of cross-area indirect neurons in cortex; they found robust task-related modulation in several cortical areas, including premotor cortex, after a multi-day learning paradigm<sup>6</sup>. This suggests that the M2 activity patterns we see here may be refined and maintained even in later learning. This parallels evidence from natural motor learning showing that the overall amount of correlated activity between M2 and M1 does not change with learning<sup>11</sup>.

### 2.4.4 Limitations and future work

Comparisons with results from prior studies are limited by differences in experimental paradigms. For example, the learning sessions were shorter than those from similar BCI tasks<sup>2,3,5,34</sup>. Consequently, our results may specifically capture an earlier stage of learning, and the role of M2 may evolve beyond what we see here during the early, exploratory stages of learning. Additionally, although only M1 direct units causally drive the BCI output, it is still unknown whether

M1 indirect neurons or neurons from other brain regions are necessary for BCI learning and performance in this task. Inactivation experiments could directly test necessity of other brain regions for BCI performance, though such inactivations may also disrupt the larger motor network function<sup>36</sup>.



## 2.5 Figures

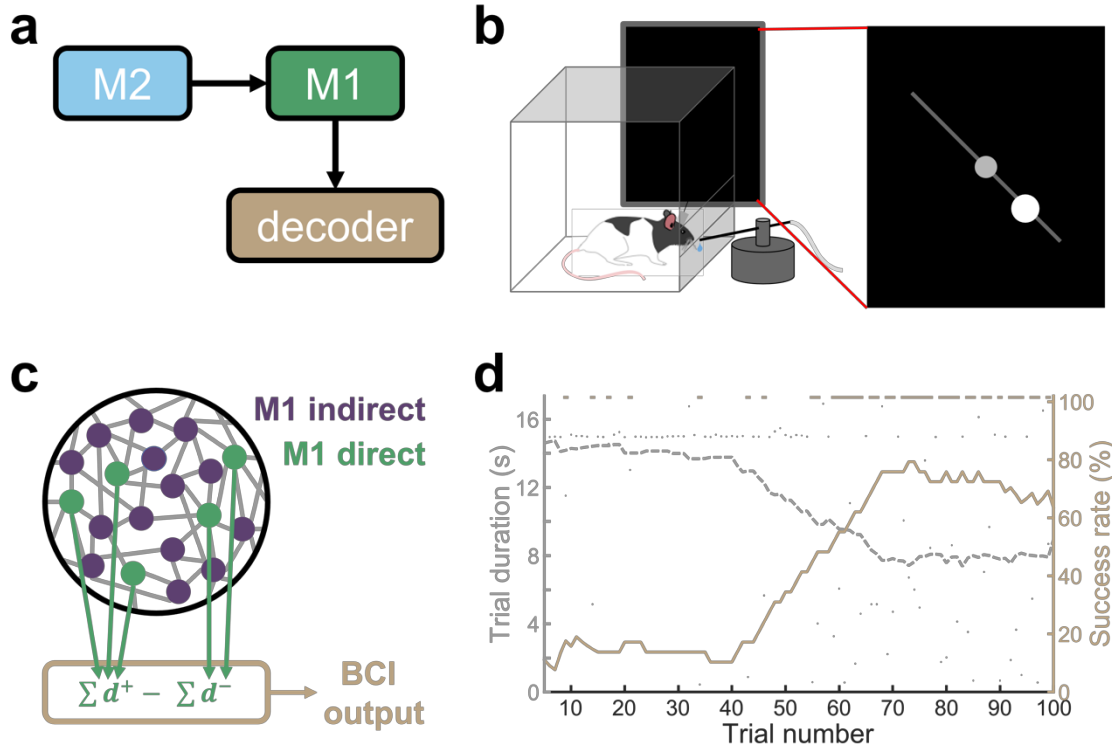


**Figure 2.1 Learning the BCI task**

**(a)** Rats learned a BCI task using only M1 neurons as inputs to the BCI decoder. Neural activity from M2 was recorded but was not directly decoded for BCI control. **(b)** Experimental setup (not to scale). Rats were allowed to move freely inside a clear plastic behavior box during the task. Online feedback about neural state was provided via a moving water spout (all  $n=4$  rats) and visual cues on a computer monitor placed outside the box ( $n=3$  rats) (see Methods). When the target neural state was reached, the water spout moved within reach and a water reward was given. Auditory cues marked trial start, reward, or task timeout. **(c)** A subset of M1 neurons were arbitrarily chosen as “direct” units (green), used to drive the BCI decoder, while the rest were considered “indirect” units (purple). 1 to 4 direct units were assigned to the “positive pool” ( $d^+$ ) and 1 to 4 direct units were assigned to the “negative pool” ( $d^-$ ). Online firing rates were summed within the pools, and then the  $d^-$  firing rate was subtracted from the  $d^+$  firing rate to obtain the neural state used to control BCI output. The neural state was compared to a baseline distribution, and when it exceeded a threshold value, the trial was considered a success (see Methods). **(d)** Example learning curve from one rat showing an improvement in success rate across the course of the BCI session. Small gray points indicate actual trial duration. Dashed gray line shows running average trial duration (smoothed over 30 trials). Light brown boxes at the top of the plot indicate successful trials. Brown line shows running average success rate (smoothed over 30 trials). X-axis is slightly cropped to remove smoothing artifact at the ends for visualization only, this session included 104 trials total.

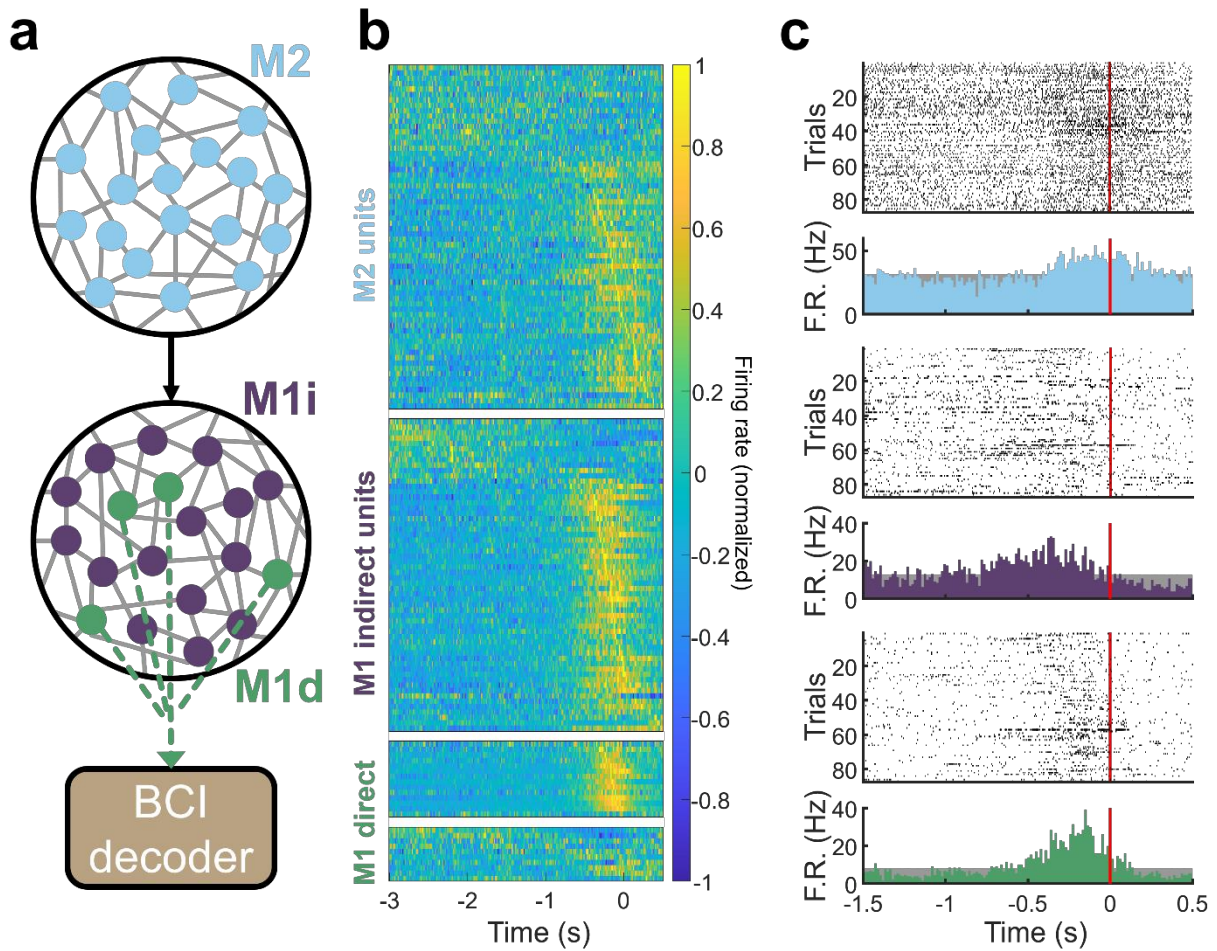


**Figure 2.2 Indirect neurons in both M2 and M1 are modulated during BCI control.**

(a) Illustration of the relationship between recorded neurons and the BCI decoder. Neurons were recorded in both M2 (blue) and M1. A subset of M1 neurons were chosen to be direct neurons (green) and used to drive the BCI, while rest of M1 neurons were indirect (purple). (b) Peri-event time histogram (PETH) showing average activity patterns from significantly modulated units in all rats. Units are grouped as: M2, M1i, M1d<sup>+</sup>, M1d<sup>-</sup>. Within each group, units are ordered by the time of their peak firing rate. Time is relative to the end of successful trials. Color indicates normalized firing rate. (n = 387 units from 7 BCI sessions in 4 animals). (c) Rasters and PETHs for example M2 (top), M1i (middle) and M1d (bottom) units. Data is aligned to the end of successful trials (red bar). Grey shaded region represents a circular shuffle test (see Methods).

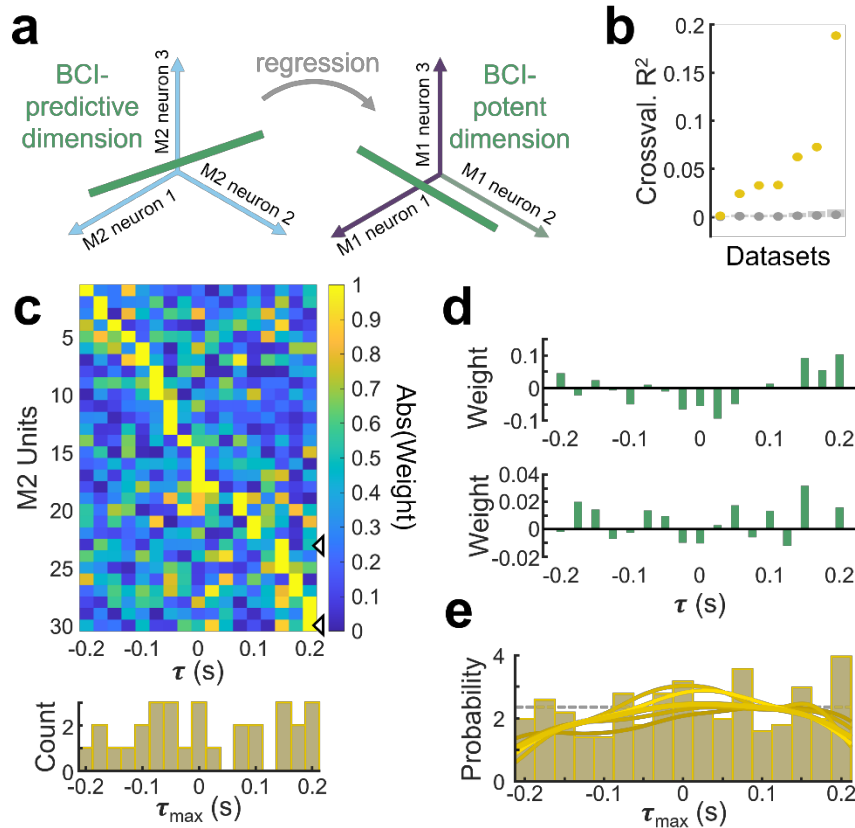


**Figure 2.3 M2 neural activity predicts M1 BCI-potent neural activity at multiple timescales.**

(a) Regression was used to identify a M2 neural population space that predicted BCI-potent M1 activity. GLMs were fit to predict the M1 BCI neural state from M2 population activity; multiple time lagged copies of each M2 unit were used as predictors. (b) Crossvalidated  $R^2$  values for GLM models (yellow) were higher than for models fit to trial shuffled data (gray, circles show mean, shaded area shows 95% confidence interval). Datasets are ordered from lowest to highest  $R^2$ . (c) Distribution of regression weight magnitude in one example session. (Top) For each M2 unit, regression weights were assigned for a variety of time lags, and the absolute value of those weights is indicated by color. Units are sorted according to the time of the largest magnitude weight. Tick marks on the right edge indicate the units shown in (d). (Bottom) Histogram of the  $\tau$  values with the largest magnitude weight for this dataset. (d) Example weights for two M2 neurons from one example session (neural data binned at 25ms). Height of green lines indicates weights for example neurons at different time lags ( $\tau$ ) relative to the M1 BCI-potent activity, with negative  $\tau$  values meaning that M2 leads. (e) Histogram of time lags that had the largest magnitude regression weight for all M2 units in all animals, for models fitted to neural data binned at 25ms. Yellow lines show kernel density fit to equivalent histograms for models fit to neural data binned at 15ms (lightest), 25ms, 35ms, 50ms, and 100ms (darkest). Dashed gray line shows theoretical uniform distribution, empirical distribution is not significantly different.

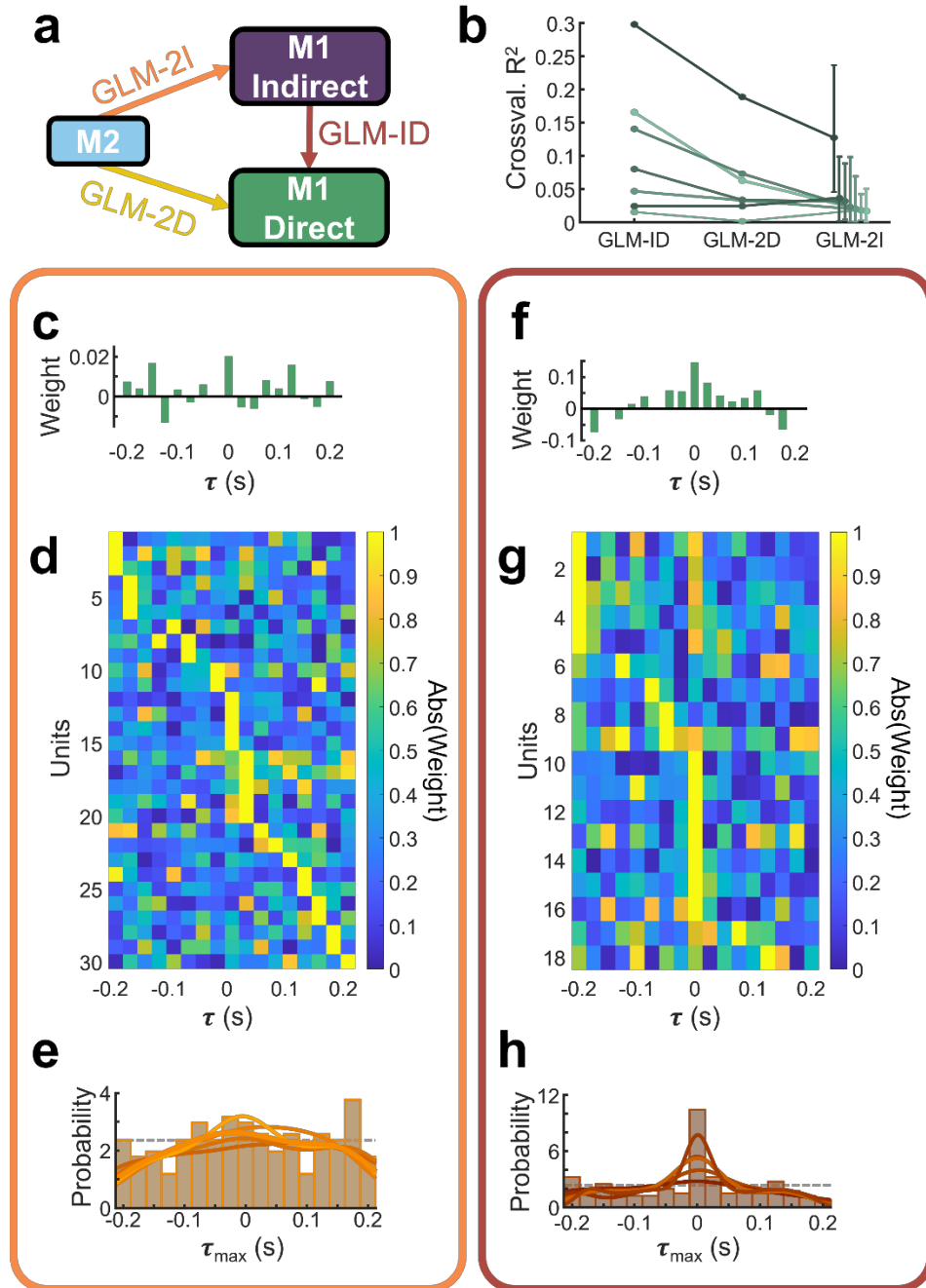


**Figure 2.4 Comparison of timescales of M2 and M1-indirect units' predictions of M1-direct units.**

**(a)** Models which predict M1 direct activity from M2 activity (“GLM-2D”, see Figure 3) were compared to models which predict M1 direct activity from M1 indirect activity (“GLM-ID”) and to models which predict a subset of M1 indirect neurons from M2 activity (“GLM-2I”). **(b)** Crossvalidated  $R^2$  values for GLM-ID, GLM-2D, and GLM-2I models. Each line is one dataset. For the GLM-2I models, 50 different models were fitted to different choices of indirect units. Circle shows mean, error bars show full range. **(c)** Example regression weights for an M2 neuron from

one example learning session, for a model fitted to neural data binned at 25ms. Height of the green lines indicates regression weights for the example neurons at different time lags ( $\tau$ ), with negative values meaning that M2 leads. **(d)** Distribution of regression weight magnitudes in one example learning session. For each unit, regression weights were assigned for a variety of time lags (as in c), and the absolute value of those weights is indicated by color. Units are sorted according to the time of the largest magnitude weight. **(e)** Histogram of time lags that had the largest magnitude regression weight for all M2 units in all animals, for models fitted to neural data binned at 25ms. Solid lines show kernel density fit to equivalent histograms for models fit to neural data binned at 15ms (lightest), 25ms, 35ms, 50ms, and 100ms (darkest). Dashed gray line shows theoretical uniform distribution. **(e)** As in (b), but for GLM-ID models. **(f)** As in (c), but for GLM-ID models. **(g)** As in (d), but for GLM-ID models.

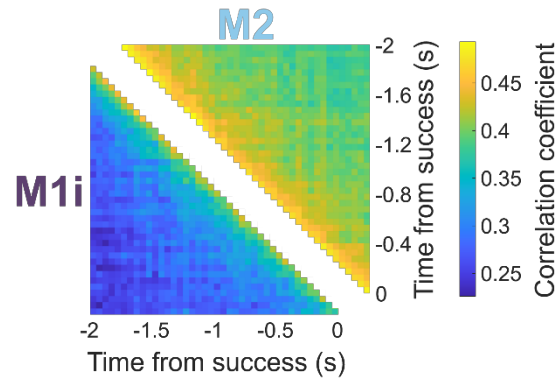


**Figure 2.5 M2 population activity evolves more slowly across trials than M1 indirect population activity.**

Correlation of population firing vectors across time for neural data binned at 50ms. Color indicates the average correlation coefficient between population vectors at the given time for all successful trials of at least 2s duration, for all animals. Data above the diagonal shows correlation coefficients for M2 population vectors; data below the diagonal shows correlation coefficients for M1i population vectors.

## **2.6 Methods**

### **Animal care**

All procedures were in accordance with protocols approved by the Institutional Animal Care and Use Committee at the San Francisco Veterans Affairs Medical Center. Adult male Long Evans rats ( $n = 10$ , 250–400 g; Charles River Laboratories) were housed in a 12-h/12-h light–dark cycle. All experiments were done during the light cycles. Rats were housed in groups of 2 animals prior to surgery and individually after surgery.

### **Surgeries**

All surgical procedures were performed using a sterile technique under 2–4% isoflurane. Surgery involved cleaning and exposure of the skull, preparation of the skull surface (using cyanoacrylate) and then implantation of the skull screws for overall headstage stability. Reference screws were implanted posterior to lambda and ipsilateral to the neural recordings. For experiments involving physiological recordings, craniotomy and durectomy were performed, followed by implantation of the neural probes. For experiments involving only infusions, burr holes were drilled in the appropriate locations, followed by implantation of the cannulas. Postoperative recovery regimen included the administration of 0.02 mg kg<sup>-1</sup> buprenorphine for 2 days, and 0.2 mg kg<sup>-1</sup> meloxicam, 0.5 mg kg<sup>-1</sup> dexamethasone and 15 mg kg<sup>-1</sup> trimethoprim sulfadiazine for 5 days. All animals were allowed to recover for 1 week prior to further behavioral training.

### **Electrode array and cannula implants**

Long-Evans hooded rats were implanted with two 32-channel tungsten wire probes (TDT or Innovative Neurophysiology), one each in M1 (+0.5 AP, +3.5 ML, -1.5 DV) and M2 (+4.0–4.5 AP, +1.5 ML, -1.5 DV). One rat (T391) had a cannula attached to the lateral side of the M2 electrode array prior to surgery for use in a different experiment<sup>11</sup>.

## **General brain-machine interface paradigm**

Rats were trained using an automated behavior box, with components controlled by Matlab R2015a and an Arduino running the Adafruit Motor Library V1. Within the box, rats were unrestrained. Neural data was recorded and sorted online using software from Tucker Davis Technologies: for spout BMI, the software used was OpenEx; for visual BMI, it was Synapse. Spike counts from online sorting were imported into Matlab and used to control the feedback stimuli (see “Spout BMI” and “Visual BMI” for details). Trials started with an auditory cue and the opening of the plastic gate covering a slot in the back of the behavior box. When rats achieved the neural firing rate target, success was indicated with an auditory cue, and water reward was delivered via a metal spout through the slot. If rats failed to achieve the target in the set time, failure was indicated with an auditory cue and the closing of the gate, followed by a timeout period. The maximum trial length and the timeout period following failures were both manipulated over the course of the experiments to encourage learning, and ranged from 10-20s and 5-10s respectively.

## **Spout BMI**

The spout BMI paradigm was used to train  $n = 1$  rat. In this paradigm, feedback about progress to the firing rate target was given via the movement of the water spout used for reward. Eight “direct” units were chosen based on having good signal-to-noise and neither unusually high nor unusually low firing rates. Of the direct units, 4 units were arbitrarily assigned to the “positive pool”, and 4 units were arbitrarily assigned to the “negative pool”. The same channels were used for all sessions, but we did not directly test for unit similarity across days. At the beginning of each session, a 30 minute baseline recording was taken and used to fit mean firing rates for each unit. During the task, for every 100ms bin, direct unit firing rates were computed, mean subtracted, and summed within pools. The “neural state” was computed as  $s = g * (p - n)$ , where  $p$  is the firing rate of the positive pool,  $n$  is the firing rate of the negative pool, and  $g$  is an experimenter-controlled gain parameter. The neural state was smoothed by averaging it with its previous value,



and then used to control the position of the water spout, such that increasing the difference between p and n moved the spout towards the rat. Once the spout crossed a threshold value, the trial was considered a success.

### **Visual BMI**

The visual BMI paradigm was used to train  $n = 3$  rats. In this paradigm, feedback about progress to the firing rate target was given via the movement of both a visual cue on a computer monitor placed outside the behavior box and of the water spout used for reward. 4-8 “direct” units were chosen based on having good signal-to-noise and neither unusually high nor unusually low firing rates. Of the direct units, 2-4 units were arbitrarily assigned to the “positive pool”, and 2-4 units were arbitrarily assigned to the “negative pool”. The same channels were used for all sessions, but we did not directly test for unit similarity across days. At the beginning of each session, a 5-10 minute baseline recording was taken. The baseline data was divided into overlapping 100ms bins. For every bin, firing rates were summed within the positive and negative pools, and the difference between the two pools was computed. Gamma distributions were fitted to the histogram of firing rate differences using the Matlab function *fitdist*. During the task, for every 100ms bin, firing rates were summed within the positive and negative pools, and the difference between the two pools was computed. This difference was fed into the cumulative distribution function of the baseline distribution to obtain the “neural state”. When the neural state crossed an experimenter-defined threshold, the trial was considered a success. Typical threshold values were 0.85 - 0.95. The neural state was smoothed by averaging it with its previous value, and then used to give rats feedback in two ways. First, a computer monitor outside the behavior box displayed a circular “cursor” that moved along a line towards a stationary “target” circle. The position of the cursor along the line was a direct readout of neural state, moving from the top left to the bottom right of the screen (i.e., closer to the rat) as neural state increased. Second, the neural state was also used to control the position of the water spout. The angular speed of the water spout was limited

to 1 degree/s, but otherwise the position of the spout was proportional to the neural state such that as neural state increased, the spout moved closer to the rat.

### **Electrophysiology data collection**

We recorded extracellular neural activity using tungsten microwire electrode arrays (MEAs, n = 8 rats, TDT or Innovative Neurophysiology). We recorded spike and LFP activity using a 128-channel TDT-RZ2 system (TDT). Spike data was sampled at 24,414 Hz and LFP data at 1,018 Hz. Analog headstages with a unity gain and high impedance (~1 GΩ) were used. Snippets of data that crossed a high signal-to noise threshold (4 standard deviations away from the mean) were time-stamped as events, and waveforms for each event were peak aligned. For BCI control, spikes were sorted online using either TDT OpenEx (1 animal) or TDT Synapse (3 animals) software. MEA recordings were sorted offline using a density-based clustering algorithm<sup>37</sup>. Clusters interpreted to be noise were discarded, but multi-units were kept for analysis. Trial-related timestamps (i.e., trial onset, trial completion) were sent to the RZ2 analog input channel using an Arduino digital board and synchronized to neural data.

### **Circular shuffle test for single unit modulation**

A circular shuffle test was used to determine if single units were significantly task-modulated. First, the unit's true peri-event time histogram (PETH) was calculated by aligning data to the end of successful trials and binning at 15ms. Then, the PETH was given a modulation score by calculating its difference from a flat mean using the Matlab function *immse*. Then, for 10<sup>5</sup> repetitions, trials were independently randomly circularly shuffled, and a shuffled PETH and modulation score were calculated. A unit was considered significantly task-modulated if its true modulation score exceeded the 95<sup>th</sup> percentile of shuffled modulation scores.

### **M1 BCI-potent space**

M1 BCI-potent activity was reconstructed from offline-sorted data by binning the data according to online timestamps and identifying the units on M1 direct channels that were most correlated with the recorded online firing rates. Once the offline-sorted M1 direct units had been identified,

neural data could be binned at any binwidth, and M1 BCI-potent activity could be computed as the difference between summed M1d<sup>+</sup> activity and summed M1d<sup>-</sup> activity and used as the response variable in the GLMs.

### **Generalized Linear Models**

Regression was performed using generalized linear models fitted with the Matlab function *fitglm*. Predictors were binned firing rates of either M2 units or M1 indirect units, and the response variable was either M1 BCI-potent space activity (described above), or surrogate M1 indirect activity (for GLM-2I models, described below). In all cases, each predictor unit was represented multiple times, with data shifted to include all time lags from -0.2 to +0.2 s relative to the response variable. For the response variable, data used was the final 2s of all trials of at least 2s duration; for the predictors, the incorporation of time lags meant that data between 2.2s before the end of the trial to 0.2s after the end of the trial was used. Models were fit to data binned at 15, 25, 35, 50, and 100ms; statistics were performed on 25ms models. In the case of GLM-2I models, a “surrogate BCI-potent space” was created from M1 indirect activity by randomly selecting matched numbers of indirect units to stand in for the true direct units. The randomly chosen indirect units were summed within pools and the difference between the pools was used as the response variable. This process was repeated for 50 choices of indirect units per dataset.

For each model, a crossvalidated  $R^2$  was computed and used as a metric of how well the model generalized to held out data. The full dataset was randomly partitioned into 10 equal folds (ignoring trial structure, i.e. timepoints from the same trial could be assigned to different folds). Then, ten different times, one fold was assigned to be the test data and the other nine to be the training data. GLM models were fit to the training dataset. The test data was then projected onto the training model, and  $R^2$  values were computed between the true response variable and the model output. The  $R^2$  values reported are the average across all 10 combinations of testing/training data.

## Population correlation

Population correlation was computed for either M2 or M1 indirect units. Neural data from the given population was binned at 50ms, and the set of firing rates at a given time bin was considered a population vector. For all successful trials of at least 2s duration, pairwise correlations were computed between population vectors for all time bins from -2s to 0s (relative to success) using the Matlab function *corrcoef*. The results were averaged across all trials and all datasets.

## Statistical Analysis

Statistical tests were done using bootstrapping and permutation tests. Unless otherwise specified, simulations had  $10^5$  repetitions, and the significance threshold was set at  $\alpha = 0.05$ , meaning that tests were significant when the true value was greater than the 95<sup>th</sup> percentile of the reference distribution.

To determine whether GLMs had significant predictive power, their crossvalidated  $R^2$  (described above) was compared to a reference distribution of crossvalidated  $R^2$  values for models fitted to trial-shuffled data. Shuffling the trials in the response variable before fitting the models created a control dataset with equivalent firing rates and the same characteristic pattern of neural state increasing at the end of successful trials, but broke true moment-by-moment correlations. Trial-shuffling was performed for 25ms models only.  $10^3$  shuffles were performed. Models were considered to have significant predictive power if the true  $R^2$  exceeded the 95<sup>th</sup> percentile of the reference distribution, which was the case for all 7 datasets.

To determine whether the distribution of timelags that had the largest magnitude GLM weight ( $\tau_{\max}$ ) were significantly non-uniform, the  $\tau_{\max}$  histograms were compared to surrogates drawn from a uniform distribution as follows: First, the probability-normalized  $\tau_{\max}$  histogram was considered to be the empirical distribution, and a theoretical discrete uniform distribution was calculated as the mean value of the empirical distribution. The difference between the empirical and theoretical distributions was computed using the Matlab function *immse*. Then, for each bootstrap repetition, a surrogate set of  $\tau_{\max}$  values was drawn from a uniform distribution using

the Matlab function *datasample*, and the difference from the theoretical distribution was calculated in the same manner to create the reference distribution.

To determine whether the GLM-2D models had significantly different  $R^2$  values from the GLM-2I models, permutation tests were performed separately on each dataset. First, for each dataset, the true difference between the GLM-2D  $R^2$  value and the mean GLM-2I  $R^2$  value was calculated. Then the true GLM-2D  $R^2$  value was pooled with the 50 GLM-2I  $R^2$  values (from different choices of indirect units, see “Generalized Linear Models” above), resulting in a set of 51  $R^2$  values. Then, for each permutation, one of the  $R^2$  values was chosen to stand in for the GLM-2D  $R^2$  value, and the difference between that and the mean of the remaining 50  $R^2$  values was calculated to create the reference distribution. By this metric, the GLM-2D  $R^2$  values were not significantly different from the GLM-ID  $R^2$  values for 6 of the 7 datasets; for the remaining dataset the GLM-2D  $R^2$  value was significantly higher than the mean GLM-ID  $R^2$  value.

To determine whether the GLM-2D models had significantly lower  $R^2$  values from the GLM-ID models, a permutation test was used. First, the mean GLM-2D and GLM-ID  $R^2$  values were calculated across datasets, and the true difference between them was computed. Then, for each permutation, the GLM-2D and GLM-ID  $R^2$  values were randomly swapped (or not) with 50% probability, and the difference in means between the two groups was calculated to create the reference distribution.

To determine whether M2 single units had a significantly wider autocorrelation function than M1 indirect units, a permutation test was used. First, the autocorrelation of each M2 and M1 indirect unit was computed using the Matlab function *xcorr*, the width-at-half-max was calculated for each autocorrelation, and the true difference in mean values between M2 and M1 indirect was calculated. Then, for each permutation, units were randomly assigned to two groups, matched in size to the true M2 and M1 indirect populations, and the difference in mean autocorrelation width between the two groups was calculated to create the reference distribution.

To determine whether M2 population activity was more correlated across time than M1 indirect population activity, a permutation test was used. First, M2 and M1 indirect population correlations were computed as described above. Then, the mean M2 and M1 indirect population correlations was taken across all time bin pairs, and the true difference between the two means was calculated. Then, for each permutation, correlation values were randomly swapped between M2 and M1 and the difference between the mean values was calculated to create the reference distribution.

**Acknowledgements:** Thank you to R. Kulkarni and N. Hoglen for providing comments on the manuscript.

**Funding:** This work was supported by fellowship awards from the National Defense Science and Engineering Graduate Fellowship (NDSEG, <https://ndseg.asee.org/>) the UCSF Discovery Fellows Program, and the Markowski-Leach Fellowship (to T.L.V.), the UCSF Medical Scientist Training Program (to T.L.V.), the UCSF Neuroscience Graduate Program (to T.L.V. and K.D.). Additional funds come from the Department of Veterans Affairs, Veterans Health Administration (VA Merit: 1I01RX001640 to K.G) and National Institute of Mental Health, NIH (5R01MH111871 to K.G.); and start-up funds from the UCSF Department of Neurology to K.G.. K.G. also holds a Career Award for Medical Scientists from the Burroughs Wellcome Fund (1009855) and an Independent Scientist Award (1K02NS093014) from the National Institute of Neurological Disorders and Stroke, NIH. The funders had no role in study design, data collection and analysis, decision to publish, or preparation of the manuscript.

## 2.7 References

1. Ganguly, K., Dimitrov, D. F., Wallis, J. D. & Carmena, J. M. Reversible large-scale modification of cortical networks during neuroprosthetic control. *Nature Neuroscience* 14, 662–667 (2011).
2. Koralek, A. C., Jin, X., Long II, J. D., Costa, R. M. & Carmena, J. M. Corticostriatal plasticity is necessary for learning intentional neuroprosthetic skills. *Nature* 483, 331–335 (2012).
3. Gulati, T., Ramanathan, D. S., Wong, C. C. & Ganguly, K. Reactivation of emergent task-related ensembles during slow-wave sleep after neuroprosthetic learning. *Nature Publishing Group* 17, 1107–1113 (2014).
4. Clancy, K. B., Koralek, A. C., Costa, R. M., Feldman, D. E. & Carmena, J. M. Volitional modulation of optically recorded calcium signals during neuroprosthetic learning. *Nature Neuroscience* 17, 807–809 (2014).
5. Kim, J., Gulati, T. & Ganguly, K. Competing Roles of Slow Oscillations and Delta Waves in Memory Consolidation versus Forgetting. *Cell* 179, 514-526.e13 (2019).
6. Liu, Z. & Schieber, M. H. Neuronal Activity Distributed in Multiple Cortical Areas during Voluntary Control of the Native Arm or a Brain-Computer Interface. *eNeuro* 7, (2020).
7. Hira, R. et al. In vivo optogenetic tracing of functional corticocortical connections between motor forelimb areas. *Frontiers in Neural Circuits* 7, 1–10 (2013).
8. Reep, R. L., Corwin, J. V., Hashimoto, A. & Watson, R. T. Afferent connections of medial precentral cortex in the rat. *Neuroscience Letters* 44, 247–252 (1984).
9. Reep, R. L., Corwin, J. V., Hashimoto, A. & Watson, R. T. Efferent Connections of the Rostral Portion of Medial Agranular Cortex in Rats. *Brain Research Bulletin* 19, 203–221 (1987).
10. Jeong, M. et al. Comparative three-dimensional connectome map of motor cortical projections in the mouse brain. *Scientific Reports* 6, 1–14 (2016).

11. Veuthey, T. L., Derosier, K., Kondapavulur, S. & Ganguly, K. Single-trial cross-area neural population dynamics during long-term skill learning. *Nature Communications* 11, 4057 (2020).
12. Cao, V. Y. et al. Motor Learning Consolidates Arc-Expressing Neuronal Ensembles in Secondary Motor Cortex. *Neuron* 86, 1385–1392 (2015).
13. Okabe, N., Narita, K. & Miyamoto, O. Axonal remodeling in the corticospinal tract after stroke: How does rehabilitative training modulate it? *Neural Regeneration Research* 12, 185–192 (2017).
14. Brown, A. R. & Teskey, G. C. Motor Cortex Is Functionally Organized as a Set of Spatially Distinct Representations for Complex Movements. *Journal of Neuroscience* 34, 13574–13585 (2014).
15. Kawai, R. et al. Motor Cortex Is Required for Learning but Not for Executing a Motor Skill. *Neuron* 86, 800–812 (2015).
16. Hyland, B. Neural activity related to reaching and grasping in rostral and caudal regions of rat motor cortex. *Behavioural Brain Research* 94, 255–269 (1998).
17. Saiki, A. et al. Different Modulation of Common Motor Information in Rat Primary and Secondary Motor Cortices. *PLoS ONE* 9, e98662 (2014).
18. Chen, T., Li, N., Daie, K. & Svoboda, K. A Map of Anticipatory Activity in Mouse Motor Cortex. *Neuron* 94, 866-879.e4 (2017).
19. Murakami, M., Vicente, M. I., Costa, G. M. & Mainen, Z. F. Neural antecedents of self-initiated actions in secondary motor cortex. *Nature neuroscience* 17, 1574–82 (2014).
20. Makino, H. et al. Transformation of Cortex-wide Emergent Properties during Motor Learning. *Neuron* 94, 880-890.e8 (2017).
21. Perich, M. G. & Miller, L. E. Altered tuning in primary motor cortex does not account for behavioral adaptation during force field learning. *Experimental Brain Research* (2017) doi:10.1007/s00221-017-4997-1.



22. Stringer, C. et al. Spontaneous behaviors drive multidimensional, brainwide activity. *Science* 364, eaav7893 (2019).
23. Runyan, C. A., Piasini, E., Panzeri, S. & Harvey, C. D. Distinct timescales of population coding across cortex. *Nature* 548, 92–96 (2017).
24. Shenoy, K. V., Sahani, M. & Churchland, M. M. Cortical control of arm movements: a dynamical systems perspective. *Annual review of neuroscience* 36, 337–59 (2013).
25. Stavisky, S. D., Kao, J. C., Sorokin, J. M., Ryu, S. I. & Shenoy, K. V. System identification of brain-machine interface control using a cursor jump perturbation. in 2015 7th International IEEE/EMBS Conference on Neural Engineering (NER) 643–647 (2015). doi:10.1109/NER.2015.7146705.
26. Xu, M., Zhang, S., Dan, Y. & Poo, M. Representation of interval timing by temporally scalable firing patterns in rat prefrontal cortex. *Proc Natl Acad Sci U S A* 111, 480–485 (2014).
27. Churchland, M. M. et al. Neural population dynamics during reaching. *Nature* 487, 51–56 (2012).
28. Collinger, J. L. et al. High-performance neuroprosthetic control by an individual with tetraplegia. *The Lancet* 381, 557–564 (2013).
29. Athalye, V. R., Ganguly, K., Costa, R. M. & Carmena, J. M. Emergence of Coordinated Neural Dynamics Underlies Neuroprosthetic Learning and Skillful Control. *Neuron* 93, 955-970.e5 (2017).
30. Luft, A. R. & Buitrago, M. M. Stages of motor skill learning. *Mol Neurobiol* 32, 205–216 (2005).
31. Kleim, J. A. Cortical Synaptogenesis and Motor Map Reorganization Occur during Late, But Not Early, Phase of Motor Skill Learning. *Journal of Neuroscience* 24, 628–633 (2004).
32. Hikosaka, O., Nakamura, K., Sakai, K. & Nakahara, H. Central mechanisms of motor skill learning. *Current Opinion in Neurobiology* 12, 217–222 (2002).

33. Floyer-Lea, A. & Matthews, P. M. Distinguishable Brain Activation Networks for Short- and Long-Term Motor Skill Learning. *Journal of Neurophysiology* 94, 512–518 (2005).
34. Gulati, T., Guo, L., Ramanathan, D. S., Bodepudi, A. & Ganguly, K. Neural reactivations during sleep determine network credit assignment. *Nature Neuroscience* 20, 1277–1284 (2017).
35. Silversmith, D. B. et al. Plug-and-play control of a brain–computer interface through neural map stabilization. *Nature Biotechnology* 1–10 (2020) doi:10.1038/s41587-020-0662-5.
36. Otchy, T. M. et al. Acute off-target effects of neural circuit manipulations. *Nature* 528, 358–363 (2015).
37. Chung, J. E. et al. A Fully Automated Approach to Spike Sorting. *Neuron* 95, 1381-1394.e6 (2017).

## CONCLUSION

In this dissertation, we studied communication between primary motor (M1) and premotor (M2) cortex while rats learned either a dexterous natural motor task or a simple linear M1 brain-computer interface (BCI) task. In both cases, we found that activity was coordinated between the two regions. In the case of natural motor learning, we found that learning did not change the strength of M2-M1 interactions, but did increase the amount of task-related information available in the cross-area dynamics, and that these cross-area dynamics were necessary for learned behavioral improvements. We also found that when M2 was inactivated, M1 neurons and population dynamics that had earlier been more strongly coordinated with M2 were more affected. In the case of BCI learning, we found that M2-M1 interactions occurred on a broader timescale than did M1-internal interactions, and that M2 population activity evolved at a slower pace. These results are consistent with a model in which M2 provides top-down contextual information to M1, which more precisely controls the output.

An important point for the interpretation of both of these studies is the distinction between using correlation to estimate neural connectivity and using correlation to estimate population signals. It has been shown that correlated activity is not a reliable predictor of true anatomical connectivity between single neurons<sup>1</sup>, and we do not wish to make any claims of connectivity between the units we have recorded here. Although there are direct projections between M2 and M1<sup>2,3</sup>, it is possible that none of the M2 neurons we recorded were directly connected to the M1 neurons we recorded. Instead, we used correlations between the neurons we did record as a method for estimating the influence of one region on the other. In this perspective, the high level of correlation between units within each population that is a confound when estimating true connectivity is instead a strength, because it means that even though experimental limitations prevent us from recording from exactly the M2 neurons that project to M1 and the M1 neurons that receive those projections, we are recording from neurons that are highly correlated with them.

Another caveat is that both the canonical correlation analysis used in Ch. 1 and the generalized linear models used in Ch. 2 are linear methods, and cannot capture higher order statistical dependencies. It is therefore likely that we were only able to estimate some of the coordination between M2 and M1, and that the true relationship is more complex.

This work could be improved by performing more extensive anatomical mapping prior to implantation. Although we had robust movement-related responses on all arrays in all animals, we were not able to verify the placement of the M2 and M1 arrays with respect to each other, and it is possible that much of the variability seen across animals is due to differences in relative anatomical placement. Concerns about surgery time prevented us from performing complete ICMS mappings of M2 and M1, but the incorporation of an abridged ICMS mapping or even of tract imaging<sup>4</sup> could be beneficial.

Both learning paradigms would also be improved by tracking the same neurons across days, and extending the training sessions to go from exploration all the way to stereotyped behavior. In the BCI task, we used a single session learning paradigm, analyzing the early exploratory stages of BCI learning. In the natural learning task, learning took place across several days, but large gaps between recording sessions prevented us from confidently identifying neurons that had been maintained between sessions. Advances in recording technology are increasing the feasibility of maintaining and identifying the same neurons across days<sup>5</sup>. Being able to match neurons between different sessions would enable characterization of the effects of learning on single units, in addition to population level analyses.

Another interesting future direction would be optogenetic inhibition of M2 during the M1 BCI task. In the natural learning task, we used muscimol to inactivate M2 in a block design. However, this required a gap of several hours between the sessions, and caused a small but significant reduction in M1 baseline firing rates, both of which would pose problems for the ability to use the same decoder before and after inactivation in the BCI task. Therefore, to test whether task-related modulation in M2 is necessary for M1 BCI performance, it may be better to use optogenetics to

briefly perturb M2 activity on a minority of trials. Viral optogenetics can be done in rats<sup>6,7</sup>, but it is often technically challenging to achieve sufficient expression. Alternatively, similar BCI tasks have been done in mice<sup>8</sup>, where genetic tools are generally considered to be more reliable.

A key innovation in both of the studies is the use of dimensionality reduction methods that optimize for coordination between the populations of interest. Many previous studies of cortical communication have used dimensionality reduction methods that optimize local properties alone (e.g., principal components analysis, factor analysis) before comparing regions<sup>9,10</sup>, or compare bulk population signals like wide-field calcium signals<sup>11,12</sup> or local field potentials<sup>13-1</sup>. These strategies run the risk of missing activity patterns that are coordinated between regions but do not dominate the local population. We think that an approach that focuses on coordination between regions first is better suited to studying inter-area communication.

Overall, this work has studied the role of M1-M2 communication in learning. We characterized cross-area activity patterns in both natural motor learning and BCI learning, and saw that M2 activity had the potential to provide contextual signals in both cases. In natural motor learning, we were able to inactivate M2 and show that it is necessary for both learned improvements in behavior and for M1 cross-area dynamics.

## References

1. Das, A., & Fiete, I. R. (2020). Systematic errors in connectivity inferred from activity in strongly recurrent networks. *Nature Neuroscience*, 23(10), 1286–1296.  
<https://doi.org/10.1038/s41593-020-0699-2>
2. Reep, R. L., Corwin, J. V., Hashimoto, A., & Watson, R. T. (1987). Efferent Connections of the Rostral Portion of Medial Agranular Cortex in Rats. *Brain Research Bulletin*, 19(2), 203–221. [https://doi.org/10.1016/0361-9230\(87\)90086-4](https://doi.org/10.1016/0361-9230(87)90086-4)
3. Hira, R., Ohkubo, F., Tanaka, Y. R., Masamizu, Y., Augustine, G. J., Kasai, H., & Matsuzaki, M. (2013). In vivo optogenetic tracing of functional corticocortical connections between motor forelimb areas. *Frontiers in Neural Circuits*, 7(April), 1–10.  
<https://doi.org/10.3389/fncir.2013.00055>
4. Jeong, M., Kim, Y., Kim, J., Ferrante, D. D., Mitra, P. P., Osten, P., & Kim, D. (2016). Comparative three-dimensional connectome map of motor cortical projections in the mouse brain. *Scientific Reports*, 6(December 2015), 1–14.  
<https://doi.org/10.1038/srep20072>
5. Chung, J. E., Joo, H. R., Smyth, C. N., Fan, J. L., Geaghan-Breiner, C., Liang, H., Liu, D. F., Roumis, D., Chen, S., Lee, K. Y., Pebbles, J. A., Tooker, A. C., Tolosa, V. M., & Frank, L. M. (2019). Chronic Implantation of Multiple Flexible Polymer Electrode Arrays. *Journal of Visualized Experiments: JoVE*, 152. <https://doi.org/10.3791/59957>
6. Gulati, T., Guo, L., Ramanathan, D. S., Bodepudi, A., & Ganguly, K. (2017). Neural reactivations during sleep determine network credit assignment. *Nature Neuroscience*, 20(9), 1277–1284. <https://doi.org/10.1038/nn.4601>
7. Kim, J., Gulati, T., & Ganguly, K. (2019). Competing Roles of Slow Oscillations and Delta Waves in Memory Consolidation versus Forgetting. *Cell*, 179(2), 514-526.e13.  
<https://doi.org/10.1016/j.cell.2019.08.040>

8. Mitani, A., Dong, M., & Komiyama, T. (2017). Brain-Computer Interface with Inhibitory Neurons Reveals Subtype-Specific Strategies. *Current Biology*, 1–7.  
<https://doi.org/10.1016/j.cub.2017.11.035>
9. Perich, M. G., & Miller, L. E. (2017). Altered tuning in primary motor cortex does not account for behavioral adaptation during force field learning. *Experimental Brain Research*. <https://doi.org/10.1007/s00221-017-4997-1>
10. Athalye, V. R., Ganguly, K., Costa, R. M., & Carmena, J. M. (2017). Emergence of Coordinated Neural Dynamics Underlies Neuroprosthetic Learning and Skillful Control. *Neuron*, 93(4), 955-970.e5. <https://doi.org/10.1016/j.neuron.2017.01.016>
11. Makino, H., Ren, C., Liu, H., Kim, A. N., Kondapaneni, N., Liu, X., & Kuzum, D. (2017). Transformation of Cortex-wide Emergent Properties during Motor Learning. *Neuron*, 94(4), 880-890.e8. <https://doi.org/10.1016/j.neuron.2017.04.015>
12. Chen, T., Li, N., Daie, K., & Svoboda, K. (2017). A Map of Anticipatory Activity in Mouse Motor Cortex. *Neuron*, 94(4), 866-879.e4. <https://doi.org/10.1016/j.neuron.2017.05.005>
13. Arce-McShane, F. I., Ross, C. F., Takahashi, K., Sessle, B. J., & Hatsopoulos, N. G. (2016). Primary motor and sensory cortical areas communicate via spatiotemporally coordinated networks at multiple frequencies. *Proceedings of the National Academy of Sciences*, 113(18), 5083–5088. <https://doi.org/10.1073/pnas.1600788113>
14. Koralek, A. C., Jin, X., Long li, J. D., Costa, R. M., & Carmena, J. M. (2012). Corticostriatal plasticity is necessary for learning intentional neuroprosthetic skills. *Nature*, 483(7389), 331–335. <https://doi.org/10.1038/nature10845>
15. Loonis, R. F., Brincat, S. L., Antzoulatos, E. G., & Miller, E. K. (2017). A Meta-Analysis Suggests Different Neural Correlates for Implicit and Explicit Learning. *Neuron*, 96(2), 521-534.e7. <https://doi.org/10.1016/j.neuron.2017.09.032>

## Publishing Agreement

It is the policy of the University to encourage open access and broad distribution of all theses, dissertations, and manuscripts. The Graduate Division will facilitate the distribution of UCSF theses, dissertations, and manuscripts to the UCSF Library for open access and distribution. UCSF will make such theses, dissertations, and manuscripts accessible to the public and will take reasonable steps to preserve these works in perpetuity.

I hereby grant the non-exclusive, perpetual right to The Regents of the University of California to reproduce, publicly display, distribute, preserve, and publish copies of my thesis, dissertation, or manuscript in any form or media, now existing or later derived, including access online for teaching, research, and public service purposes.

DocuSigned by:

*Katherine Derosier*

1456253957E34E3...

Author Signature

12/15/2020

Date